Mapping root water uptake stress and carrying capacity using satellite observed soil moisture data

Herman Brink

Master's Thesis

Mapping root water uptake stress and carrying capacity using satellite observed soil moisture data

Herman Brink
Bsc., Civil Engineering (University of Twente, Enschede)

In partial fulfillment of the requirements
for the degree of

Master of Science in Civil Engineering and Management

University of Twente

February 7, 2014

Under supervision of the following committee:
Dr. ir. D.C.M. Augustijn
University of Twente, Department of Water Engineering and Management

Dr. ir. R. van der Velde
University of Twente, Faculty of Geo-Informations Science and Earth Observations

Ing. W.J.M. Heijkers
SAT-water/Hoogheemraadschap de Stichtse Rijnlanden

M.B.A. ter Haar - Leuverink MSc.
SAT-water/Waterschap Groot-Salland

A. Peters MSc.
SAT-water/Waterschap Aa en Maas

Abstract

The waterboards responsibility for freshwater availability is managed by monitoring surface and ground water levels. These levels are influencing the soil moisture content in the soil, which is an important parameter for crop growing (root water uptake stress) and the carrying capacity. Knowledge of the soil moisture content can improve the management of the available water resources. In this research the soil moisture is retrieved from satellite observations and used to quantify the carrying capacity and root water uptake stress.

Soil moisture is inhomogeneous over an area and can change rapidly in time due to atmospheric forcings (e.g. rainfall and evapotranspiration) and irrigation. Therefore fine resolution spatial and temporal soil moisture data are needed for good estimations of root water uptake stress and the carrying capacity at field scale. These fine spatial and temporal resolution data are produced by downscaling low spatial and high temporal Advance SCATerometer data (ASCAT, 12.5 km x 12.5 km, 1 day) with high spatial, low temporal resolution satellite data (RADARSAT-2, 25 m x 25m, 24 days). Four downscaling methods are applied and results are compared to in-situ soil moisture measurements of the soil moisture and soil temperature network located in the eastern part of the Netherlands for the year 2012. The downscaling method which uses a daily changing soil sensitivity parameter (β) shows the best fit between in-situ and satellite retrieved soil moisture data, using the ASCAT SWI 1 product for coarse resolution soil moisture, with correlation coefficients (R^2) ranging up to 0.69 over the whole year. When only RADARSAT-2 observation dates are considered R^2 increases even to 0.77.

Maps of the retrieved soil moisture data show wet and dry areas at the expected locations. Grassland on peat in the western part of the study area presents a higher volumetric soil moisture content than high situated grasslands with sandy soils grounds in the east. The soil moisture values are transformed to a soil status using the Soil-Moisture-Stress indication (SMS-i) diagram. A SMS-i diagram is developed for each soil type of the Policy Analysis of Water Management for the Netherlands (PAWN) classification consisting of the combination of water or oxygen stress for root take up and the carrying capacity. Resulting SMS-i maps show that the contours of the different soil statuses are following the contours of the PAWN soil type map. This indicates that the soil status as defined in this research is more dominated by the soil type than by the retrieved volumetric soil moisture content.

The status of the soil strongly depends on the soil type because i) each soil type has its own unique SMS-i diagram based on its water retention curve and ii) the coarse resolution satellite data has to be multiplied by the porosity of the soil to obtain the volumetric soil moisture content. The influence of the coarse resolution soil moisture data and the soil porosity are equal because their values are multiplied with each other in the used downscaling method. Because the used soil map, based on the Policy Analysis of Water Management for the Netherlands (PAWN) classification, has only 21 soil types for the Netherlands, soil properties are averaged and spatial heterogeneity within soil types is neglected. This research has shown that satellite retrieved data can be used to produce fine resolution soil moisture maps which can be translated to classes indicating the root water uptake stress and the carrying capacity. However, the average Mean Absolute Error of 0.08 m^3/m^3 over all grass covered in-situ stations after validation is high compared to the average porosity of 0.42. Accuracy and reliability of the retrieved maps should be improved to make them useful for operational water management.

Acknowledgements

This Master's Thesis concludes my study in Civil Engineering and Management at the University of Twente. The research has been carried out at Waterboard Groot Salland in Zwolle with the aim to investigate if satellite data can be used for water management at field scale. I found it interesting to learn how satellite data is retrieved and which information can be derived from this data.

This research could not be done without the help of my supervisors. I would like to thank my supervisors of the University of Twente Denie Augustijn and Rogier van der Velde for providing constructive feedback on my reports. Rogier his expert knowledge about satellite data helped a lot, especially during the start of the project. Than I would like to thanks the external supervisors. Marloes ter Haar, who take over the daily supervision at Waterboard Groot Salland after Veronique Kaiser was send on maternity leave, Veronique thanks for the warm welcome at the start of the project. Joost Heijkers for his input mostly regarding hydrological and soil aspects and Arjan Peeters for his feedback on the designed classification system.

Next to my supervisors I would like to thank the office mates at Waterboard Groot Salland. Their sceptic view about satellite data held me critical towards it. The SAT-water group for give me the opportunity to join their meetings and discus about the use of satellite data for water management. The cooperation between Waterboard Groot Salland and the Inkomatie Catchment Management Agency which gave me the opportunity to learn and see more about water management in South-Africa where the water related problems are different then in the Netherlands but the solutions is searched in the same direction: satellite data.

Of course I would like to thank the data suppliers because without data there would be no research. The Netherland Space Office I would like to thank for making available the RADARSAT-2 data, the ITC for their in-situ measurements, TU Wien for their ASCAT products and the NASA for the GLDAS-Noah data.

I want to thank my friends and family for their support during my study. My friends from Enschede for the good times during the study and some remarkable nights. All my friends at home for the distraction they gave me during the weekends, so I could recharge myself. Finally I would thank my family, especially my parents for giving me the opportunity to study and supporting me during the years.

Herman Brink
Onnen, February 2014

Table of contents

I List of Figures

II List of tables

III List of abbreviations

AHN	Actueel Hoogtebestand Nederland
AMSR-E	Advanced Microwave Scanning Radiometer Observing System
ASCAT	Advanced Scatterometer
CBS	Centraal Bureau voor de Statistiek
Cfb	Maritime temperature climate according to the Köppen Classification System
EC-TM ECH_2O	Soil moisture probe by Decagon
Em50 ECH_2O	Datalogger by Decagon
EUMETSAT	European Organization for the Exploitation of Meteorological Satellites
FIFE	Field Experiment
FTP-server	File Transfer Protocol server
GES DISC	Goddard Earth Science Data and Information Services Center
GLDAS	Global Land Data Assimilation System
gr.	Grass
GSFC	Goddard Space Flight Center
HH-polarization	Horizontal transmission and reception of the electromagnetic wave
HV-polarization	Horizontal transmission and vertical reception of the electromagnetic wave
IPF-TU Wien	Institute of Photogrammetry and Remote Sensing from the Vienna University of Technology
ISLSCP	International Satellite Land Surface Climatology Project
ITC	Faculty of Geo-Information Science and Earth Observations of the University of Twente
ITCSM	The soil moisture and soil temperature network of the ITC
KNMI	Royal Dutch Metrological Institute
MAE	Mean Absolute Error
MetOp	Meteorological Operational satellite programme
MSL	Mean Sea Level
NAP	Normaal Amsterdams Peil (dutch for MSL)
NASA	National Aeronautics and Space Administration
NCEP	National Centers for Environmental Prediction
NHI	National Hydrologic Instruments
NOAA	National Oceanic and Atmospheric Administration
Noah	Name of the Oregon State University / NCEP Eta Land-Surface model afther 2000
NSO	Neterlands Space Office
OSU	Oregon State University
OSU LSM	Oregon State University / NCEP Eta Land-Surface model
PALSAR	Phased Array L-band Synthetic Aperture
PAWN	Policy Analysis of Water Management for the Netherlands
R^2	Coefficient of determination
RADARSAT-2	Earth Observation Satellite with a SAR
RMSE	Root Mean Squar Error
SAR	Synthetic Aperture Radar
SEBAL	Surface Energy Balance Algorithm for Land
SEBS	Surface Energy Balance System
SMAP	Soil Moisture Active and Passive
SMS-i	Soil-Moisture-Stress indication
SSM	Surface Soil Moisture

St.dev.	Standard deviation
SWI	Soil Water Index
SWI_x	Soil Water Index with time leg x
val.	Validation
VV-polarization	Vertical transmission and reception of the electromagnetic wave
$WARP^{NT}$	Water Retrieval Package for Near-Real Time
WGS	Waterboard Groot Salland
WRD	Waterboard Regge and Dinkel
WRIJ	Waterboard Rijn and IJssel

IV List of symbols

°	Degrees
°C	Degrees Celsius
A_1	Slope of the trend line with $\Theta_{in\text{-}situ}$ as base (-)
A_2	Slope of the trend line with $\Theta_{m,bbc}$ as base (-)
B_1	Offset of the trend line with $\Theta_{in\text{-}situ}$ as base (m^3/m^3)
B_2	Offset of the trend line with $\Theta_{m,bbc}$ as base (m^3/m^3)
BX	Staringreeks code of the upper soil type X
GHz	GigaHertz
h_X	Matric head X in the reduction function of Feddes et al. (1978)
I	Intensity of RADARSAT-2 backscatter (W/m^2)
MPa	Mega Pascal
n	Porosity (m^3/m^3)
n_{max}	porosity of the soil, maximal value of a. the porosity of the PAWN-classification or b. the maximal Θ observed at the in-situ location in 2012 (-)
OX	Staringreeks code of the under soil type X
S_{dry}	Scaling term for "dry" retrievals (-)
S_{wet}	Scaling term for "wet" retrievals (-)
T	Characteristic time length (days)
t	Time
t_i	Initial time (days)
α_c	Calibration parameter depending on vegetation cover, type and surface roughness (-)
β	Soil moisture sensitivity parameter (m^3/m^3 dB^{-1})
β_c	Soil moisture sensitivity parameter of a coarse grid (m^3/m^3 dB^{-1})
$\beta_{c,24}$	Soil moisture sensitivity parameter fixed per RADARSAT-2 observation (m^3/m^3 dB^{-1})
$\beta_{c,day}$	Soil moisture sensitivity parameter daily changing (m^3/m^3 dB^{-1})
$\beta_{c,year}$	Soil moisture sensitivity parameter for the whole year (m^3/m^3 dB^{-1})
θ	Volumetric soil moisture content (m^3/m^3)
$\theta_{ECH2O,cal}$	calibrated volumetric soil moisture measured by the EC-TM ECH_2O probes (m^3/m^3)
$\theta_{ECH2O,cal}$	volumetric soil moisture measured by the EC-TM ECH_2O probes (m^3/m^3)
$\theta_{GLDAS\text{-}Noah}$	Volumetric soil moisture of the GLDAS-Noah product (m^3/m^3)
$\theta_{ITCSM\ XX}$ *or* $\theta_{in\text{-}situ\ XX}$	Volumetric soil moisture measured by the ITCSM at location XX (m^3/m^3)
θ_m	Volumetric soil moisture of a medium pixel (m^3/m^3)
$\theta_{m,abc}$	Volumetric soil moisture of a medium pixel after bias correction (m^3/m^3)
$\theta_{m,abc,III}$	Volumetric soil moisture of a medium pixel after downscaling with method III and bias correction(m^3/m^3)
θ_{m1}	Volumetric soil moisture of a medium pixel after the left bias correction side (m^3/m^3)
θ_{m2}	Volumetric soil moisture of a medium pixel after the right bias correction side (m^3/m^3)
θ_{SSM}	Surface soil moisture (m^3/m^3)
$\theta_{SWI\ X}$	Volumetric soil moisture of the ASCAT SWI X product (m^3/m^3)
σ	RADARSAT-2 backscatter (-dB)
σ_c°	Average RADARSAT-2 backscattering of the ASCAT-grid (-dB)
σ_m°	Average of the 3x3 RADARSAT-2 backscattering pixel s(-dB)
σ_{max}	Maximal RADARSAT-2 backscatter assumed to be wet (-dB)
σ_{min}	Minimal RADARSAT-2 backscatter assumed to be dry (-dB)

1. Introduction

1.1. Motivation

Flood protection, freshwater availability and water quality are the main management tasks of Dutch waterboards (Unie van Waterschappen, 2007). Freshwater availability can be divided in the availability of surface and ground water which are both monitored and managed by waterboards.

According to Bakker (2013) waterboards should focus more on soil moisture status management instead of surface and groundwater level management to provide water availability for crops. This is because too low or too high soil moisture content will result in lower crop yield and farmers are one of the most important stakeholders for waterboards. Yield and financial losses of crops due to soil oxygen or water stress will occur when the matric head is too high or too low, respectively. The damage for grassland for example can be determined using the 'Waterhuishoudkundige schadefuncties op grasland' of Peerboom (1990). Good estimations of the soil moisture content need an acceptable level of soil moisture data.

Besides crop yield, the carrying capacity is also related to the soil moisture content of the topsoil. The carrying capacity is commonly measured as penetration resistance. It is important for waterboards to know if the carrying capacity is sufficient, because of maintenance (mowing and dredging) of ditches and canals whereby in the new management and maintenance structure (in Dutch Beheer en Onderhoud) of Waterboard Groot Salland (WGS) farmers ground is entered. For farmers the carrying capacity is essential when they have to enter fields with heavy machinery to prepare the land, treat or harvest their crops or for cattle grazing. This makes the carrying capacity one of the control parameters of waterboards which is estimated nowadays with a combination of area knowledge and surface water levels.

The penetration resistance, used to determine the carrying capacity, is commonly measured with hand-operated cone penetrometers because of their easy, rapid and economical operation (Perumpral, 1987). Disadvantage of the penetrometer is the local point measurement which causes the need for many measurements when the carrying capacity of a certain area is needed. The resulting high costs when these measurements have to be taken regularly, forces the need for new methods of carrying capacity prediction. Dexter et al. (2007) have shown that the penetrometer resistance can be predicted from basic soil properties such as the soil composition, bulk density and water content. Linking the carrying capacity to area covering satellite soil moisture data may be an attractive alternative.

With the expectation that remote sensing, including satellite data, will have a future in water management, a group of enthusiastic water managers bounded their forces in the SAT-water group to investigate the possibilities of this data source. According to Verkerk et al. (2012) waterboards can use remote sensing data in the future for determining, for example, flood prediction, flood areas inundation depths, water scarcity, dike strength and soil moisture content. These expectations provided the motivation to use remote sensing for this research.

To support their decisions, operational water managers want to use spatial data of important parameters. These data have to be presented in a clear and unambiguous way to make them useful for decision making.

1.2. Research objective

The main research objective is:

To provide fine resolution maps that represent oxygen or water stress for root take up in and the carrying capacity of the topsoil at field scale, based on satellite observed soil moisture data and soil texture information.

Delineation is made for the study area, the management area of Waterboard Groot Salland (WGS), Waterboard Regge and Dinkel (WRD) and the northern part of Waterboard Rijn and Ijssel (WRIJ), to secure focus during the project. Another important delineation is made based on land cover. Because grassland is the largest land cover in rural areas of the Netherlands and the dependency of grass yield and carrying capacity of the soil by different soil moisture contents is known from scientific research, only grassland will be considered here. Field scale in the objective means a pixel size smaller than common agricultural plots which are approximately 100 m x 100 m for the Netherlands.

1.3. Research questions and deliverables

Main research question of the master thesis project is:

How can satellite derived soil moisture data be used to generate fine resolution maps of topsoil water or oxygen stress and carrying capacity of grasslands?

Sub-questions that need to be addressed to answer the main question are:

I. How can fine spatial resolution soil moisture maps be generated from available remote sensing data sources?
II. How can the water or oxygen stress for root take up and the topsoil carrying capacity of grassland be determined when the soil moisture content is known?
III. How can a clear combined map be produced that represents both the status of oxygen or water stress and the carrying capacity?

The outcome of these questions will be fine resolution (field scale) maps displaying the status of the soil regarding oxygen or water stress for root take up and the carrying capacity presented in a clear way. The different classes will be based on relations between soil moisture, matric head, critical values of the carrying capacity and critical values for oxygen or water stress for root take up for different soil types. Also recommendations to waterboards will be made if and how they can use the produced maps in their (operational) water management, for example, in the water managers dashboards HydroNET or Lizard.

1.4. Research model, methodology and report outline

Figure 1 presents an overview of the research model. The model has three main components corresponding to the research questions: retrieving fine resolution soil moisture data, determination of the carrying capacity and oxygen or water stress for root take up based on soil moisture and construction of maps representing the physical status and associated desirability.

General information about the study area, in-situ and satellite data sets and their availability is presented in chapter 2. Downscaling of the coarse resolution soil moisture data with fine resolution data are indicated in box A. The downscaling algorithm will be explained in chapter 3. Bias-correction and validation of the downscaled product is done in sections 5.2 and 5.3 and the result

will be a volumetric soil moisture map. Box B describes the classification of the carrying capacity status (good, only machinery or bad) based on a combination of volumetric soil moisture content and soil type. In section 4.3 the key matric heads for root uptake for different soil types will be determined resulting in the output table of box C. Results of box B en C are combined together in section 4.4 (box D) making a unique Soil-Moisture-Stress indication (SMS-i) diagram for all soil types. Pixels representing other land use than agriculture are filtered out of the fine resolution soil moisture content maps of box A in box E (section 5.4). Resulting volumetric soil moisture content of each pixel in box E will be compared to its SMS-i diagram based on its soil type in box F (section 5.5). This will produce maps presenting the soil status classification for the retrieved fine resolution satellite data. The results will be discussed in chapter 6. Conclusions and recommendations for further research and the use of satellite data for operational use by waterboards can be found in chapter 7.

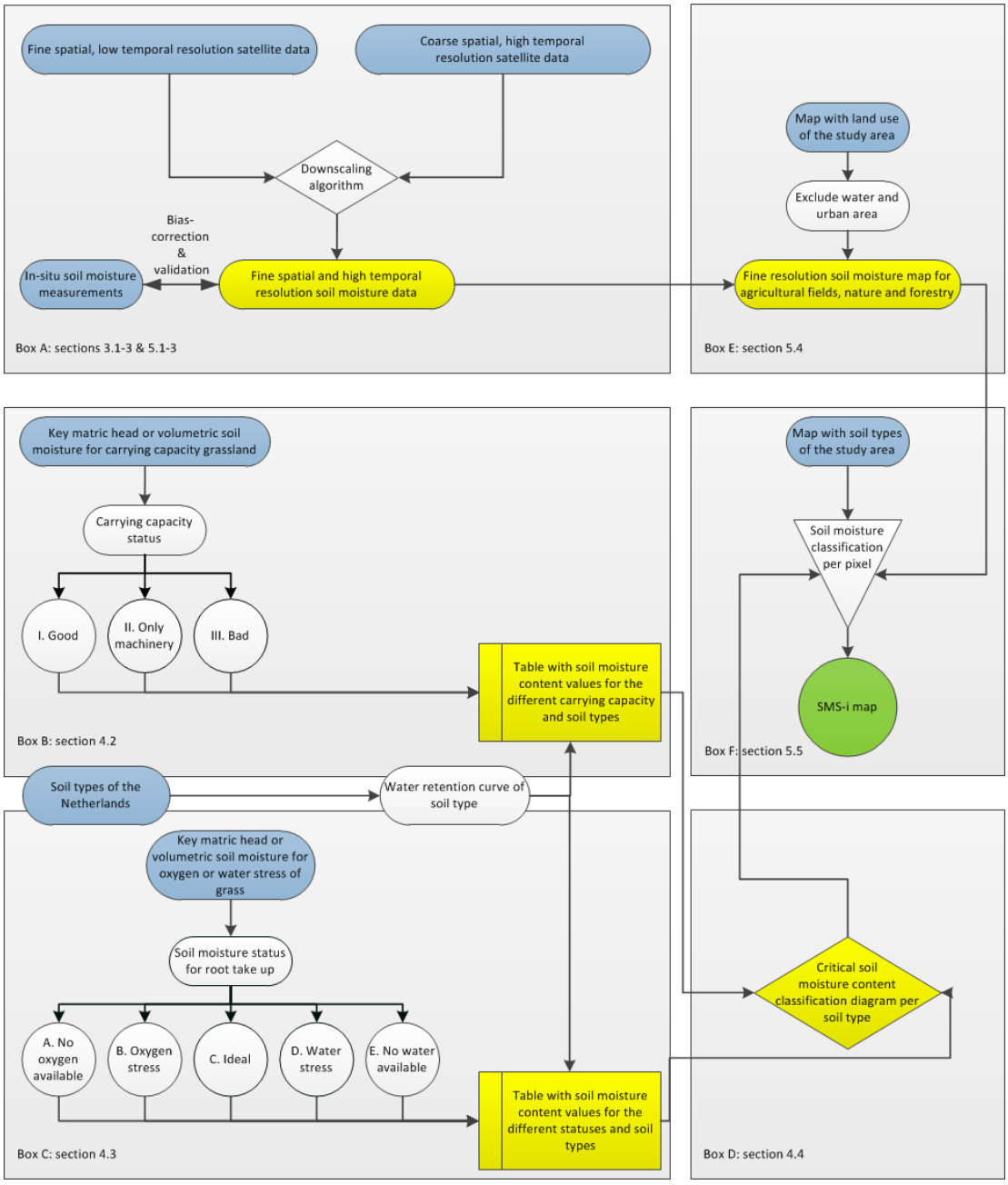

Figure 1: Research model: blue indicates input data, yellow intermediate results and green the outcome of this study.

2. Study area and data sets

This chapter describes the study area and the available data sets. The description of the study area (2.1) is followed by the in-situ measurements of soil moisture, precipitation, potential evapotranspiration and temperature (2.2). After this the coarse resolution soil moisture data (2.3) and high resolution RADARSAT-2 (2.4) data are introduced. An overview of the available data over 2012 is given in 2.5.

2.1. Description of the study area

Most of the study area is covered by the management area of Waterboard Groot Salland and Waterboard Regge en Dinkel (since 2014 merged with Waterboard Velt en Vecht to Waterboard Vechtstromen). Small parts in the south belong to Waterboard Rijn en IJssel. This area is taken because WGS is the initiator of this research and the in-situ soil moisture stations are also located in the management areas of WRD and WRIJ. The study area covers most of province Overijssel of The Netherlands (52°8-52°41'N latitude and 5°46- 7°40'E longitude, Figure 2). Circa 10 percent of the area is below mean sea level (MSL), in Dutch: Normaal Amsterdams Peil (NAP). Field level varies between -2.5 m NAP at the Koekoekspolder (Waterschap Groot Salland, 2010) in the west up to 85 m +NAP locally at the Tankenberg in the east (Figure 3).

Soil types in the study area can be divided into clay, loam, sand and peat. Figure 4 shows that sand is the most common soil type (70%) followed by peat (15%) and clay (10%). Grassland is the main land cover with a share of 60 percent, followed by maize having a share of almost 10 percent. The spatial distribution of the different land covers can be found in Figure 5.

Figure 2: Location of study area in The Netherlands, purple = Waterboard Groot Salland, dark blue = Waterboard Regge & Dinkel and light blue is Waterboard Rijn and IJssel.

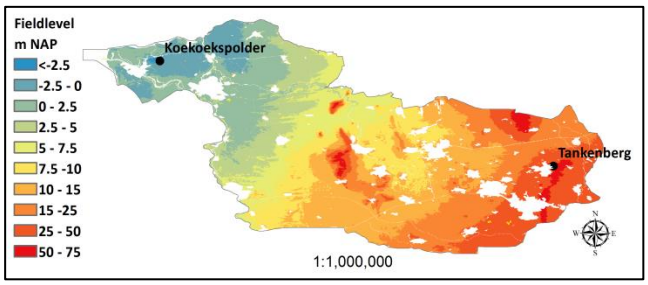

Figure 3: Field level of the study area. White indicates that the area is urbanized. Based on digital field level maps of the Actueel Hoogtebestand Nederland (AHN).

The supply route of fresh water in dry periods and the effects of desiccation are mentioned in the report “Klimaat en Droogte“ (Capel et al., 2011). During dry periods, water can be let in the study area from the rivers IJssel and Vecht, the Twentekanalen and the Zwarte Meer (see Figure 6). Some parts in the study area cannot be irrigated because their field levels are too high to pump the water effectively towards them in use for agriculture.

The study area has a maritime temperate climate (Cfb) according to Köppen Classification System. The climate is year round dominated by the polar front resulting in relatively cool summers and warm but cloudy winters (McKnight & Hess, 2000). Average air temperature during the summer is just above 20°C, long periods with frost can occur in the winter season. Rainfall is well-distributed around the year and total average precipitation for the stations Heino and Twente (see Figure 7 for their locations) is 765 mm yearly (KNMI, 2013).

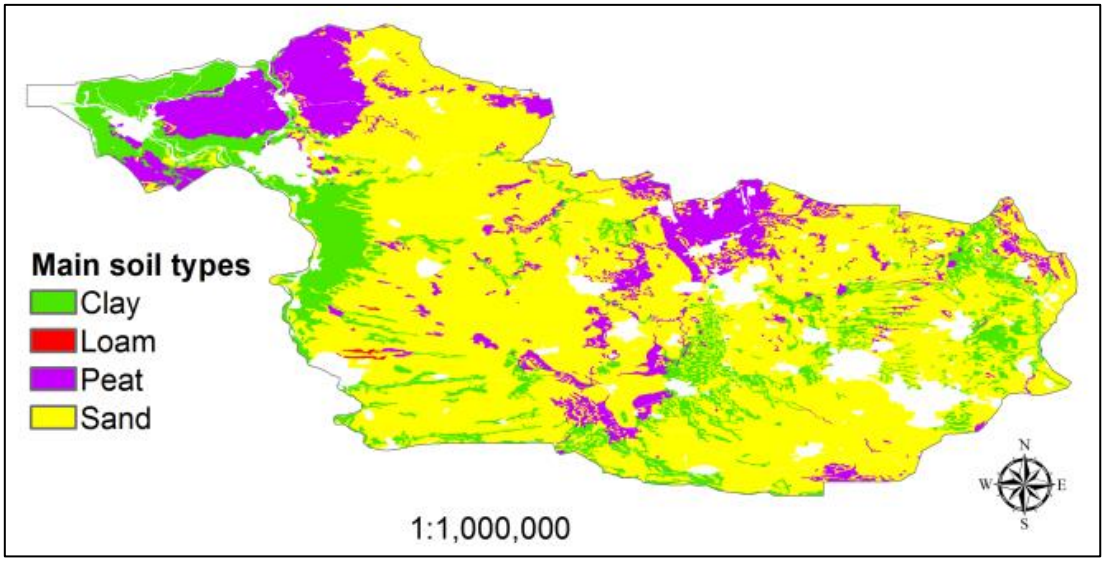

Figure 4: Main soil types of the study area, white indicates that the area is urbanized. Based on the digital PAWN soil maps.

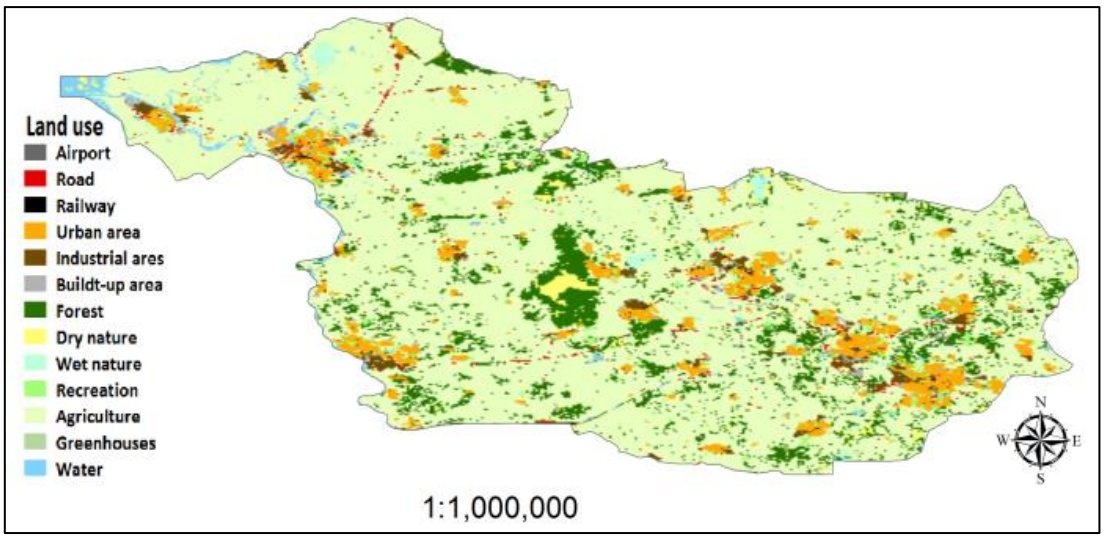

Figure 5: Land use of the study area. Adapted from the digital maps Bestand Bodemgebruik of Centraal Bureau voor de Statistiek (CBS)

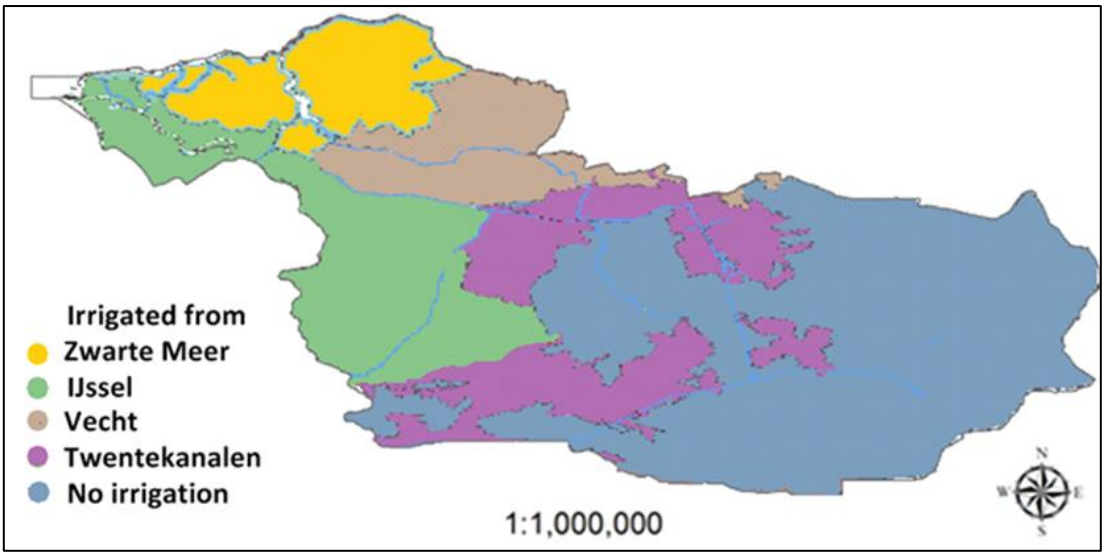

Figure 6: Irrigation sources in dry periods of the study are. Modified from Capel et l., (2011).

2.2. In-situ measurements

Twenty-one in-situ soil moisture measuring stations are located in the study area. One of WGS at Boetelerveld and 20 from the soil moisture/temperature monitoring network operated by the Faculty of Geo-Information Science and Earth Observations (ITC) of the University of Twente. Because 2012 was the first year in which the in-situ station at Boetelerveld was used by WGS, the station was not calibrated and validated yet. Therefore only the ITC soil moisture and soil temperature network (ITCSM) will be used for bias-correction and validation of the satellite data. Also some ITCSM stations will not be used, their data was not available due to instrument failures. The location of Boetelerveld, the 12 used ITCSM and two KNMI, the Royal Netherlands Meteorological Institute, stations can be found in Figure 7.

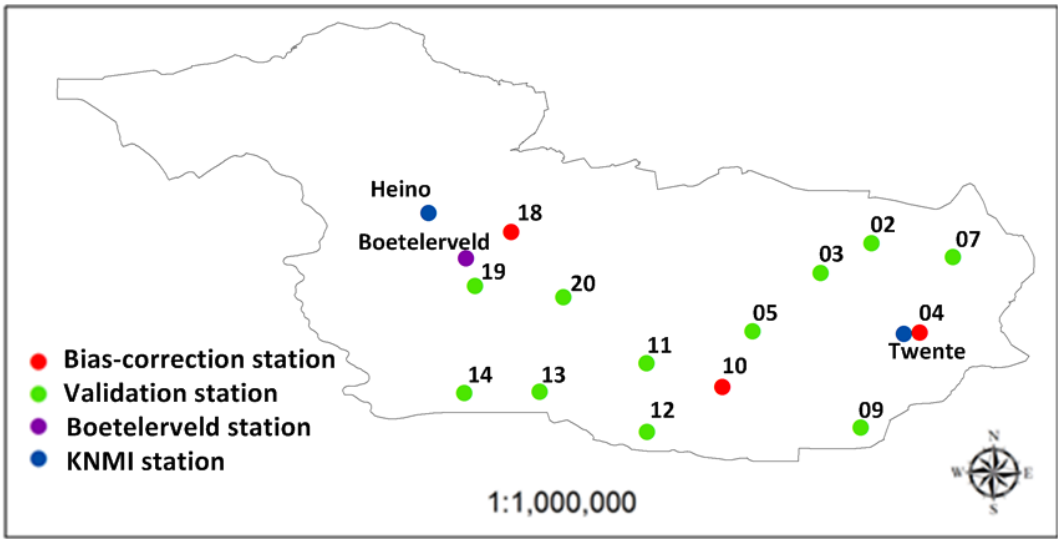

Figure 7: Locations of the measuring stations in the study area.

Twente soil moisture and soil temperature network

The soil moisture and soil temperature network of the faculty ITC of the University of Twente is described in several papers. Dente et al. (2011) describes the network and the working of its instruments. Information about the used stations can be found in Table 1. Station ITCSM 04, ITCSM 10 and ITCSM 18 will be used for the calibration because together they provided soil moisture data during the whole year of 2012, only ITCSM 18 has a small interruption of 10 days, are well distributed over the study area and have the land cover type grassland. The other stations are used for the validation, whereby the different land covers for station ITCSM 07 (corn), ITCSM 09 (corn) and ITCSM 20 (forest) have to be kept in mind. They can provide an indication of the performance of the method for other land covers than grass.

Table 1: Network station information (station name, geographical coordinates, elevation above MSL, depth of probes, land cover, soil type (Staringreeks name based on the PAWN-classification), porosity (based on PAWN-classification), the maximal volumetric soil moisture measured in 2012 and the nearest KNMI weather station

Station	Coordinates (Latitude/ Longitude)	Elevation (m NAP)	Depth (cm)	Land cover	Soil type (PAWN)	Porosity (PAWN)	Maximal volume-tric soil moisture over 2012 (m^3/m^3)	Nearest KNMI station
ITCSM 02	52°23'24"/ 6°51'26"	28	5, 10, 20	Grass	Loamy fine sand	0.40	0.35	Twente
ITCSM 03	52°21'20"/ 6°47'24"	7	5, 10	Grass	Moderate light silt	0.43	0.51	Twente
ITCSM 04	52°16'18"/ 6°55'16"	44	5, 10, 20	Grass	Mild-loamy fine sand	0.42	0.61	Twente
ITCSM 05	52°16'24"/ 6°41'58"	17	5, 10, 20, 40	Grass	Mild loamy fine sand	0.42	0.34	Twente
ITCSM 07	52°22'18"/ 6°57'55"	17	5, 10	Corn	Moderate light silt	0.43	0.35	Twente
ITCSM 09	52°08'47"/ 6°50'35"	29	5, 10	Corn	Mild-loamy fine sand	0.42	0.32	Twente
ITCSM 10	52°12'00"/ 6°39'34"	11	5, 10, 20	Grass	Mild-loamy fine sand	0.42	0.56	Twente
ITCSM 11	52°13'52"/ 6°33'32"	7	5, 10	Grass	Mild loamy fine sand	0.42	0.40	Twente
ITCSM 12	52°08'25"/ 6°33'35"	8	5, 10, 20	Grass	Moderate light silt	0.43	0.51	Twente
ITCSM 13	52°11'38"/ 6°25'30"	8	5, 10	Grass	Mild-loamy fine sand	0.42	0.35	Heino
ITCSM 18	52°24'19"/ 6°22'48"	-3	5, 10, 20	Grass	Mild-loamy fine sand	0.42	0.58	Heino
ITCSM 19	52°19'54"/ 6°19'54"	3	5, 10, 20, 40	Grass	Mild-loamy fine sand	0.42	0.32	Heino
ITCSM 20	52°19'80"/ 6°26'55"	17	5, 10, 20	Forest	Loamless fine sand	0.43	0.51	Heino

To obtain the bulk density and particle size distribution of the soils, samples were taken during installation of the measuring equipment. Samples for particle size distribution were collected between 5 cm and 20 cm depth, bulk density samples at 5 cm depth. Measurements of the porosity are not available. Approximation of the porosity can be done using the bulk density, but this is unavailable for the whole study area thus another source is used. The PAWN-classification (Policy Analysis for Watermanagement in the Netherlands (Wösten et al., 1988) and "De Staringreeks" (Wösten et al., 2001) are used to determine the porosity for the stations, which can be found in Table 1. The maximal volumetric soil moisture measured at the in-situ locations over 2012 exceeds this porosity in six of the thirteen times. Because the maximum volumetric soil moisture should always be equal or lower than the porosity, the decision is made to use the maximum value of the porosity or maximum volumetric soil moisture as porosity of the soil at the ITCSM locations. Soil analysis showed that all soil samples have a very low clay content, this coincides with the low clay contents in the PAWN-classifications at the locations of the stations.

In situ soil moisture is measured by two to four EC-TM ECH_2O probes (by Decagon), consisting of three flat 5.2 cm pins. Installation depth of the pins varies per station and is given in Table 1. The pins measure the dielectric permittivity of the surrounding soil and convert it to volumetric soil moisture content (θ) according to a standard calibration equation. Soil temperature is measured by the probe using a thermistor. Data are stored every 15 minutes by a Em50 ECH_2O datalogger (by Decagon), which is uploaded twice a year. The standard calibration equation has a 3% accuracy for all fine textured mineral soils. Soil specific calibration can increase the accuracy to 1-2%. The probe calibration was done at the ITC laboratory following the instructions of Decagon. Having similar soil texture and organic matter content makes it possible to use one general calibration equation for all the ITCSM stations:

$$\theta_{ECH2O,cal} = 0.7751 * \theta_{ECH2O} + 0.0706 \quad \text{(I)}$$

With:

$\theta_{ECH2O,cal}$ = calibrated volumetric soil moisture measured by the EC-TM ECH_2O probes (m^3/m^3)

θ_{ECH2O} = volumetric soil moisture measured by the EC-TM ECH_2O probes (m^3/m^3)

Calibration over ten ITCSM stations, representing all soil types in the area, results in a decrease of the root-mean-square-error (RMSE) of 0.054 m^3/m^3 to 0.023 m^3/m^3 for direct θ from the ECH_2O measuring devices (Dente et al., 2011). The quality of the data are checked by comparing the data of one station with data from the other stations and with precipitation data of the KNMI. The data show the expected: after precipitation the θ is higher (Figure 8). It also shows low θ_{ECH2O} during soil temperatures below 0°, because when the water contents freezes permittivity will decline and thus observed θ_{ECH2O} will be lower.

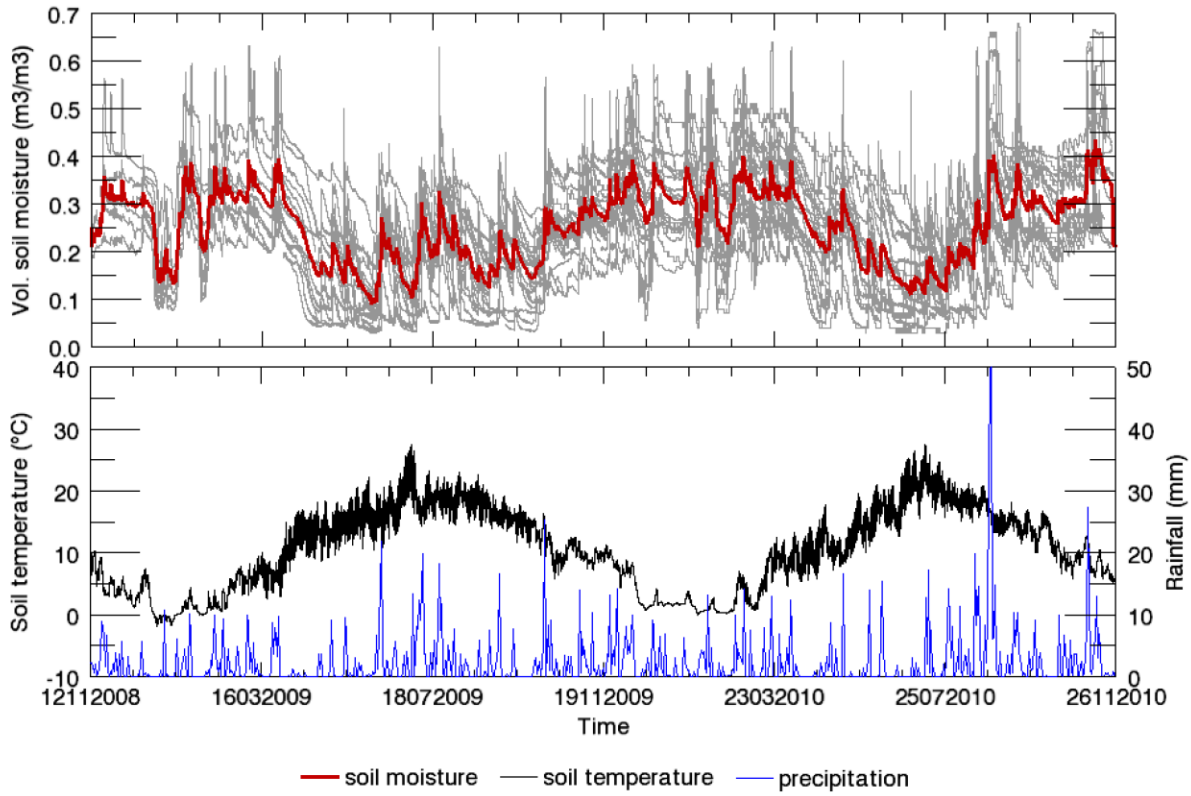

Figure 8: Mean volumetric soil moisture and mean soil temperature obtained for quality control of the ITCSM network by computing a spatial average of the data collected at all 20 sites of the Twente Soil Moisture and Soil Temperature network, at 5 cm depth, compared with the average daily precipitation recorded in the area. (Dente et al., 2011)

Weather data

The weather data are provided by the main KNMI-stations in the study area: Heino (52°26'; 06°16') and Twente (52°16'; 06°54'). Daily precipitation (Figure 10a), reference evapotranspiration based on Makkink (Figure 10b) and the temperature (Figure 10c) can be used to give an explanation for the difference between in-situ and satellite measured soil moisture. Differences between both stations can be found in precipitation especially during the summer, as a result of more intense and spatially distributed rainfall events, and in temperature where the influence of warm water during autumn and cold water during spring from the IJsselmeer at Heino is stronger than at Twente.

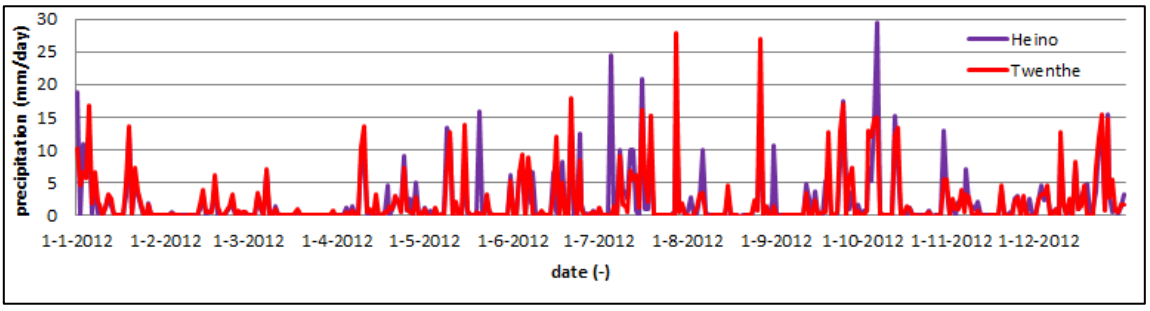

(a)

Figure 9: KNMI stations Heino and Twente: (a) precipitation, (b) reference evapotranspiration (Makkink) and (c) daily average air temperature.

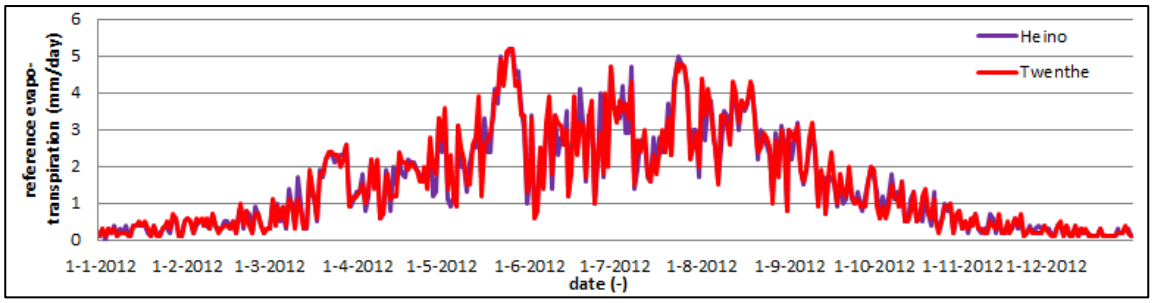

(b)

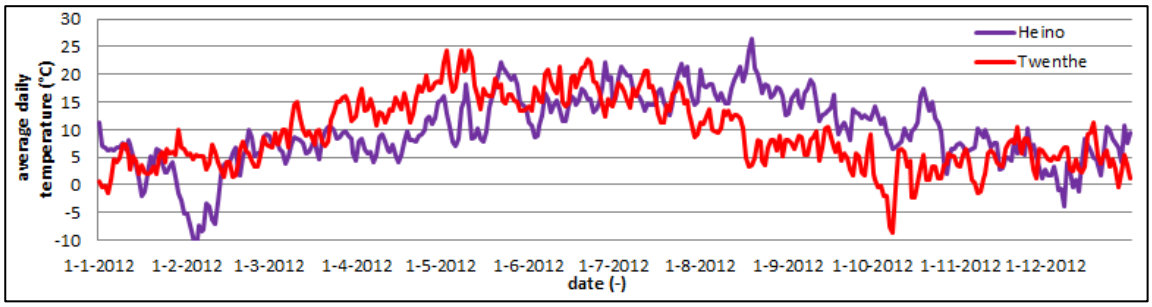

(c)

Figure 10: KNMI stations Heino and Twente: (a) precipitation, (b) reference evapotranspiration (Makkink) and (c) daily average air temperature.

2.3. Coarse resolution soil moisture data

Coarse resolution satellite based soil moisture data will be used as input in the downscaling method. These data contain the average soil moisture status of a coarse pixel. Two ways to obtain coarse resolution soil moisture data are compared i) a land surface model that uses satellite data to model soil moisture (GLDAS Noah) and ii) only satellite data (ASCAT).

GLDAS-Noah

The Global Land Data Assimilation System (GLDAS) is developed by the National Aeronautics and Space Administration Goddard Space Flight Center (NASA GSFC) and is capable of running various land surface models. The Noah model, maintained by the National Oceanic and Atmospheric Administration National Centers for Environmental Prediction (NOAA NCEP), is one of the models and produces near-real time, global estimations of terrestrial water end energy storages at coarse spatial resolution. The GLDAS-product uses both satellite- and ground-based data and is used as input for predicting climate change, weather, biological, agricultural productivity, flooding and other biogeosciences studies (Rodell et al., 2004).

In 2000, a land surface model developed in the 1990s by NCEP under the name Oregon State University / NCEP Eta Land-Surface Model (OSU LSM) was renamed to Noah (Mitchell, 2005). Characteristic for the OSU model is the Penman potential evapotranspiration of Mahrt and Ek (1987), the multilayer soil model of Mahrt and Pan (1984) and the primitive canopy model of Pan and Mahrt (1987). Chen et al. (1996) concluded that the OSU-model simulates seasonal and diurnal variations in evapotranspiration, soil moisture and surface skin temperature well compared to area-averaged observations over the 15 km x 15 km First International Satellite Land Surface Climatology Project (ISLSCP) Field Experiment (FIFE) area. Until 2002, important updates of the OSU-model are the implementation of a four layer model instead of a two layer model and the self-cycling of soil

moisture and temperature (Ek et al., 2003).

The used GLDAS-Noah product has a spatial resolution of 0.25° longitude and 0.25° latitude, approximately equal to 28 km x 28 km, making the study area covered by 14 grids (Figure 11). GLDAS-Noah is modeled with a 30 minutes temporal resolution. The used soil moisture data-set is obtained by filtering the 06:00 AM data, similar to the observation time of the used RADARSAT-2 product (see section 2.4), out of the modeled three hours output data downloaded from NASA's Goddard Earth Sciences Data and Information Services Center (GES DISC) website (http://disc.sci.gsfc.nasa.gov/). Four different layers of soil moisture are given by the model with following depths: 0-0.1, 0.1-0.4, 0.4-1.0 and 1.0-2.0 m. This study considers the top layer, so the shallow 0-0.1 m soil moisture data will be used. GLDAS expresses the soil moisture in kg/m^2 for the 0.1 m meter thick layer.

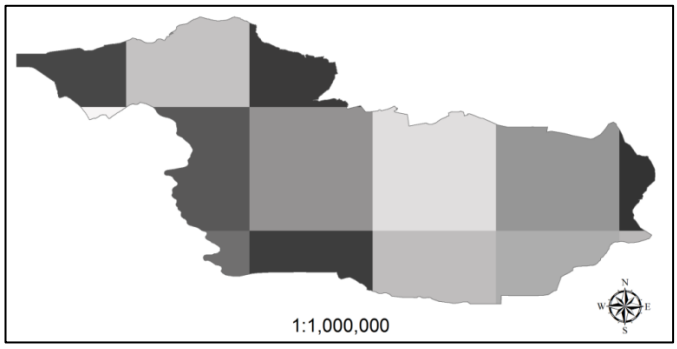

Figure 11: Spatial coverage of GLDAS-Noah grids over the study area (grid size approximately 28 km x 28 km).

ASCAT

Delivered by the European Organization for the Exploitation of Meteorological Satellites (EUMETSAT), the Advanced Scatterometer (ASCAT) is a C-band 5.255 GHz (5.67 cm) VV-polarized (vertical transmission and reception of the electromagnetic wave) real aperture radar onboard the MetOp satellite. The C-band electromagnetic waves are cloud, rain, dust and haze penetrating and can be used for day and night-time observations. ASCAT soil moisture products are produced using the change detection algorithm of the Institute of Photogrammetry and Remote Sensing from the Vienna University of Technology (IPF-TU Wien) under the name $WARP^{NRT}$ (Water Retrieval Package for Near-Real Time). There are two products: Level 2 product ASCAT Surface Soil Moisture (*SSM*) representing the soil moisture content within a thin soil surface layer (5 cm) during the time of overflight of the satellite and Level 3 product ASCAT Soil Water Index (*SWI*) representing the water content in the soil profile by filtering the surface soil moisture time series with an exponential function, regularly sampled in space and time (IPF TU Wien, 2012). The data sets used in this study are made available from the File Transfer Protocol (FTP) server of the TU Wien and has a spatial resolution of 25 km (12.5 km grid spacing). The grid distribution over the study area is shown in Figure 12. Except for December, the ASCAT data were available daily for the whole of 2012.

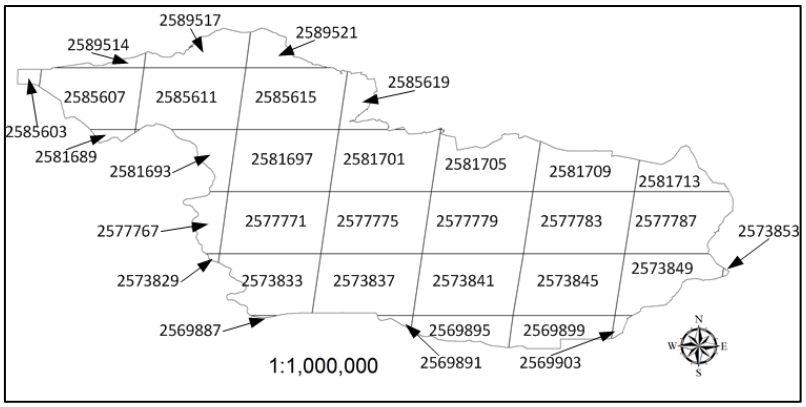

Figure 12: Spatial coverage of ASCAT grids over the study area and their WARP-id (grid size 12.5 km x 12.5 km).

The change detection method of IPF/TU Wien uses the radar backscattering coefficients to determine the *SSM*. The angle of the radar backscatter is first normalized to a reference incidence angle of 40°. Resulting backscattering coefficients are scaled in a range between 0% and 100%. 0% means that the radar backscattering has its lowest measured value corresponding to a dry soil resulting in a *SSM* of 0%. A *SSM* of 100% is obtained when the maximum backscatter, corresponding to a wet soil, is measured. *SSM* represents the soil moisture content in the top 5 cm soil layer (Bartalis et al., 2008). Disadvantage of the IPF/TU Wien change detection method is its assembled backscatter from soil moisture, vegetation phenology and static components such as surface roughness, soil composition and land cover (Figure 13) (Chung et al., 2013). This means that backscatter not only reflects soil moisture but also noise from other components that influence the backscatter. Figure 12 shows that soil moisture provides the greatest influence in the changing measured backscatter, making the disadvantage of IPF/TU Wien method acceptable.

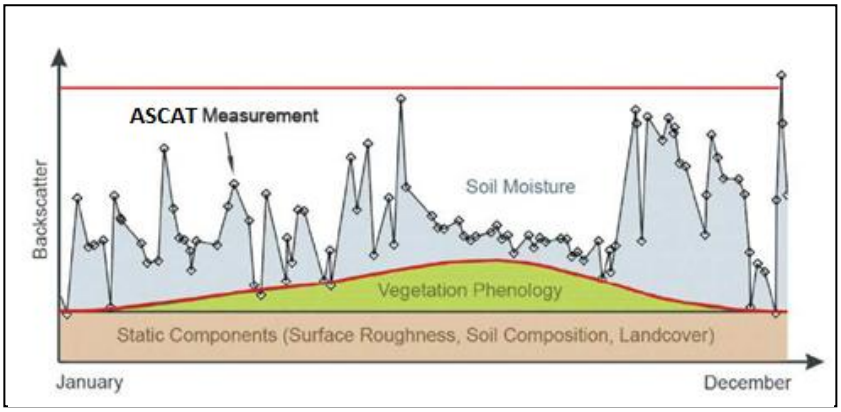

Figure 13: TU-Wien change detection algorithm for soil moisture retrieval using radar backscatter signal according to Wagner. The figure shows the different sources of the assembled ASCAT backscatter. (Pradhan et al., 2011)

Because *SSM* reacts strong on precipitation and evapotranspiration, it can change significant in a few hours. Therefore the *SWI* is derived from *SSM* for agro-meteorological applications considering a thicker layer depth than the topsoil. The *SWI* is a dimensionless index presenting the relative percentage of soil moisture (saturation). A *SWI* of 0 means that the volumetric soil moisture is minimal and a *SWI* of 100 means maximal volumetric soil moisture assumed equivalent to porosity. A simplified two-layer model is introduced by Wagner et al. (1999) in which the upper layer strongly reacts on precipitation and evapotranspiration and the lower layer is a reservoir of which the

moisture content changes slower. The water content in the soil profile is estimated by convoluting the surface soil moisture (*SSM*) time series with an exponential filter of the form exp(-*t*/*T*). *T* is the characteristic time length in days and increases with the depth of the reservoir. For a 10 cm layer depth *T*=19.5 days gives the best results (Brocca et al., 2010). Because this research looks to the upper soil layer, *T* has to be smaller than 19.5 days. For this study we evaluate the products obtained with *T*=1, *T*=5, *T*=10 and *T*=15 days. The soil water index is defined by the following equation:

$$SWI(t) = \frac{\sum_i SSM(t_i) e^{-(t-t_i)/T}}{\sum_i e^{-(t-t_i)/T}}, for\ t_i \leq t. \quad \text{(II)}$$

With:

SWI = Soil Water Index (%)
SSM = Surface Soil Moisture (%)
t_i = initial time (days)

t = time (days)
T = characteristic time length (days)

ASCAT compared to GLDAS-Noah as coarse resolution soil moisture input data

The coarse resolution ASCAT soil moisture data (*SSM* and *SWI*) and the GLDAS-Noah estimated soil moisture at 0-10 cm depth will be compared to in-situ measurements. For this comparison it has to be realized that coarse resolution data, 12,5 km x 12.5 km for ASCAT and 28 km x 28 km for GLDAS-Noah, are compared to in-situ measurements at point locations. The comparison will be based on the mean absolute error (*MAE*) and the coefficient of determination (R^2) between both coarse resolution products and the in-situ measurements at location ITCSM 04, ITCSM 10 and ITCSM 18 (the locations that will also be used for bias-correction). The *MAE* is used to measure accuracy and the R^2 will be used to assess the predictive power of the satellite data. Equations of both statistic tools and the meaning of their results can be found in section 3.3.

Before the comparison is made, the ASCAT *SSM* and ASCAT *SWI* data are converted to volumetric soil moisture. Multiplying the ASCAT *SSM* and *SWI* values with the porosity (*n*) and multiplying it by 0.01 results in the volumetric soil moisture in m^3/m^3. For example for the ASCAT *SSM*:

$$\theta_{SSM} = 0.01 \times n \times SSM \quad \text{(III)}$$

With:

θ_{SSM} = volumetric soil moisture derived from the Surface Soil Moisture (m^3/m^3)
n = porosity of the soil (m^3/m^3)
SSM = Surface Soil Moisture (%)

For porosity (*n*) the porosity according to the PAWN-classification is taken, only for the grids in which the measurement points are located the maximum value is taken of the PAWN porosity and the maximal volumetric content measured (see Table 1).

Results of the statistical comparison between the coarse resolution soil moisture products and the in-situ measurements can be found in Table 2A and 2B for the MAE and the R^2, respectively.

Table 2A shows that the MAE of the θ_{SWI} products are almost identical for the different characteristic time lengths and are in almost all cases better than the MAE of $\theta_{GLDAS\text{-}Noah}$. Different MAE for the locations is a result of location specific bias. The MAE of θ_{SSM} gives for both depths at ITCSM 10 the best results but the results at the two other locations are significantly worse than the MAE of $\theta_{GLDAS\text{-}Noah}$ or the θ_{SWI}. The R^2 values of $\theta_{GLDAS\text{-}Noah}$ are in the same range of θ_{SSM}, close to zero. This means that the relation between $\theta_{GLDAS\text{-}Noah}$ or θ_{SSM} and $\theta_{in\text{-}situ}$ is weak. Results for R^2 of the θ_{SWI} are much better varying between 0.17 and 0.58. Best overall results of R^2 for both measuring depths are obtained with $\theta_{SWI\ 1}$.

Table 2A: Mean absolute error (MAE) in m^3/m^3 of satellite based soil moisture compared to in-situ measurements in m^3/m^3 over the period January-November 2012 .

In-situ location	In-situ depth (cm)	$\theta_{GLDAS\text{-}Noah}$ (0-10 cm)	θ_{SSM}	$\theta_{SWI\ 1}$	$\theta_{SWI\ 5}$	$\theta_{SWI\ 10}$	$\theta_{SWI\ 15}$
ITCSM 04	5	0.11	0.17	0.10	0.09	0.09	0.08
ITCSM 04	10	0.12	0.18	0.11	0.10	0.09	0.09
ITCSM 10	5	0.17	0.14	0.17	0.17	0.17	0.17
ITCSM 10	10	0.17	0.15	0.17	0.18	0.18	0.18
ITCSM 18	5	0.11	0.17	0.11	0.10	0.10	0.10
ITCSM 18	10	0.11	0.17	0.10	0.10	0.09	0.09

Table 2B: Coefficient of determination (R^2) of satellite based soil moisture compared to in-situ measurements over the period January-November 2012.

In-situ location	In-situ depth (cm)	$\theta_{GLDAS\text{-}Noah}$ (0-10 cm)	θ_{SSM}	$\theta_{SWI\ 1}$	$\theta_{SWI\ 5}$	$\theta_{SWI\ 10}$	$\theta_{SWI\ 15}$
ITCSM 04	5	0.08	0.05	0.38	0.50	0.54	0.56
ITCSM 04	10	0.07	0.05	0.37	0.51	0.56	0.58
ITCSM 10	5	0.01	0.04	0.23	0.20	0.18	0.17
ITCSM 10	10	0.00	0.04	0.25	0.20	0.18	0.17
ITCSM 18	5	0.02	0.00	0.31	0.28	0.25	0.22
ITCSM 18	10	0.02	0.01	0.30	0.30	0.28	0.27

Figure 14 shows the volumetric soil moisture content in m^3/m^3 of the different products for 2012. Soil temperatures below zero, like in February 2012, become visible as drops in the volumetric soil moisture observed in the in-situ and ASCAT measurement and as a peak in the GLDAS-Noah data. The volumetric soil moisture drop can be explained by frozen water particles resulting in lower permittivity measured by the in-situ stations (Dente, Vekerdy, Su, & Ucer, 2011) and a decreasing soil dielectric constant due to inability of the soil water molecules to align themselves to the external electromagnetic field (Wagner et al., 2013). The peak in the GLDAS-Noah data shows that this model reacts in an opposite way to frost. The figures also show that $\theta_{GLDAS\text{-}Noah}$ does not vary much during the year, it varies between 0.15 m^3/m^3 and 0.37 m^3/m^3, compared to the in-situ and ASCAT products. More variation is present in the θ_{SSM} product, which can be related to the thin surface layer that is measured. This makes the ASCAT SSM product usable to generate actual surface soil moisture but less useful when the soil moisture below the surface layer is needed. The variance of the θ_{SWI} is between the θ_{SSM} and $\theta_{GLDAS\text{-}Noah}$. Because of this, the fact that the trend in the $\theta_{SWI's}$ and the in-situ measurements are quite similar to each other and the results in Table 2A and B, the decision is made to use ASCAT SWI 1 data as coarse soil moisture input data.

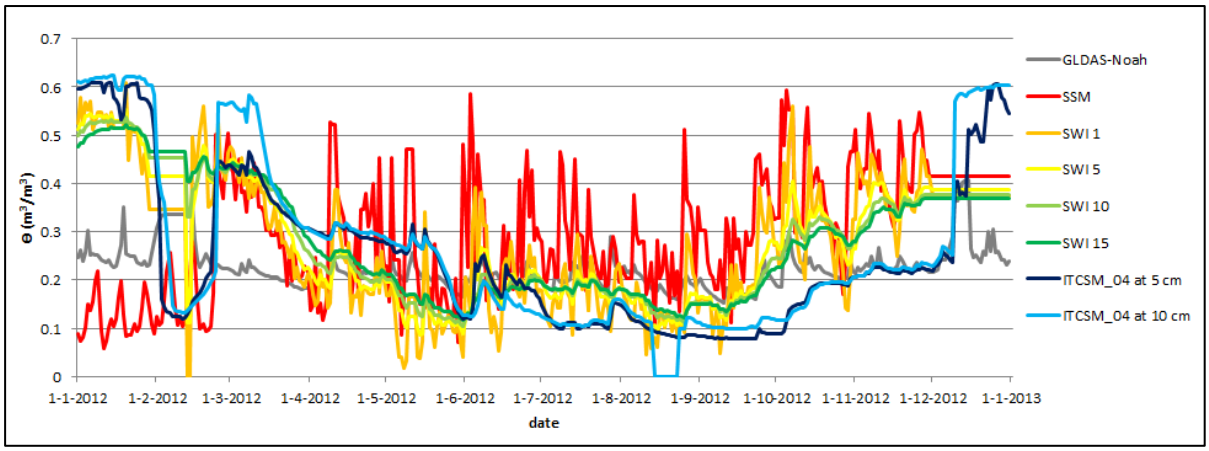

(a)

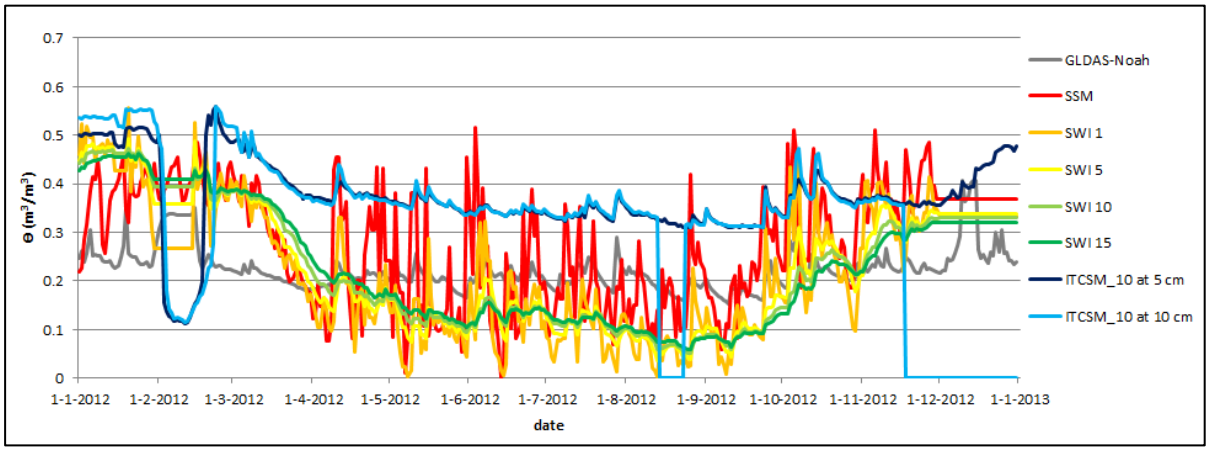

(b)

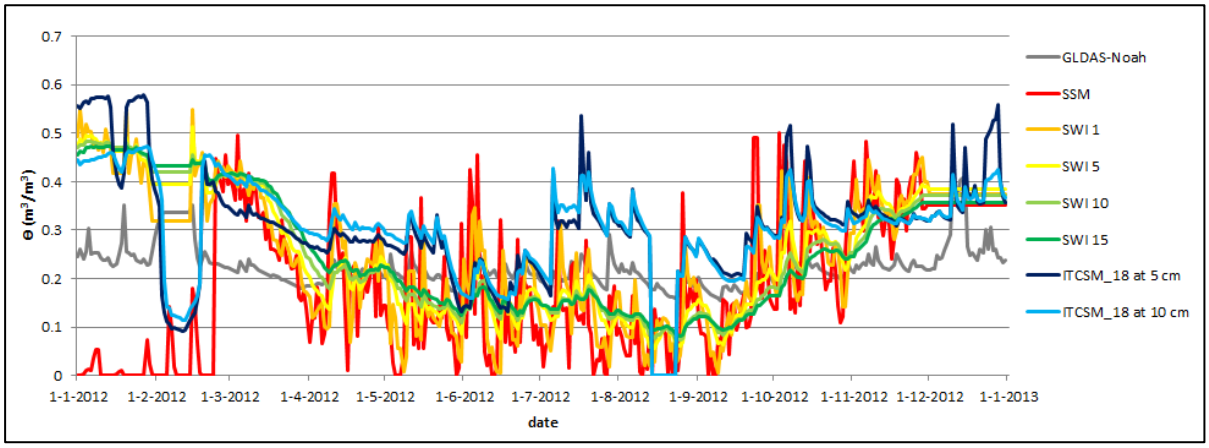

(c)

Figure 14: GLDAS-Noah and ASCAT SSM/SWI's compared to in-situ measurements at the locations (a) ITCSM 04, (b) ITCSM 10 and (c) ITCSM 18.

2.4. Fine resolution satellite data

Synthetic Aperture Radar

Synthetic Aperture Radar (SAR) makes use of aperture synthesis to obtain high resolution remote sensing data and can be used for soil moisture retrieval. Aperture synthesis means that only a small antenna is installed on the satellite and software is used to simulate a larger antenna using time-multiplex measurements. This software is based on the Doppler effect, invented by Carl Wiley in the 1950s, and the spatial resolution is determined by the Doppler bandwidth of the received signal instead of the azimuthal width of radars antenna beam pattern (McCandless & Jackson, 2005). Change in backscatter can be a result of a change in soil moisture, surface roughness or electrical properties (RADARSAT International, 1995). SAR products of the RADARSAT-2 satellite will be used in this research because its products over the year 2012 are made available by the Netherlands Space Office (NSO).

RADARSAT-2

The RADARSAT-2 data are operating in the C-band microwave with a frequency of 5.3 GHz. The eastern part of The Netherlands is only covered by the descending RADARSAT-2 satellite passes from north to south, and has a HH- and HV-polarization. Having a HH-polarization means horizontal transmission and reception of the electromagnetic wave, HV-polarization has horizontal transmission and vertical reception. Standard beam mode width, S3 (30-37 degrees), is used with a swath width of 100 km and a spatial resolution of 25 m (Figure 15). It takes 24 days before the RADARSAT-2 satellite returns at the same location and gives an image of the same area. Fly over dates in 2012, used in this research can be found in Table 3 and take all place around 06:00 AM. Recurrence time can be reduced to 6 days when images from different modes are combined. Another advantage of the descending mode in this study is its year round availability, the ascending mode is made available between May and October by the NSO.

Table 3: The 13 used Radarsat2 fly-over dates in 2012.

RADARSAT-2 fly-over dates in 2012
12-3-2012
5-4-2012
29-4-2012
23-5-2012
16-6-2012
10-7-2012
3-8-2012
27-8-2012
20-9-2012
14-10-2012
7-11-2012
1-12-2012
25-12-2012

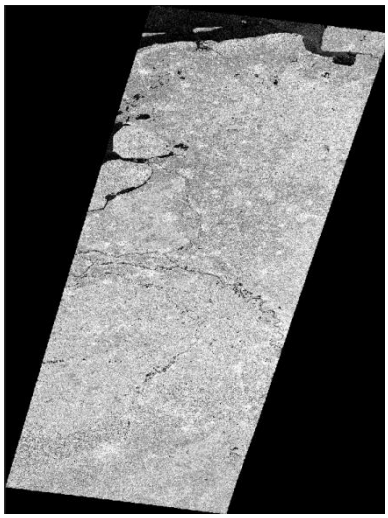

Figure 15: RADARSAT-2 backscattering, HH-polarization and 100 km beam width, image of the eastern part of The Netherlands on 16-6-2012.

Backscatter (σ) data are given in decibels (dB; $10log\frac{I}{10^{-12}}$, where I is the intensity in W/m^2). Because the I values are low (< 10^{-12}) the backscatter values are negative, commonly between -5 for high θ values (wet) and -16 for low θ values (dry). Only the HH-polarization images will be used because they are more sensitive to the soil moisture content than the HV-polarization (Gyo et al., 2013). Sanli et al. (2008) conclude that there is an 81% correlation (R^2=0.81) between the soil moisture content and RADARSAT-2 C-band HH-polarized SAR backscattering. Another advantage of the HH-polarization is its potential in vegetation penetration by minimizing the impact of vertical stalks and trunks (Kornelsen & Coulibaly, 2013).

2.5. Availability of data-sets over the year 2012

The Gantt chart in Figure 16 gives an overview of the data availability for the year 2012. The blue bar represents dates when the data are available. When the bar is interrupted, it indicates that data are missing. The availability of satellite-based data (ASCAT, GLDAS and RADARSAT-2) is more secured than in-situ measurements (ITCSM and WGS-boetelerveld). Problems of some in-situ measurements are the data-logs during spring (April-May), which is the start of the growing season.

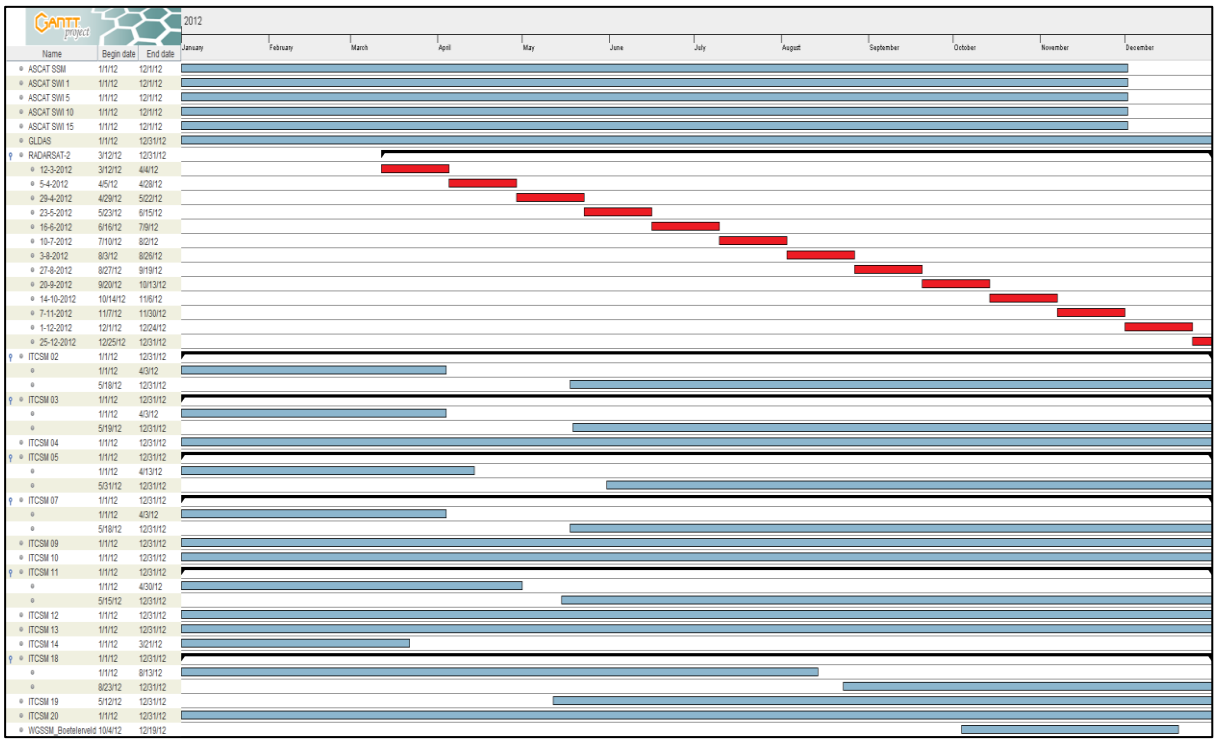

Figure 16: Gantt chart of dates with available data (RADARSAT-2 dates are indicated in red because the observation of the fly over day will be used 24 days).

3. Fine resolution soil moisture retrieval

Fine resolution soil moisture data will be retrieved using four different downscaling methods, of which three are based on Das et al. (2011). These methods will downscale coarse resolution ASCAT-data to fine resolution soil moisture data using fine resolution RADARSAT-2 data. The four methods will be introduced in section 3.1. The four combinations will be bias-corrected for the ITCSM locations 04, 10 and 18 compared to the in-situ measurements using the bias-correction method explained in section 3.2. Validation of the soil moisture results will be done by comparing the downscaled results with in-situ measurements at the other ITCSM locations in section 3.3.

3.1. Downscaling

The downscaling method used in this research is a modified version of the downscaling method described by Das et al. (2011). They have retrieved high spatial and temporal resolution soil moisture data by merging radiometer and radar data that serve as a candidate retrieval algorithm for the combined active/passive soil moisture product of NASA's Soil Moisture Active and Passive (SMAP) mission. To minimize the error that can occur during geo-referencing the different datasets to each other, not one but nine (3x3) RADARSAT-2 pixels are used as reference for one ITCSM network location (Figure 17). Grid topology of the downscaling method is illustrated in Figure 18. On the top it shows the input products ASCAT and RADARSAT-2 at coarse and fine resolution products, respectively. These products are input for the downscaling algorithm that will be explained below. Output of the downscaling algorithm is the downscaled product, having a medium-size grid of 75 m x 75 m and is shown on the bottom of Figure 18. The downscaling algorithm to compute the downscaled volumetric soil moisture product is:

$$\theta_m = \theta_{SWI\,1} \times \beta_c\left(\sigma_m^\circ - \sigma_c^\circ\right) \qquad \text{(IV)}$$

With:

θ_m = volumetric soil moisture of downscaled product at medium resolution (m^3/m^3)

$\theta_{SWI\,1}$ = volumetric soil moisture of the ASCAT SWI 1 product (m^3/m^3)

β_c = soil moisture sensitivity parameter of the course grid depending on vegetation cover and type and surface roughness (m^3/m^3 dB^{-1})

σ_m° = average of the 9 backscatter values of the 3x3 RADARSAT-2 medium grid backscatter pixel (dB)

σ_c° = average of the 27889 (~12,500/75 x 12,500/75) RADARSAT-2 backscatter values of the course grid (dB)

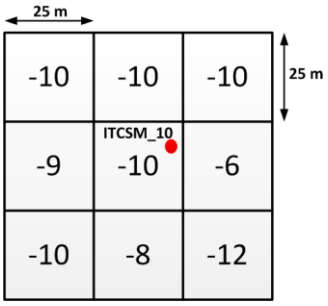

Figure 17: ITCSM 10 and the surrounding 3x3 RADARSAT-2 pixels at 12-03-2012, backscatter-value for this ITCSM-station will be the average of the 9 pixels (-9.57 dB).

The soil sensitivity parameter β_c will be determined for every coarse ASCAT-grid independently using the linear relation between $\theta_{SWI\ 1}$ and σ_c° for three time intervals: yearly ($\beta_{c,year}$), 24-days ($\beta_{c,24}$) and daily ($\beta_{c,day}$). Equation V gives the relation for the yearly product using α_c, a calibrated parameter depending on vegetation cover, vegetation type and surface roughness that is assumed to be homogeneous across the coarse grid cell.

$$\theta_{SWI\ 1} = \alpha_c + \beta_{c,year} \times \sigma_c^\circ \qquad \text{(V)}$$

By both the $\beta_{c,24}$ and $\beta_{c,day,}$ parameter α_c is set to 0 and β is calculated by dividing $\theta_{SWI\ 1}$ of the (RADARSAT-2 fly-over) day, by σ_c°. $\beta_{c,24}$ is calculated every 24 days when a new RADARSAT-2 image is available and will be used for the next 24 days from that moment on till the next RADARSAT-2 image is available. For $\beta_{c,day}$, the relation between $\theta_{SWI\ 1}$ and σ_c° is calculated per day holding σ_c° constant for 24 days with combination of the daily $\theta_{SWI\ 1}$. Spatial variation of $\beta_{c,24}$ will change daily while the spatial variation of the other beta's will change once every 24 days. In both equations for $\beta_{c,24}$ and $\beta_{c,day}$ is a multiplication by -1 added to neutralize the negative value of the backscatter.

$$\beta_{c,24} = -\frac{\theta_{SWI\ 1}}{\sigma_c^\circ}, for\ every\ RADARSAT-2\ observing\ date \qquad \text{(VI)}$$

With:

$\beta_{c,24}$ = soil moisture sensitivity parameter that is constant for the 24 days after a RADARSAT-2 observation ($m^3/m^3\ dB^{-1}$)

$\theta_{SWI\ 1}$ = ASCAT SWI 1 soil moisture content at the RADARSAT-2 observation date (m^3/m^3)

σ_c° = average RADARSAT-2 backscatter of the coarse grid at the RADARSAT-2 observation date (dB)

$$\beta_{c,day} = -\frac{\theta_{SWI\ 1}}{\sigma_c^\circ}, for\ every\ day \qquad \text{(VII)}$$

With:

$\beta_{c,day}$ = soil moisture sensitivity parameter that is determined daily ($m^3/m^3\ dB^{-1}$)

$\theta_{SWI\ 1}$ = ASCAT SWI 1 soil moisture content of the day (m^3/m^3)

σ_c° = average RADARSAT-2 backscatter of the coarse grid of the last RADARSAT-2 observation (dB)

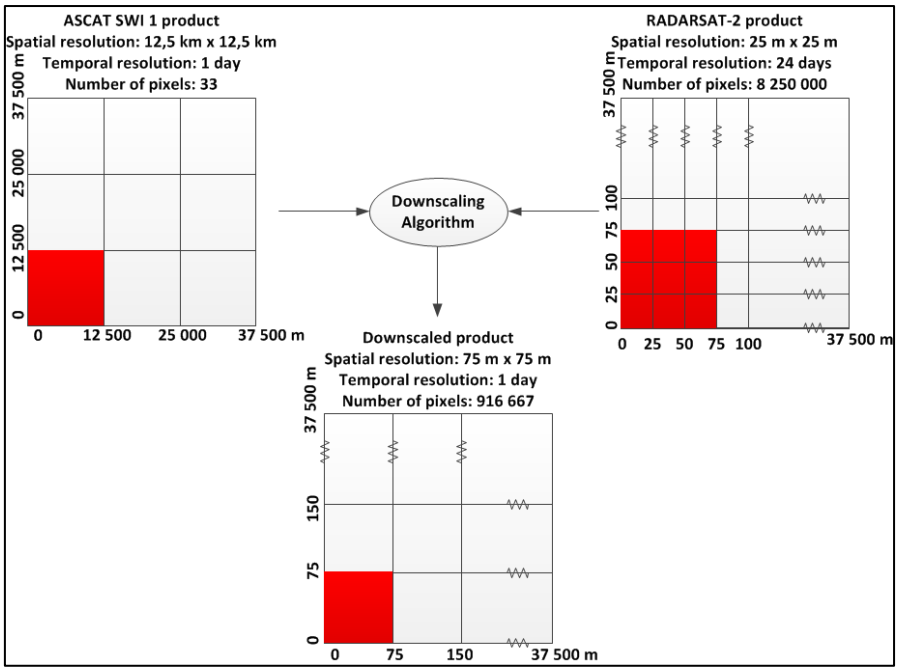

Figure 18: Grid topology of ASCAT SWI 1, RADARSAT-2 and the downscaled product.

Disadvantage of the downscaling method described by Das et al. (2011) is the possibility of over- and underestimating of the soil moisture content under extreme wet and extreme dry conditions, respectively. These under- and overestimations are negative values for the volumetric water content and values exceeding the soils porosity, both unrealistic. Solution for this problem can be found in scaling the volumetric soil moisture between dry ($\theta_{SWI\ 1}$ = 0) and wet ($\theta_{SWI\ 1}$ = n). This solution includes a linear scaling of the volumetric water content based on the difference in RASARSAT-2 backscatter in a coarse grid. For medium grid RADARSAT-2 backscatter values lower than the coarse grid average ($\sigma^\circ_m < \sigma^\circ_c$) the linear interpolation of the volumetric soil moisture is between dry and $\theta_{SWI\ 1}$, for medium grid RADARSAT-2 backscatter values greater than the coarse grid average ($\sigma^\circ_m > \sigma^\circ_c$) the linear interpolation is between $\theta_{SWI\ 1}$ and n and when the medium and coarse grid RADARSAT-2 backscatter are equal ($\sigma^\circ_m = \sigma^\circ_c$) the volumetric soil moisture is $\theta_{SWI\ 1}$. Minimal and maximal RADARSAT-2 backscatter over all periods is set to -16 dB and -5 dB is this study and $\theta_{SWI\ 1}$ has a daily temporal resolution.

$$\text{If } \sigma^\circ_m > \sigma^\circ_c: \ \theta_m = \theta_{SWI\ 1} + \frac{n_{max} - (\theta_{SWI\ 1})}{(\sigma^\circ_{max} - \sigma^\circ_c)} (\sigma^\circ_m - \sigma^\circ_c) \qquad \text{(VIII)}$$

$$\text{Else}: \theta_m = \theta_{SWI\ 1} - \frac{(\theta_{SWI\ 1})}{(\sigma^\circ_{min} - \sigma^\circ_c)} (\sigma^\circ_m - \sigma^\circ_c) \qquad \text{(IX)}$$

Using the above scaling method has two disadvantages: beta drops out and the average θ_m (=θ_c) after implementation of the simple scaling method differs from $\theta_{SWI\ 1}$. The loss of beta results in a spatial distribution depending strongly on the assumed linear relation between minimal, maximal and average RADARSAT-2 backscatter and $\theta_{SWI\ 1}$, resulting in a daily changing spatial distribution.

Four downscaling methods will be evaluate in this report: the downscaling combination of Das et al. (2011) with (I) yearly, (II) 24 days and (III) daily beta and (IV) the linear scaling method. To these methods will be referred in the following sections as method I till IV.

3.2. Bias-correction

The downscaled results of ITCSM stations 04, 10 and 18 will be bias-corrected using the average results of the bias-correction method presented by Piani et al. (2010). They use a trend (not a regression) line with in-situ measurements on the horizontal axis. Here the trend line is calculated using the LINEST function in Microsoft Excel. This is shown on the left side on the second line in Figure 19 (bias-correction 1). The trend line for this plot can be described by $\theta_m = A_1\theta_{in\ situ} + B_1$, with A_1 = 0.75 and B_1 = -0.05. The corrected θ_m (θ_{m1}) is the estimated $\theta_{in\ situ}$ based on this trend line, i.e. $\theta_{m1} = (\theta_m - B_1)/A_1$. The result is shown in Figure 17 (third line, left side). Using this bias-correction, the peaks are elevated, but MAE between the bias-corrected θ_{m1} (blue bars) and $\theta_{in\text{-}situ}$ (red line) is larger than desired. When the axes are reversed, a different trend line is obtained (right side on the second line in Figure 19). The trend line for this plot can be described by $\theta_{in\ situ} = A_2\theta_m + B_2$, with A_2 = 0.28 and B_2 = 0.24. The bias correction based on this trend line ($\theta_{m2} = A_2\theta_m + B_2$) shows a flatter line for θ for the year 2012 with a good MAE value but the peaks are smoothed out (Figure 17, third line right side). Combining both bias-correction methods, by taking the average $\theta_{m,abc}\left(=\frac{\theta_{m1}+\theta_{m2}}{2}\right)$, results in a corrected θ_m having the best properties of both: peaks are present and the MAE is relative low (see bottom Figure 19). The bias-correction is determined separately for ITCSM stations 04, 10 and 18 using the following equation:

$$\theta_{m,abc} = \frac{\theta_m\left(\frac{1}{A_1} + A_2\right) + \frac{B_1}{A_1} + B_2}{2} \qquad \text{(X)}$$

With:

$\theta_{m,abc}$ = volumetric soil moisture after bias correction (m^3/m^3)
θ_m = volumetric soil moisture before bias correction (m^3/m^3)
A_1 = slope of the trend line with $\theta_{in\text{-}situ}$ as base (-)
A_2 = slope of the trend line with θ_m as base (-)
B_1 = offset of the trend line with $\theta_{in\text{-}situ}$ as base (m^3/m^3)
B_2 = offset of the trend line with θ_m as base (m^3/m^3)

The average result of the bias-correction over station 04, 10 and 18 is set to the standard bias-correction. These average bias-correction values for A_1, A_2, B_1, and B_2 will be applied to all stations.

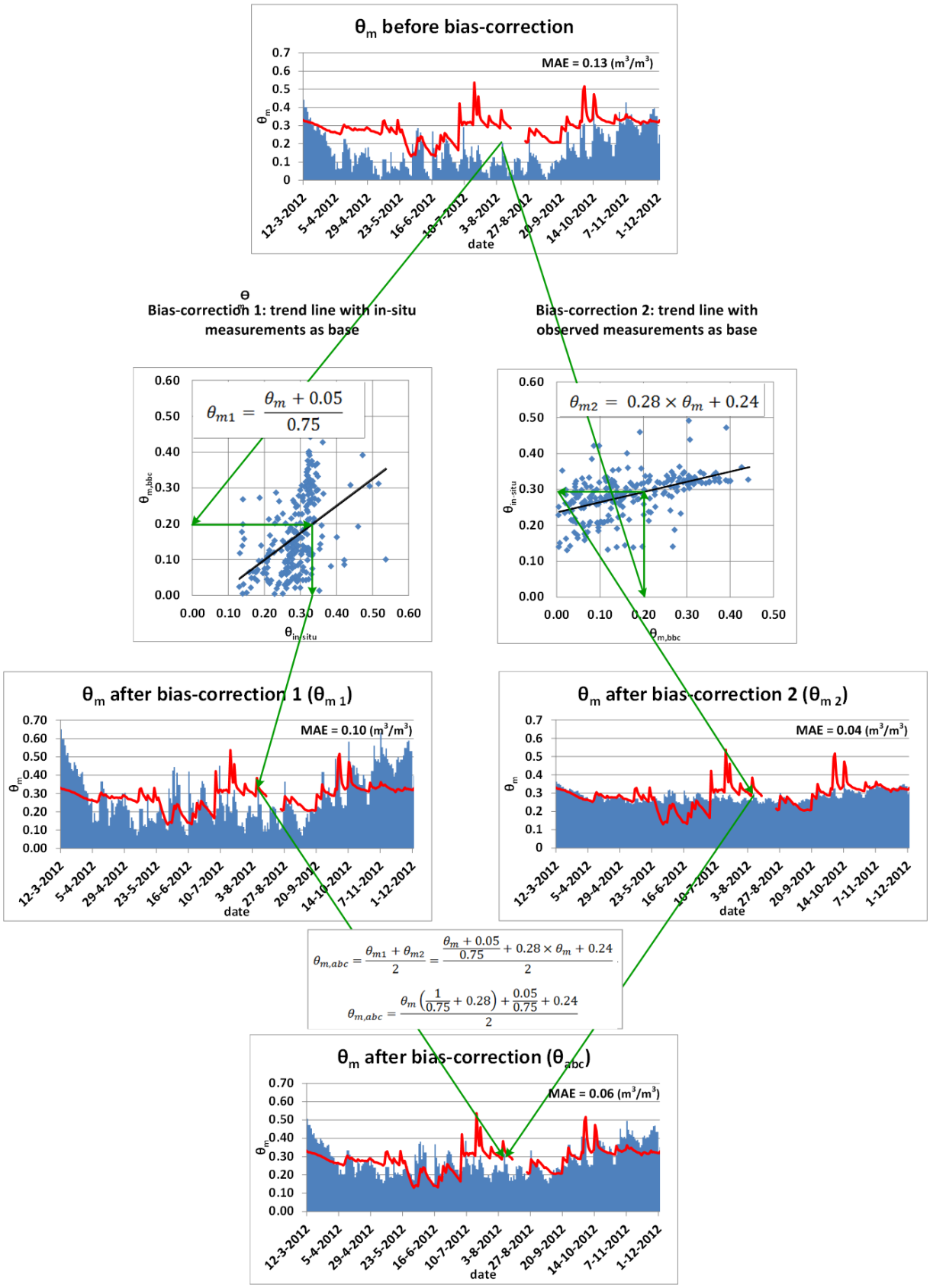

Figure 19: Bias-correction method; the left side is according to Hageman et al. (2010) and the right side uses the same principle only the x- and y-axes are changed. Blue bars representing estimated θ_m and the red line $\theta_{in\text{-}situ}$ for ITCSM 18 with n_{max}=0.58.

3.3. Validation

Validation is done by comparing $\theta_{m,abc}$ with $\theta_{in\text{-}situ}$ for the locations 02, 03, 05, 07, 09, 11-13, 19 and 20 of ITCSM-network points. Results are expressed as the coefficient of determination (R^2) and the Mean Absolute Error (MAE). The Root Mean Square Error ($RMSE$) is also explained because it is used several times in this report.

Coefficient of determination (R^2)

$$R^2 = 1 - \frac{\sum_{t=1}^{T}\left(\theta_{in-situ}^{t} - \theta_{m,abc}^{t}\right)^2}{\sum_{t=1}^{T}\left(\theta_{in-situ}^{t} - \overline{\theta_{in-situ}}\right)^2} \quad \text{(XI)}$$

The coefficient of determination denotes the linear relation between two variables. R^2 values range from 0 to 1, with 1 representing a perfect linear fit between two variables and a value of zero indicating no relation at all between both variables.

Mean Absolute Error (MAE)

$$MAE = \frac{1}{T}\sum_{t=1}^{T}\left|\theta_{in-situ}^{t} - \theta_{m,abc}^{t}\right| \quad \text{(XII)}$$

The MAE is the average of the absolute differences between the derived and measured values. Larger accuracy of the model will result in lower MAE values.

Root Mean Square Error (RMSE)

$$RMSE = \sqrt{\frac{1}{T}\sum_{t=1}^{T}\left(\theta_{in-situ}^{t} - \theta_{m,abc}^{t}\right)^2} \quad \text{(XIII)}$$

The RMSE is the square root of the average squared differences between the derived and measured values. Smaller $RMSE$ values signify larger accuracy of the model. Although $RMSE$ is one of the most widely reported error measures in climatic en environmental literature the MAE is a more natural measure for the average error and is unlike $RMSE$ unambiguous (Willmott & Matsuura, 2005).

4. Soil status classification

The status of the soil will be classified on three aspects: i) the carrying capacity of the topsoil ii) the soil water availability for root uptake and iii) oxygen availability for roots. The different aspects will be combined together resulting in one classification system. Because the status is a result of a combination between the volumetric soil moisture content and soil type, the different soil types in the study area have to be known first.

4.1. Soil classification

In the Netherlands there are different soil classification systems. In this research The Policy Analysis for Water management in the Netherlands (PAWN) (NHI, 2008) classification is used because it is most commonly used in hydrological modeling. The PAWN classification map is available at 25 m x 25 m resolution and distinguishes 23 different classes: 21 soil types, built-up area and water. Wösten et al. (2013) linked the PAWN classification to soil types of the Staringreeks (Wösten et al.,2001). By just taking the topsoil layer into account, the 23 PAWN soil classifications can be replaced with eleven soil types from the Staringreeks (Table 4). Appendix 2 gives an overview of the soil types and their Staringreeks codes and PAWN numbers.

Table 4: PAWN classification and the Staringreeks for Dutch soils. B represents upper soil layers and O represents exposed lower soil layers.

Staringreeks code	PAWN number	Classification	Porosity (m^3/m^3)
B1	8 & 14	Loamless fine to moderate fine sand	0.43
B2	5, 9, 10 & 12	Mild loamy, fine to moderate fine sand	0.42
B3	11 & 13	Loamy, fine to moderate fine sand	0.46
B8	15, 19 & 20	Moderate mild zavel	0.43
B10	16	Light clay	0.43
B11	3 & 4	Moderate heavy clay	0.59
B12	17 & 18	Heavy clay	0.54
B16	2	(sandy) Peat	0.80
B18	1 & 6	Clayey peat	0.77
O1	7	Loamless fine to moderate fine sand	0.36
O15	21	Silty loam	0.41

4.2. Carrying capacity

The topsoil carrying capacity can be expressed as the penetration resistance which depends on many variables, with soil type and soil water content as most important. The different topsoil types in the study area are classified first. After this classification the critical soil moisture content values related to the critical carrying capacity are determined because penetration resistance can vary significantly with the soil water content (Lapen et al., 2004).

The critical carrying capacity of grasslands is 0.5 mega Pascal (MPa) for machinery and 0.6 MPa for grazing cattle (Cultuurtechnische Vereniging, 1992). The carrying capacity of a soil varies with different volumetric soil water contents. Two sources are used to determine the volumetric water content belonging to the critical carrying capacity of the topsoils mentioned in Table 4. Schothorst (1982) investigated the relation between the penetration resistance and matric head of peat soils with an organic matter content of 40 to 50% (Staringreeks B16). Peerboom (1990) has

derived relations between matric head and penetration resistance for the Staringreeks B1, B3, B12 and B18. The water-retention/pF-curve is used to translate the matric head values to volumetric soil moisture content. The critical soil moisture content for the remaining soil types is determined using linear interpolation between the critical values of the matric head of the soil types surrounding in the Staringreeks. The critical matric head value is then translated to a volumetric soil moisture content using the water-retention/pF-curve. More detailed information about how the critical soil moisture content values are determined can be found in Appendix 4.

Table 5: Critical soil moisture content volume for a carrying capacity of 0.5 MPa and 0.6 MPa.

Staringreeks classification	Matric head (cm)		Soil moisture content (volumetric)		Source
	0.5 MPa	0.6 MPa	0.5 MPa	0.6 MPa	
B1	-2	-14	0.42	0.38	Peerboom (1990)
B2	-10	-24	0.39	0.36	Linear interpolation of matric head between B1 and B3
B3	-18	-33	0.43	0.41	Peerboom (1990)
B8	-47	-65	0.40	0.39	Linear interpolation of matric head between B3 and B12
B10	-58	-77	0.41	0.40	
B11	-64	-84	0.55	0.54	
B12	-70	-90	0.50	0.49	Peerboom (1990)
B16			0.68	0.65	Schothorst (1982)
B18	-56	-78	0.70	0.68	Peerboom (1990)
O1	-2	-14	0.35	0.31	Matric head assumed to be equal as B1
O15	-82	-103	0.37	0.36	Linear extrapolation of matric head between B3 and B12 (neglecting extra clay layer in the lower soils class (see Appendix 4))

4.3. Soil moisture and oxygen availability for root uptake

Soil moisture and oxygen availability for root uptake by plants is important for the growing process. When the soil conditions are too wet, the growing process will be disturbed as a consequence of oxygen stress. On the other hand when the soil conditions are too dry, soil moisture stress will disturb the growing process. For crops, in this research grass, it results in lower yield per hectare.

Key values of the matric head for root water uptake by grass are given by Van den Akker (2001) and are identical for all soil types. The key values are related to the reduction function of Feddes et al. (1978) of which a modified version is shown in Figure 20. The reduction function has two dehydration curves: one for high transpiration and one for low transpiration. Because wilting problems are more common during the growing season the decision is made to use only the dehydration curve associated with high transpiration (h_{3h}). When the matric head is higher than h_2, the soil becomes saturated and less oxygen is available for the roots. From h_1 and higher no oxygen is available in the soil for roots at all. On the dehydration side, water stress will occur from h_{3h} and lower with absolute desiccation from h_4 and lower. The critical values of the matric head for grassland are: h_1=-10 cm, h_2=-25 cm, h_{3h}=-200 cm and h_4=-8000 cm.

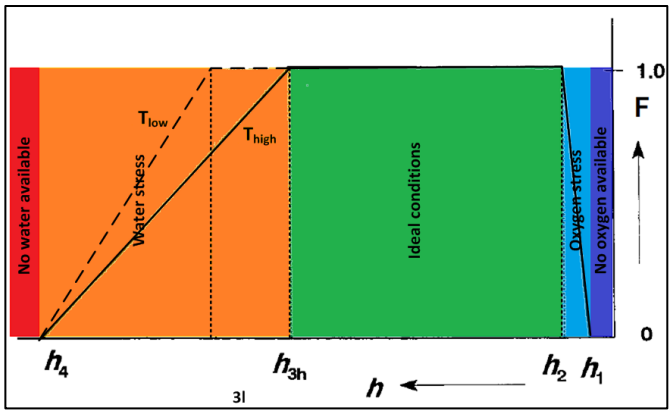

Figure 20: Modified reduction function of Feddes et al. (1978), at the dehydration side the high transpiration curve is normative. The five colors indicates the state of the soil for root take up of water.

Using the water retention/pF-curve for every soil type of the Staringreeks (Wösten et al., 2001), the volumetric soil moisture content can be derived for each critical value of the matric head (Table 6).

Table 6: Critical values for root take up of grassland.

Staringreeks classification	θ (m^3/m^3)			
	pF=1 (h_1=-10 cm)	pF=1.4 (h_2=-25 cm)	pF=2.3 (h_{3h}=-200 cm)	pF=3.9 (h_4=-8000 cm)
B1	0.39	0.35	0.21	0.06
B2	0.39	0.36	0.24	0.09
B3	0.44	0.42	0.30	0.11
B8	0.42	0.41	0.34	0.17
B10	0.43	0.42	0.37	0.22
B11	0.58	0.57	0.51	0.36
B12	0.53	0.52	0.47	0.35
B16	0.77	0.74	0.57	0.27
B18	0.75	0.73	0.62	0.39
O1	0.32	0.28	0.14	0.03
O15	0.40	0.40	0.34	0.17

4.4. Combined soil moisture or oxygen stress and carrying capacity classification

The carrying capacity status and the water and oxygen availability for root uptake are determined using the volumetric soil moisture content. The critical soil moisture content values for both the carrying capacity and water and oxygen availability for root uptake are soil dependent. The range of critical soil moisture values of all soils together are presented in Figure 21. A longer bar means more dispersion of the critical value between the different soil types. Because all soils are presented in this diagram, a high degree of overlap exists. This makes it impossible to use soil type independent standard values for the critical values. For example a volumetric soil moisture content of 0.40 means for soil type B4 that there is no oxygen in the soil available while in soil type B18 there is water stress

for root take up. To tackle this problem, a Soil Moisture Stress indication diagram (SMS-i diagram) is made for each soil type.

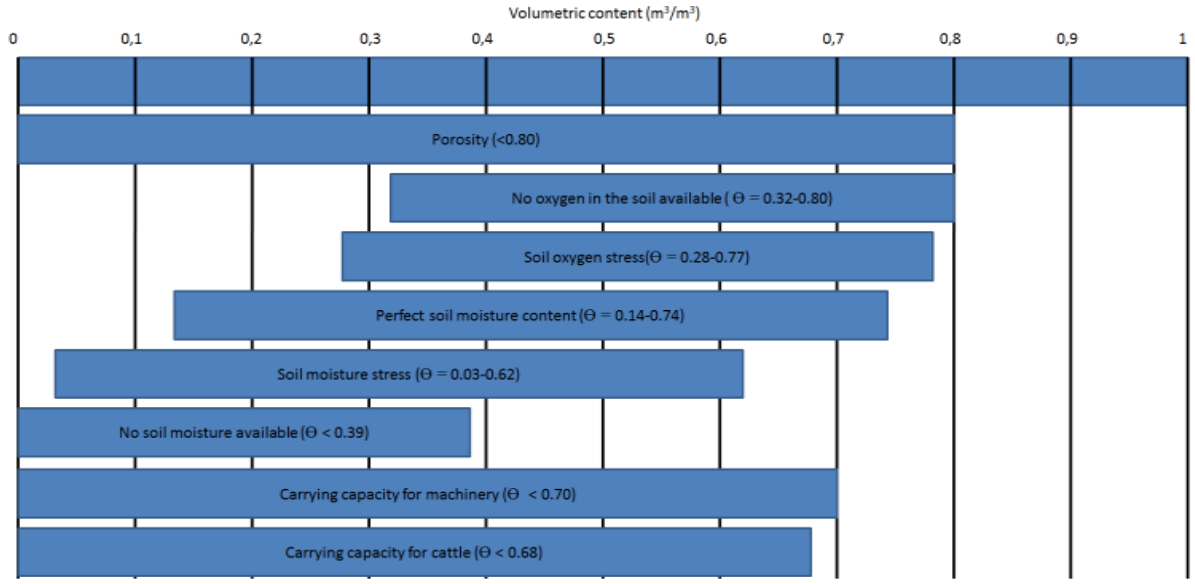

Figure 21: Overview diagram of the range in critical soil moisture content values; the bar represents the spatial distribution for the critical values for all soil types together.

The SMS-i diagram for the soil type loamless fine to moderate fine sand (B1) is presented in Figure 23, the diagram of the other soil types can be found in Appendix 5. The diagram displays the overlay between the carrying capacity and the soil moisture availability dependent of volumetric soil moisture content values. The upper bar shows the colors that will be presented on the map based on the different values of the volumetric soil moisture content. The fifteen different classes that can be distinguished are shown in Figure 22. Classes B I, C I, B II and C II only occur in peaty soils and are not present in this research.

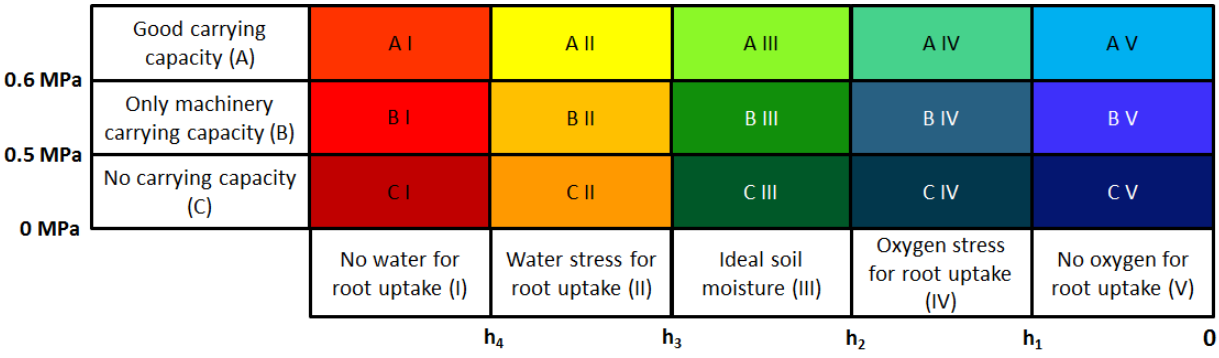

Figure 22: Soil Moisture Stress indication diagram class colours.

The diagram of Staringreeks B1 has only 8 different colors, representing 7 different classes. Not all classes are available in each soil because it depends on the soil composition and when soil moisture classes of a soil changes, for example when the status changes from A I to A II the next change cannot be from A II to B I.

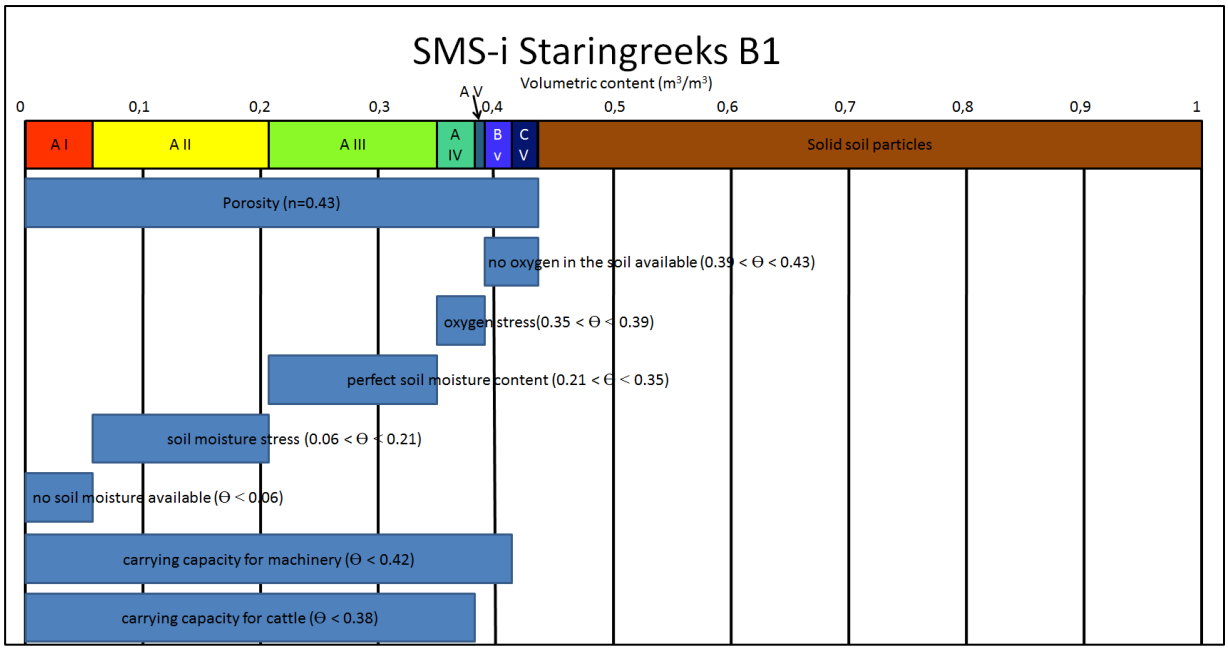

Figure 23: SMS-i diagram for loamless fine to moderate fine sand (B1).

Table 7: Range of the SMS-i classifications for all soil types present using the Staringreeks classification. SMS-i classes B I, B II, C I and C II are left out because they do not occur in this case.

Staring-reeks type	SMS-i classification										
	A I	**A II**	**A III**	**A IV**	**A V**	**B III**	**B IV**	**B V**	**C III**	**C IV**	**C V**
B1	0-0.06	0.06-0.21	0.21-0.35	0.35-0.38	-	-	0.38-0.39	0.39-0.42	-	-	0.42-0.43
B2	0-0.09	0.09-0.24	0.24-0.36	-	-	-	0.36-0.39	-	-	-	0.39-0.42
B3	0-0.11	0.11-0.30	0.30-0.41	-	-	0.41-0.42	0.42-0.43	0.42-0.44	-	-	0.44-0.46
B8	0-0.17	0.17-0.34	0.34-0.39	-	-	0.39-0.40	-	-	0.40-0.41	0.41-0.42	0.42-0.43
B10	0-0.22	0.22-0.37	0.37-0.40	-	-	0.40-0.41	-	-	0.41-0.42	0.42-0.43	0.43
B11	0-0.36	0.36-0.51	0.51-0.54	-	-	0.54-0.56	-	-	0.56-0.57	0.57-0.58	0.58-0.59
B12	0-0.35	0.35-0.47	0.47-0.49	-	-	0.49-0.50	-	-	0.50-0.52	0.52-0.53	0.53-0.54
B16	0-0.27	0.27-0.57	0.57-0.65	-	-	0.65-0.68	-	-	0.68-0.74	0.74-0.77	0.77-0.80
B18	0-0.39	0.39-0.62	0.62-0.68	-	-	0.67-0.70	-	-	0.70-0.73	0.73-0.75	0.75-0.77
O1	0-0.03	0.03-0.14	0.14-0.28	0.28-0.31	0.31-0.32	-	-	0.32-0.35	-	-	0.35-0.36
O15	0-0.17	0.17-0.34	0.34-0.36	-	-	0.36-0.37	-	-	0.37-0.40	-	0.40-0.41

5. Results

Because the soil moisture sensitivity parameter β is needed for three of the four methods, this will be calculated first. β_c will be used in section 5.2 for the bias-correction and in section 5.3 for validation of the four downscaling methods plus bias correction. Soil moisture maps from a wet to dry period (23-08-2012 till 28-08-2012) of the best downscaling method will be presented in section 0 and derived soil classification maps in section 5.5. Section 5.6 zooms in on a small area located in the north of the study area.

5.1. Soil moisture sensitivity parameter

The year round soil moisture sensitivity parameter $\beta_{c,\ year}$ is obtained for all WARP^{NT}-pixels in the study (Table 8). Scatter plots of the average RADARSAT-2 backscatter (σ) versus the $\theta_{SWI\ 1}$ per WARP^{NT}-pixel for the twelve RADARSAT-2 observation dates between 12-03-2012 and 01-12-2012 can be found in Appendix 6a. RADARSAT-2 observation date 25-12-2012 is not taken into account because no ASCAT SWI 1 data are available for this date. Table 8 shows $\beta_{c,\ year}$ values between 0.038 and 0.174 ($m^3/m^3\ dB^{-1}$) and correlation coefficients R^2 varying between 0.411 and 0.821. Reason for a high $\beta_{c,\ year}$ of WARP^{NT}-grid 2589517 can be a lake and wetlands covering the area. Values of the 24-days β ($\beta_{c,\ 24}$), ranging from 0.002 $m^3/m^3\ dB^{-1}$ till 0.05 $m^3/m^3\ dB^{-1}$, can be found in Appendix 6a, daily β values ($\beta_{c,\ day}$) are because of the large amount not presented and ranges from 0 $m^3/m^3\ dB^{-1}$ till 0.052 $m^3/m^3\ dB^{-1}$.

Table 8: Yearly soil moisture sensitivity parameter $\beta_{c,\ year}$ per WARP-pixel (see Figure 12).

WARP^{NT}-ID	$\beta_{c,\ year}$	R^2	WARP^{NT}-ID	$\beta_{c,\ year}$	R^2	WARP^{NT}-ID	$\beta_{c,\ year}$	R^2
2569887	0.100	0.588	**2577767**	0.092	0.570	**2581709**	0.075	0.537
2569891	0.112	0.670	**2577771**	0.082	0.611	**2581713**	0.085	0.593
2569895	0.077	0.515	**2577775**	0.119	0.583	**2585603**	0.106	0.821
2569899	0.080	0.421	**2577779**	0.105	0.550	**2585607**	0.103	0.554
2569903	0.038	0.662	**2577783**	0.089	0.555	**2585611**	0.113	0.459
2573829	0.094	0.596	**2577787**	0.104	0.571	**2585615**	0.085	0.556
2573833	0.095	0.573	**2581689**	0.125	0.636	**2585619**	0.070	0.478
2573837	0.109	0.625	**2581693**	0.107	0.575	**2585623**	0.075	0.554
2573841	0.088	0.547	**2581697**	0.089	0.581	**2589513**	0.086	0.753
2573845	0.084	0.411	**2581701**	0.105	0.622	**2589517**	0.174	0.436
2573849	0.042	0.599	**2581705**	0.096	0.591	**2589521**	0.086	0.392
2573853	0.065	0.390						

5.2. Bias-correction

ITCSM stations 04, 10 and 18 are used for bias-correction of the four downscaling combinations. The remark has to be made that the porosity is set to the maximum of the highest measured in-situ soil moisture or the PAWN-porosity (see Table 1) at each in-situ location. Calibration results for the retrieved soil moisture using the four methods and the in-situ measurements are presented in Table 9 (values) and Appendix 6 (graphic daily representation). Bias-correction parameter A_1 is the slope of the in-situ versus modelled soil moisture scatter plot and B_1 is its offset. A_2 and B_2 are the slope and offset after exchanging the axes. Before bias-correction takes place methods III and IV are the most promising, method I gives the worst results. This is likely a result of the ignorance of changing beta during the year. Station ITCSM 04 has low R^2 and high MAE values for all combinations. The weak

correlation between RADARSAT-2 backscatter (σ°_{m}) or $\theta_{SWI\,1}$ and $\theta_{in\text{-}situ}$ for the stations location can be a good explanation for this (Appendix 60). The station is grass covered but the location is surrounded by forest (see Appendix 1) which influences RADARSAT-2 backscatter. This lack of correlation is endorsed by the results after bias-correction; for all methods the value of the MAE for ITCSM 04 increases while a decrease is expected. Remarkable is that for method IV the coefficient of determination R^2 stays equal while for the other methods R^2 decreases.

Table 9: Bias-correction results; comparison between in-situ and retrieved soil moisture at ITCSM 04, ITCSM 10 and ITCSM 18 for the methods I-IV with n = max n (in situ or PAWN).

Method		**I ($\beta_{c,\,year}$)**			**II ($\beta_{c,\,24}$)**			**III ($\beta_{c,\,day}$)**			**IV (no β_c)**		
Location ITCSM XX		**04**	**10**	**18**	**04**	**10**	**18**	**04**	**10**	**18**	**04**	**10**	**18**
Before bias-correction	**R^2**	0.10	0.59	0.08	0.03	0.15	0.25	0.10	0.53	0.20	0.08	0.62	0.15
	MAE (m^3/m^3)	0.11	0.29	0.29	0.11	0.15	0.08	0.10	0.20	0.12	0.11	0.24	0.16
Bias-correction parameters (for all locations)		A_1 = 1.872 B_1 = -0.560 A_2 = 0.157 B_2 = 0.256			A_1 = 0.895 B_1 = -0.054 A_2 = 0.166 B_2 = 0.236			A_1 = 1.046 B_1 = -0.150 A_2 = 0.261 B_2 = 0.228			A_1 = 1.107 B_1 = -0.193 A_2 = 0.267 B_2 = 0.233		
After bias-correction	**R^2**	0.10	0.62	0.08	0.03	0.03	0.20	0.10	0.43	0.22	0.08	0.62	0.15
	MAE (m^3/m^3)	0.18	0.08	0.07	0.12	0.07	0.07	0.14	0.06	0.05	0.17	0.09	0.06

5.3. Validation

A validation is done using the bias-correction parameters given in Table 9 and all available ITCSM stations. The validation results are presented in Table 10A (only RADARSAT-2 observation dates) and Table 10B (all dates between 12-03-2012 and 01-12-2012). Beside validation results of the individual points also the average results and standard deviation are given for (i) all validation stations, these are the stations with land cover type grassland that are not used for the bias-correction, (ii) all grassland stations and (iii) all available stations.

Both tables are showing the poorest validation results for downscaling method I. This is remarkable because this is the downscaling method suggested by Das et al. (2011). Method II gives the best results when only the thirteen RADARSAT-2dates are taken into account, but when the soil moisture for all dates between 12-03-2012 and 01-12-2012 is retrieved, the best results are obtained using method III. Overall the results for only the RADARSAT-2dates (Table 10A) are better than for all dates (Table 10B). The results for average values and standard deviation of R^2 and MAE are better for the validation locations than for all grassland stations or all stations.

For different stations it is visible that the downscaling method influences the coefficient of determination. For example stations ITCSM 11 and 12 are having half R^2 values for method I than their values for the other methods. Results for ITCSM 04, used for obtaining the bias-correction parameters, stands out for its low R^2 and high MAE for all methods in both Table 10A and Table 10B**.**

Looking at the average and standard deviation of R^2 and the MAE, best results are realized using downscaling method III followed by method II. Validation results of method III and IV are almost equal when only the RADARSAT-2dates are taken into account. Downscaling method IV

outperforms method I for almost all combinations, in the other cases its value is almost equal. Retrieved $\theta_{m,abc}$ using downscaling method III, measured $\theta_{in\text{-}situ}$ and the difference between both for all ITCSM-network station locations is presented in Figure 25. Figure 25a shows that $\theta_{m,abc}$ varies between 0.2 m^3/m^3 and 0.52 m^3/m^3 while $\theta_{in\text{-}situ}$ varies between 0 m^3/m and 0.52 m^3/m^3. The average overestimation of θ by method III is 0.06 m^3/m^3 with most extreme peaks for ITCSM 04 and ITCSM 09 (see Figure 25c). The same peaks are present when the over- or underestimation is expressed in percentage of $\theta_{in\text{-}situ}$ (Figure 25d).

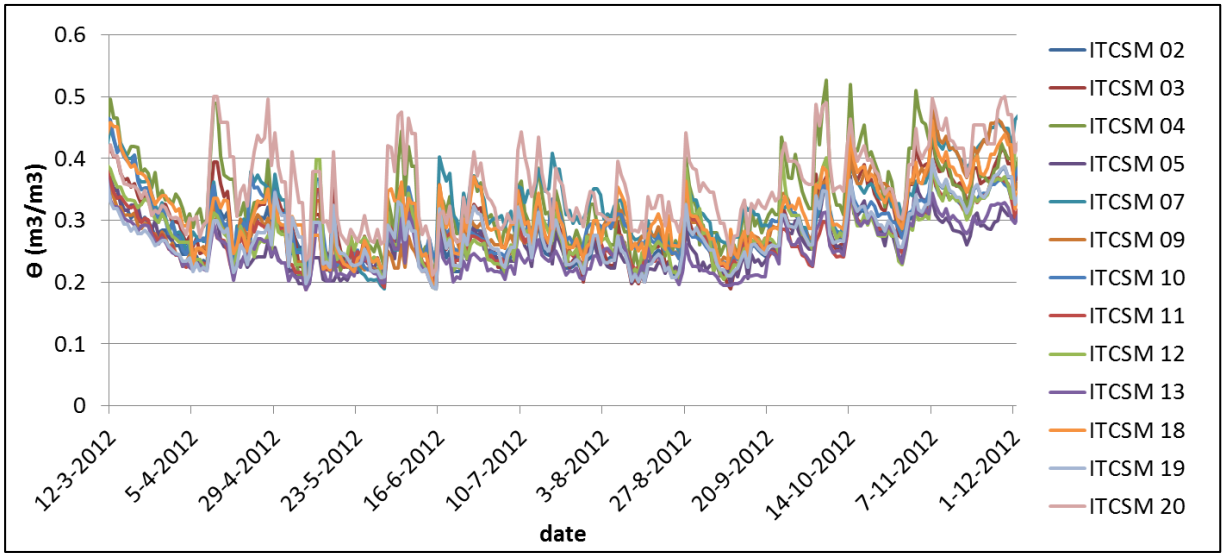

(a)

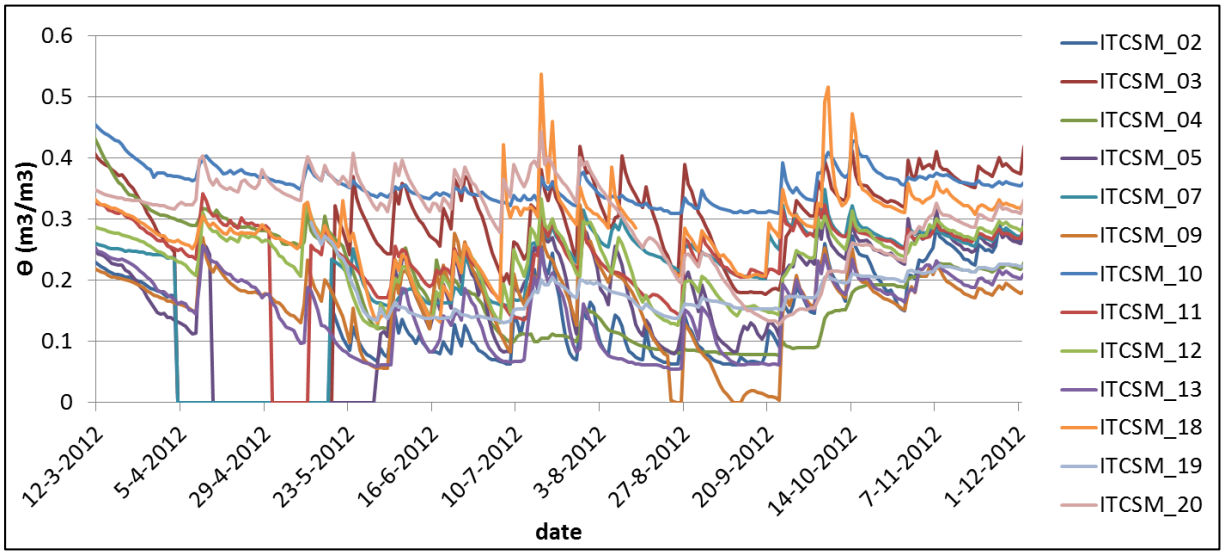

(b)

Figure 24: (a) Retrieved $\vartheta_{m,\,abc}$ using downscaling method III for the ITCSM-locations, (b) $\vartheta_{in\text{-}situ}$ for all ITCSM locations, (c) difference between retrieved and measured ϑ at all stations (retrieved-measured) and (d) difference between retrieved and measured ϑ at all stations expressed in percentage of the measured ϑ.

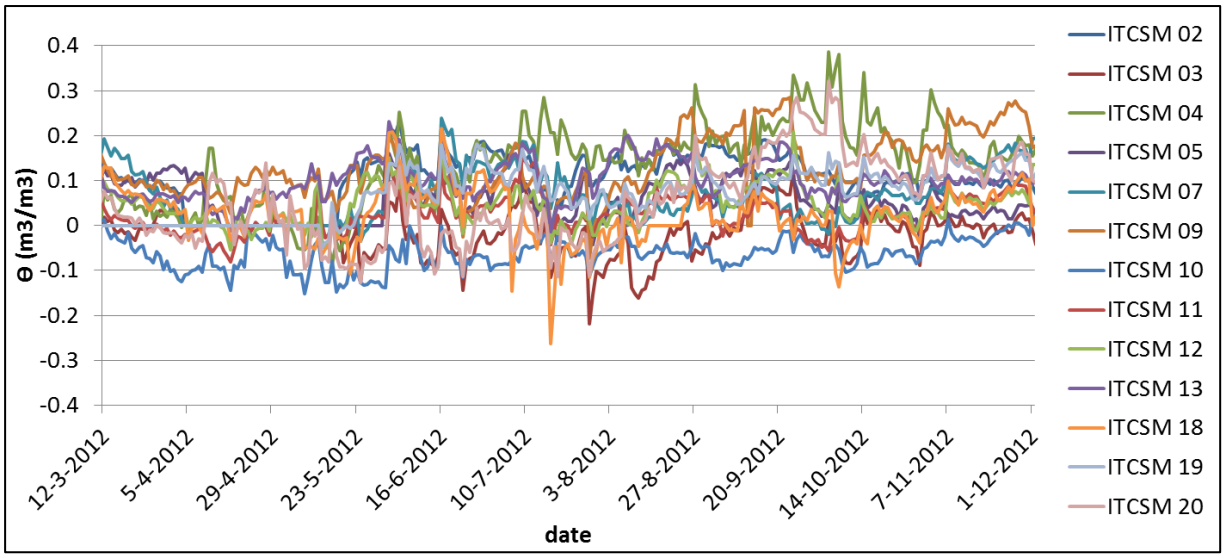

(c)

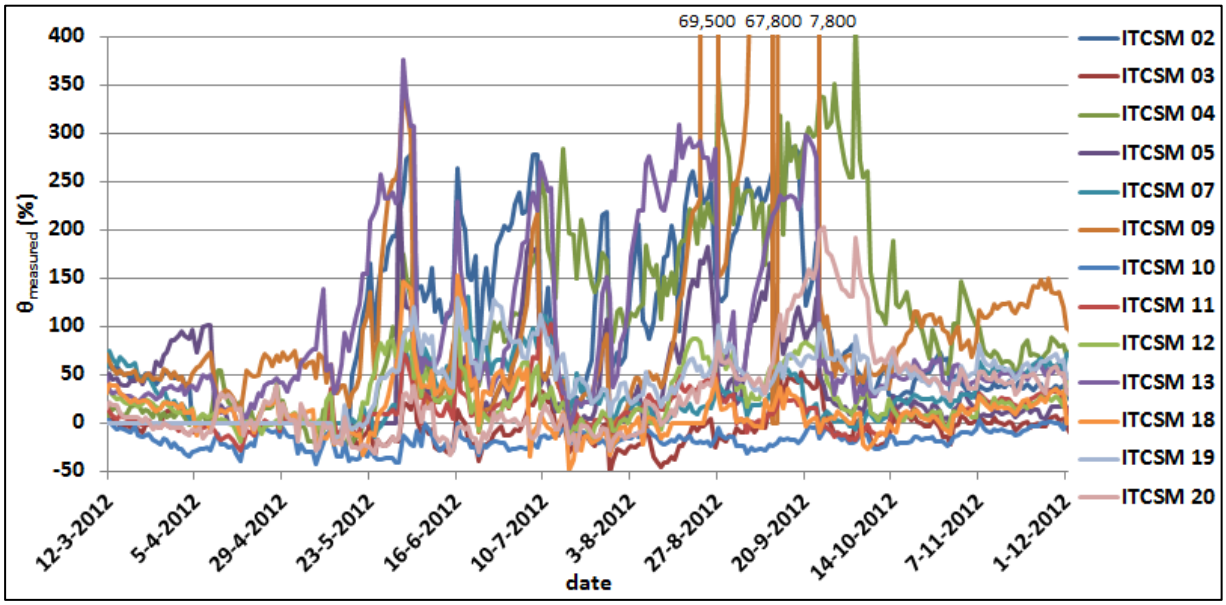

(d)

Figure 25: (a) Retrieved $\vartheta_{m,\,abc}$ using downscaling method III for the ITCSM-locations, (b) $\vartheta_{in\text{-}situ}$ for all ITCSM locations, (c) difference between retrieved and measured ϑ at all stations (retrieved-measured) and (d) difference between retrieved and measured ϑ at all stations expressed in percentage of the measured ϑ.

Table 10A: Validation results for only the thirteen RADARSAT-2 observation dates; val. means all the points taken into account for validation (ITCSM 02, 03, 05, 11-13 and 19), gr. means all the locations having a grass cover and all means all locations (best results are bold).

Method	**I ($\beta_{c,\ year}$)**		**II ($\beta_{c,\ 24}$)**		**III ($\beta_{c,\ day}$)**		**IV (no β_c)**	
Station	**R^2**	**MAE**	**R^2**	**MAE**	**R^2**	**MAE**	**R^2**	**MAE**
ITCSM 02	0.66	0.15	**0.88**	**0.10**	0.77	**0.10**	0.85	0.11
ITCSM 03	**0.82**	**0.04**	0.40	0.08	0.65	0.07	0.81	0.06
ITCSM 04	0.05	0.18	0.05	**0.12**	**0.06**	0.13	0.05	0.13
ITCSM 05	0.46	0.08	**0.87**	**0.07**	0.70	**0.07**	0.65	**0.07**
ITCSM 07	0.05	0.19	**0.68**	**0.03**	0.06	0.06	0.01	0.07
ITCSM 09	0.27	0.20	0.14	**0.09**	**0.35**	0.12	0.34	0.12
ITCSM 10	0.70	**0.07**	0.16	0.08	0.54	0.08	**0.76**	0.09
ITCSM 11	0.14	0.07	0.31	0.04	0.33	**0.03**	**0.39**	**0.03**
ITCSM 12	0.05	0.12	**0.41**	**0.06**	0.15	**0.06**	0.21	0.07
ITCSM 13	0.16	**0.10**	0.58	0.12	**0.59**	0.11	0.35	**0.10**
ITCSM 18	0.10	0.08	0.21	0.06	**0.25**	**0.05**	0.22	0.06
ITCSM 19	0.00	0.12	**0.31**	**0.08**	0.08	0.09	0.04	**0.08**
ITCSM 20	**0.10**	0.12	0.01	0.08	0.00	0.06	**0.10**	**0.05**
Average val.	0.33	0.10	**0.54**	0.09	0.47	0.08	0.47	**0.07**
St.dev. val.	0.30	0.03	**0.23**	0.03	0.26	**0.02**	0.28	**0.02**
Average gr.	0.31	0.12	0.34	**0.08**	0.41	**0.08**	**0.43**	**0.08**
St. dev. gr.	0.30	0.04	**0.23**	**0.03**	0.25	**0.03**	0.30	**0.03**
Average all	0.27	0.12	**0.38**	**0.08**	0.35	**0.08**	0.37	**0.08**
St. dev. all	0.28	0.05	0.28	**0.03**	**0.26**	**0.03**	0.29	**0.03**

Table 10B: Validation results for all dates from 12-03-2012 till 01-12-2012; val. means all the points taken into account for validation (ITCSM 02, 03, 05, 11-13 and 19), gr. means all the locations having a grass cover and all means all locations (best results are bold).

Method	**I ($\beta_{c,\ year}$)**		**II ($\beta_{c,\ 24}$)**		**III ($\beta_{c,\ day}$)**		**IV (no β_c)**	
Station	**R^2**	**MAE**	**R^2**	**MAE**	**R^2**	**MAE**	**R^2**	**MAE**
ITCSM 02	0.67	0.15	0.66	**0.12**	0.69	**0.12**	**0.73**	0.13
ITCSM 03	0.33	**0.04**	0.28	0.06	0.37	**0.04**	**0.41**	**0.04**
ITCSM 04	**0.10**	0.18	0.03	**0.12**	**0.10**	0.14	0.08	0.17
ITCSM 05	0.30	0.08	**0.52**	0.08	0.51	**0.07**	0.42	**0.07**
ITCSM 07	0.02	0.15	**0.51**	**0.03**	0.18	0.08	0.00	0.11
ITCSM 09	0.07	0.18	**0.15**	**0.08**	0.13	0.13	0.10	0.15
ITCSM 10	**0.62**	0.08	0.03	0.07	0.43	**0.06**	**0.62**	0.09
ITCSM 11	0.02	0.06	**0.33**	**0.04**	0.28	**0.04**	0.10	0.05
ITCSM 12	0.00	0.10	**0.52**	**0.04**	0.33	0.05	0.02	0.08
ITCSM 13	0.10	**0.08**	0.41	0.12	**0.49**	0.10	0.25	0.09
ITCSM 18	0.08	0.07	0.20	0.07	**0.22**	**0.05**	0.15	0.06
ITCSM 19	0.28	0.12	0.20	**0.08**	0.23	0.10	**0.31**	0.09
ITCSM 20	**0.07**	0.12	0.00	**0.08**	0.00	0.09	0.04	0.09
Average val.	0.24	0.09	**0.42**	**0.08**	0.41	**0.08**	0.32	**0.08**
St.dev. val.	0.21	**0.03**	**0.15**	**0.03**	**0.15**	**0.03**	0.22	**0.03**
Average gr.	0.25	0.10	0.28	**0.08**	**0.36**	**0.08**	0.31	0.09
St. dev. gr.	0.22	0.04	0.19	**0.03**	**0.16**	**0.03**	0.22	0.04
Average all	0.20	0.11	**0.30**	**0.08**	**0.30**	**0.08**	0.25	0.09
St. dev. all	0.21	0.04	0.21	**0.03**	**0.18**	**0.03**	0.23	0.04

5.4.Soil moisture maps of the study area

Figure 26 presents the $\theta_{m,abc,III}$ for a 6-day period (23-08-2012 – 28-08-2012) containing a rainfall event on the 26th of August. Starting at the end of an almost completely dry period, from 07-08-2012 till 26-08-2012 (see Figure 10), $\theta_{m,abc,III}$ is expected to be low at the 23th of August. Because in-situ measurements are not area covering, the porosity of the PAWN-classification of the soil types is used to obtain the soil moisture maps of the study area.

All dates show higher $\theta_{m,abc,III}$ values at the northwest and southeast corners of the study area. The outstanding high $\beta_{c,day}$ values of WARP^{NT}-grid 2589517, due to wetlands, can be the reason for the higher values in the northwest. The higher values in the southeast are caused by "no-data" values for RADARSAT-2 backscatter outside the study area (in Germany and therefore not available by the NSO) that influence the mean RADARSAT-2 data of WARP^{NT}-grids 2569903, 2573849 and 2573853. There are distinctions visible between the other WARP^{NT}-grids in the study area, caused by different $\theta_{SWI\ 1}$ values per grid at the same time. The peaty area in the north western part is slightly visible during the dry period and pops out after the precipitation event took place.

The colour of the area transforms from orange on 23-08-2013 to yellow-orange on 28-08-2012 passing through darker orange on 25-08-2012 and brighter yellow on 27-08-2012. Transformation to a lighter colour is a result of increasing $\theta_{SWI\ 1}$ values in response to precipitation events. New RADARSAT-2 observations at 27-08-2012 makes the spatial distribution more diverse, the difference between measured σ°_{m} in one coarse ASCAT-grid varies more resulting in a wider spread of the $\theta_{m,abc,III}$ values.

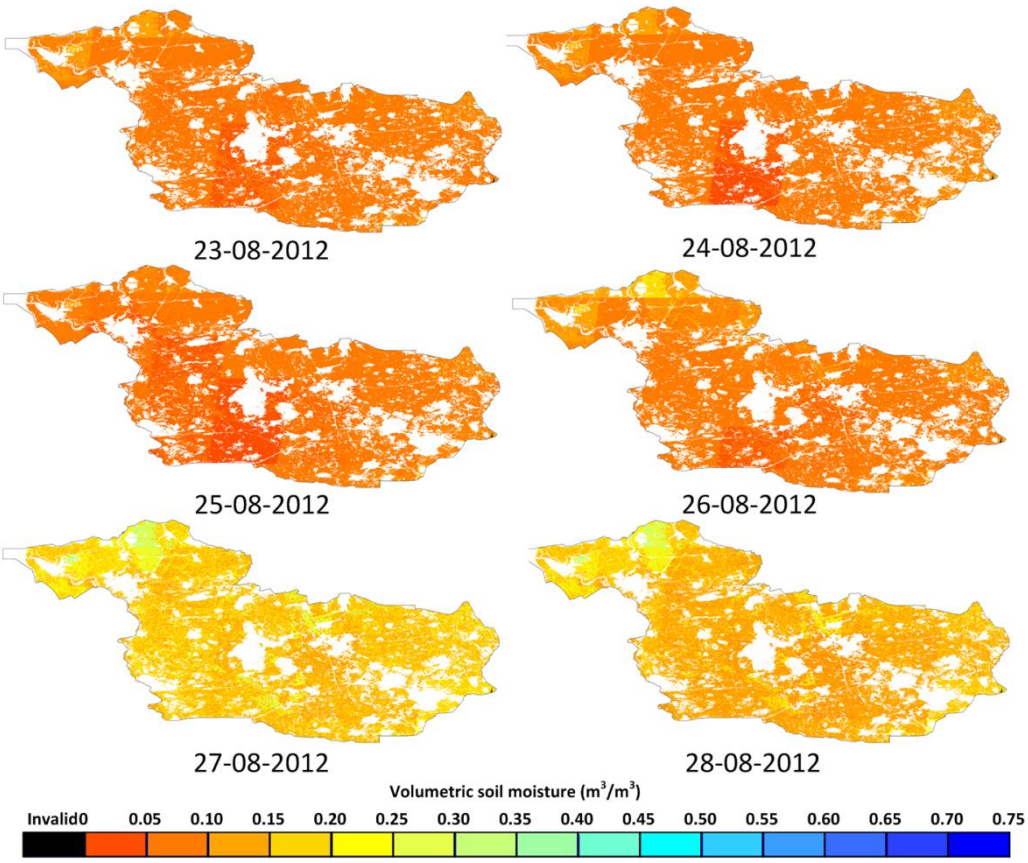

Figure 26: Observed volumetric soil moisture at agricultural fields for the period 23-08-2012 till 28-08-2012, high precipitation (10-25 mm) is measured at 26-08-2012 after a dry period up from 07-08-2012.

5.5. Soil status classification maps of the study area

The same period as for the soil moisture maps is used for the soil status classification maps (23-08-2012 till 28-08-2012). The classification is done using conditions set up of the Soil-Moisture-Stress-indication (SMS-i, section 4.4).

The first days the most dominant colour is red, representing the driest soil status (A I). This may be expected at the end of a dry period but it is remarkable that this status is present on the western side after the rainfall event. Significant parts turn into a better status, orange (A II) on 26-08-2012. After the precipitation of 26-08-2012 A II is the dominating status and even green pixels, representing the A III status, are visible.

Boundaries of the different Staringreeks classes of the topsoil are bright visible in the SMS-i classification maps. This and the fact that the A II status pixels (orange) on 25-08-2012 are mostly similar to the A III status pixels (green) on 27-08-2012 after a change in spatial distribution per WARP^{NT}-grid by a new RADARSAT-2 image on 27-08-2012, shows that the influence of the soil type is stronger than the influence of the RADARSAT-2 backscatter for determining the SMS-i class.

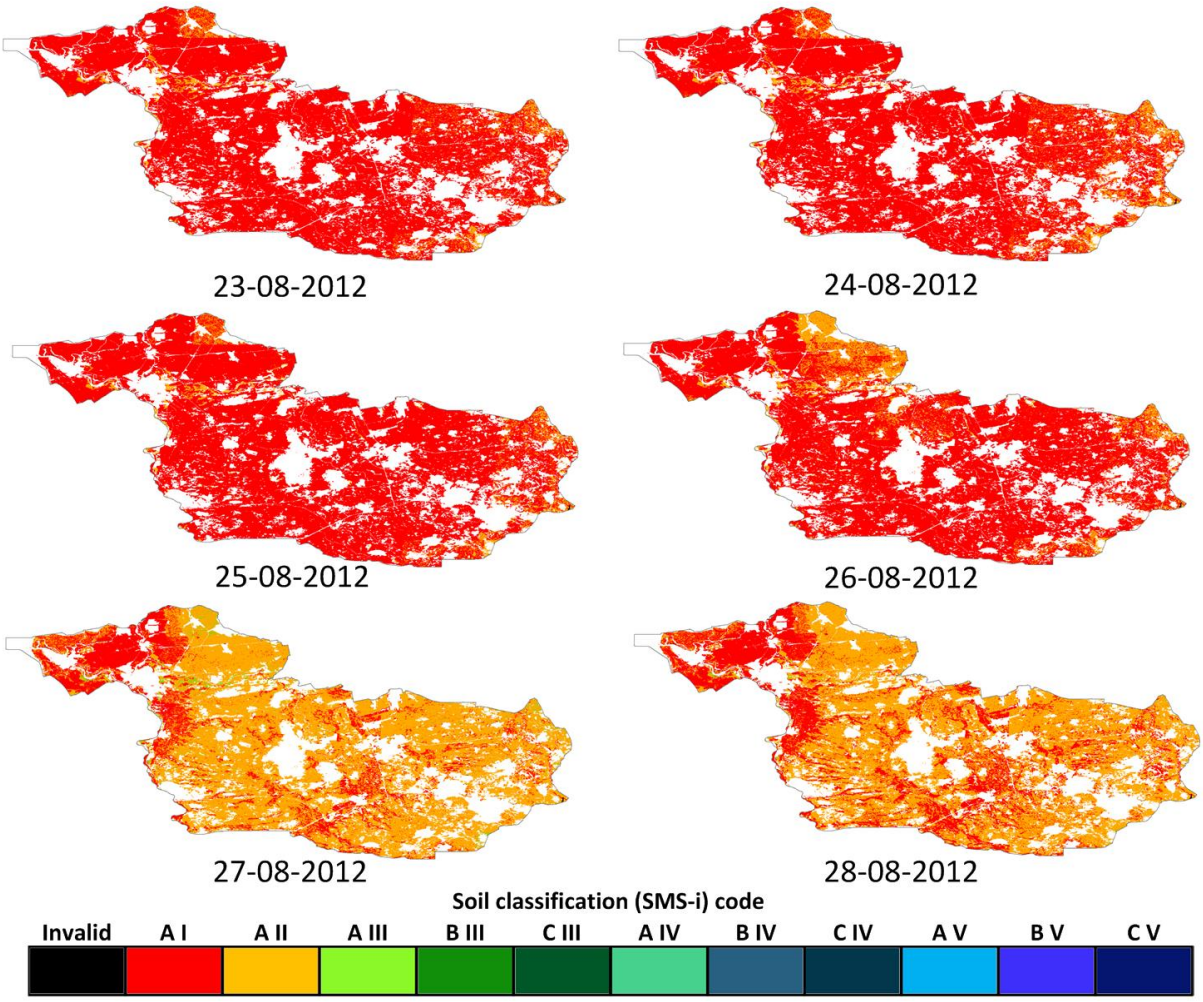

Figure 27: Soil status classification (SMS-i) derived from observed volumetric soil moisture for the period 23-08-2012 till 28-08-2012, high precipitation (10-25mm) is measured on 26-08-2012 after a dry period starting on 07-08-2012.

5.6. Soil moisture and classification of a small area

Section 0 and 5.5 are presenting the volumetric soil moisture content and soil status for the study area. These figures give a general overview, but the objective is to obtain fine resolution maps so a closer look will be taken at a smaller area in the north of the study area. The zoomed area is at the intersection between WARP^{NT}-grids 2589517, 2589521, 2585611 and 2585615 and has a 5 km x 5 km dimension (Figure 28). Values of ASCAT SWI 1 and the mean RADARSAT-2 backscatter (σ_c°) of the grids during the 23-08-2012 till 28-08-2012 period is presented in Table 11. Figure 28 shows multiple maps of the fine resolution input parameters PAWN and RADARSAT-2 backscatter.

Results of downscaling method III and following SMS-i classes of the small area are presented in Figure 29. Change of soil moisture and soil status over time shows that the soil status is stronger related to the PAWN-classes than the soil moisture content. Similarities between both maps are clear, pixels representing lower volumetric soil moisture results in a dryer soils status class. Different ASCAT SWI 1 values for WARP^{NT}-grids at the same time results in clear boundaries, especially for the dates before 27-08-2012.

Table 11: Input values of ASCAT SWI 1 and the coarse (mean) RADARSAT-2 backscatter for the WARP-grids 2589517, 2589521, 2585611 and 2585615 over the period (23-08-2012 - 28-08-2012).

		ASCAT SWI 1 (%)						σ_c° (dB)	
	date	**23-08-2012**	**24-08-2012**	**25-08-2012**	**26-08-2012**	**27-08-2012**	**28-08-2012**	**03-08-2012**	**27-08-2012**
WARP^{NT}-id	**2589517**	16	16.5	10.5	29.5	51	48	-12.26	-12.38
	2589521	20	20	19.5	33.5	60.5	49	-10.60	-10.69
	2585611	8.5	6.5	3	13.5	44.5	40.5	-11.57	-11.52
	2585615	7.5	8	5.5	20.5	48.5	40	-11.10	-10.96

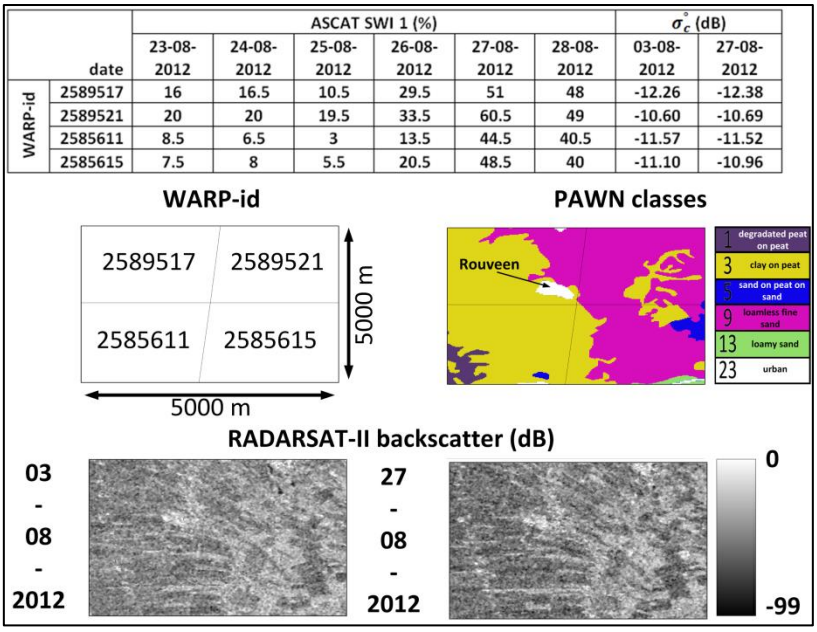

Figure 28: The 5 km x 5 km zoomed in area and related WARP-grid distribution (upper left), the PAWN classes in this small area (upper right) and RADARSAT-2 backscatter images of the small area for 03-08-2012 and 27-08-2012 (down).

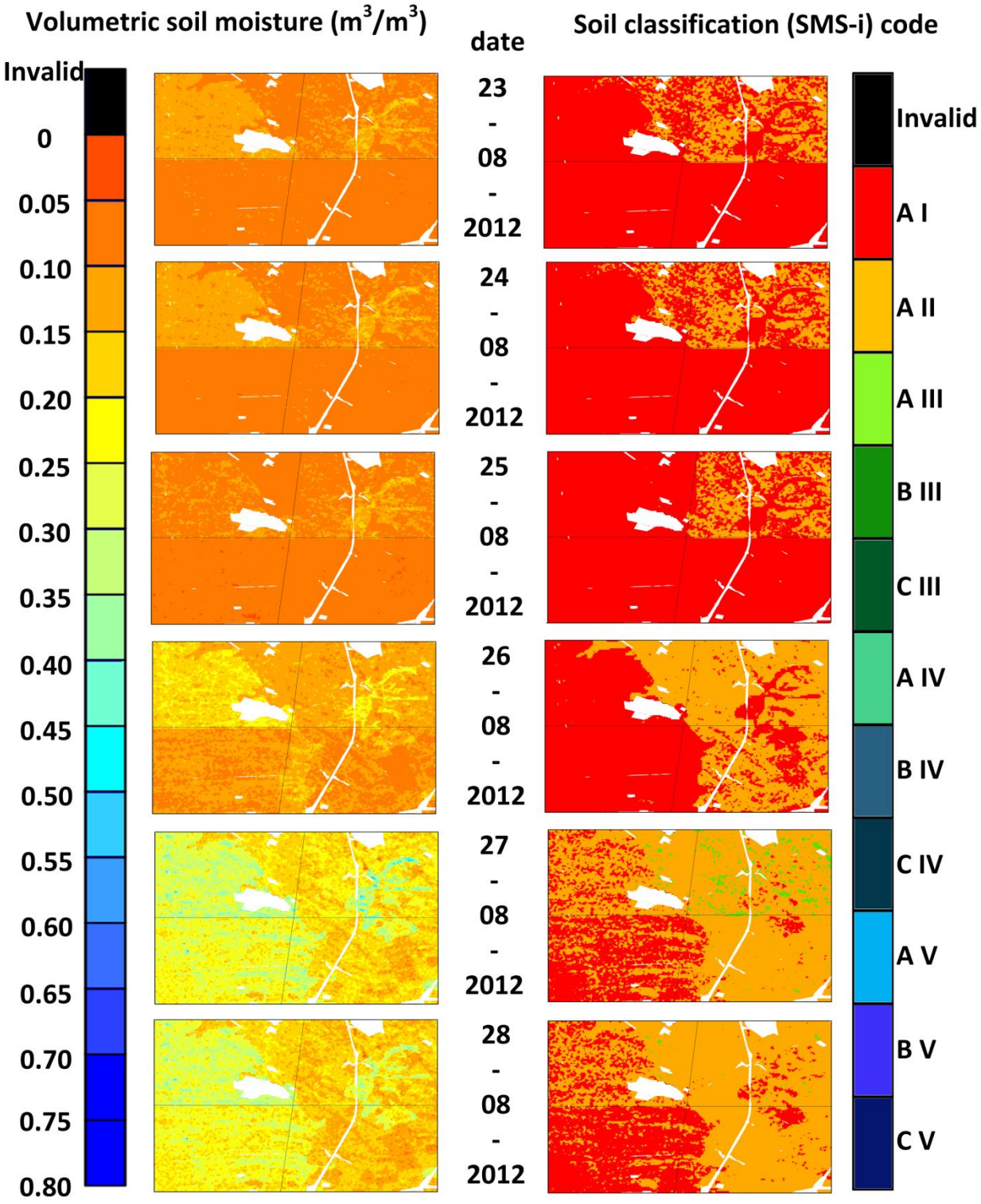

Figure 29: Output values for the volumetric soil moisture (left) and soil status classification (SMS-i, right) for agricultural fields in the zoomed area using downscaling method 3.

6. Discussion

Assumptions, decisions and used methods will be discussed and their influence will be explained. This will be done for the retrieved fine resolution soil moisture (section 6.1), the soil porosity (section 6.2) and the comparison of retrieved soil moisture with other research (section 6.3). The SMS-i classification is discussed in section 6.4 followed by its key aspects: oxygen or water stress for uptake by plants in section 6.5 and the penetration resistance in section 6.6.

6.1. Retrieved fine resolution soil moisture

Validation results show a maximal spatial variation of 0.33 m^3/m^3 for $\theta_{m,III,abc}$ between the used ITCSM-locations (Figure 25). This variation is almost 50% bigger than the spatial variation of 0.25 m^3/m^3 mentioned by Dente et al. (2011) over the same area. RADARSAT-2 backscatter is the forcing data for the spatial variation and the 24 days recurrence time is visible in the results. Differences between the validation locations stay almost equal during the 24 days periods, indicating that the difference between ASCAT SWI 1 values of the grids is limited during this year. Disadvantage of the low temporal resolution RADARSAT-2 backscatter is that variation coming from local rainfall events or the status of the grassland (for instance mowed, grazed and the cut number) stay present 24 days. Herold et al. (2000) suggest that the grassland status influence can be taken away using VV-polarized L-band backscatter.

Despite the visible influence of RADARSAT-2 backscatter in the results, used downscaling method III partly ignores the linear relation between RADARSAT-2 backscatter and the volumetric soil moisture. This relation is used for the spatial variation of volumetric soil moisture within one coarse grid but does not cross the border between two coarse grids. This because of the RADARSAT-2 backscatter at medium resolution is compared to the average of a coarse grid and not to the relation between RADARSAT-2 backscatter and volumetric soil moisture. This should be added to the soil sensitivity parameter (β) but because these are calculated per coarse grid, the relation between RADARSAT-2 backscatter and retrieved soil moisture is different per coarse grid. This can result in-situations where equal RADARSAT-2 backscatter values of two medium pixels have different volumetric soil moisture contents, even when ASCAT SWI 1 values for both coarse grids are the same.

6.2. Porosity of the soil

Porosity of the soil is an important input for the conversion of ASCAT SWI 1 to $\theta_{SWI\ 1}$. ASCAT SWI 1 data are multiplied by the porosity making the influence of porosity and ASCAT SWI 1 data similar to the output. Before bias-correction this results in a change in $\theta_{SWI\ 1}$ of 20% when the porosity or ASCAT SWI 1 is changed by 50%. Some of the porosity used for bias-correction and calibration, is retrieved by taking the maximum volumetric soil moisture measured at the in-situ locations, differs almost 50% to the porosity obtained from the PAWN-classification. Causes for this difference can be super saturated soil, inaccuracy of the ITCSM-network sensors for high θ, soil life (for example corridors of earthworms), higher percentage of organic matter in the topsoil (5 cm layer) than assumed in the PAWN-classifications, compaction of the ground and the low number of soil types using the PAWN-classification maps (resulting in variability in one PAWN class). Van Bakel et al. (2012) discussed this when using the Staringreeks, here indirectly used by applying the PAWN classification, it results in unrealistic values for soil physical properties due to generalisation of soil types. This generalisation results in more general values and less spatial variations of soil properties. Their conclusion is supported by Wösten et al. (2013). Soil saturation degrees instead of volumetric soil moisture content values can be a solution to leave out the soils porosity. Disadvantage of

saturation degrees is that it cannot be used for the SMS-i classification as presented. On the other hand, the degree of saturation can be used by waterboards when they want global information of an area for (operational) management decisions and plans.

6.3. Comparison of retrieved soil moisture with other researches

The porosity issue cannot be separated from the *MAE* values obtained during the bias-correction and validation. The *MAE* is influenced by the error in porosity, the impact is however not measurable because there is no information about the actual porosity at each location in the study area. The value of R^2 depends more on the ASCAT SWI 1 data and generating values up to 0.69 for downscaling method III (0.73 for method IV) shows that there are good results. The average R^2 value of 0.36 for all the used grass covered stations equals R^2 presented by Sabah et al. (2013). They have retrieved soil moisture using active passive microwave observations over the east part of the Netherlands using a combination of Phased Array L-band Synthetic Aperture (PALSAR) backscatter and the C-band Advanced Microwave Scanning Radiometer Observing System (AMSR-E) of the NASA for the year 2010. Only the *MAE* of ITCSM stations 04, 10 and 18 can be compared to the bias-corrected results of Sabah et al. (2013). They have bias-corrected every location independently, the used bias-correction in this research is based on the bias of retrieved soil moisture at ITCSM stations 04, 10 and 18. The results are various compared to the bias-corrected results of Sabah et al. (2013). Retrieved ITCSM 04 gives a *MAE* 0.08 m^3/m^3 higher than Sabah et al. (2013), for ITCSM 10 is the *MAE* 0.1 m^3/m^3 worse and for ITCSM 18 0.1 m^3/m^3 better. Comparing the results of the bias-corrected other stations gives a mixed picture with maximal difference of 0.08m^3/m^3 for the *MAE*.

Maximum *MAE* values of 0.14 m^3/m^3 are having a greater impact on the allocated soil status than it appears at first sight. The average soil porosity in the Netherlands is 0.42 (not explicitly for the top 5 cm layer) making an error of 0.14 m^3/m^3 an error of 33 %. Assuming that the topsoil layer has a higher porosity will decrease this percentage, but with maximum porosities of 0.80 it is still 17.5 %.

6.4. Soil status classification

The spatial variance of the volumetric soil moisture disappears almost completely when these values are translated to a status of the soil. During this translation, the influence of the PAWN-classification discussed above becomes even greater (see section 5.5 and 5.6). This is visible in Figure 27, where most contours of the different SMS-i classes match the contours of the different soil types.

The *MAE's* are big compared to the porosity and different statuses of the soil. Errors of, for example 0.10 m^3/m^3 means that the soil status can be in a different status than determined. For soil type B11 this error gives a range of six soil statuses between 0.5 m^3/m^3 and 0.6 m^3/m^3. This means that the retrieved volumetric soil moisture values cannot be used to give a reliable soil status because of the high *MAE*. Even the 0.04 m^3/m^3 accuracy of NASA his SMAP (Soil Moisture Active Passive) mission is too high to use it for retrieving reliable SMS-i classes.

6.5. Oxygen or water stress for root uptake by plants

Feddes et al. (1978) reports that his reduction function uses a fixed anaerobiosis point (h_2) that may be incorrect because there is no direct relation between pressure heads and the soils aeration status. Oxygen stress in the root zone depends on a combination of soil temperature, growth stage of the plant, soil texture and microbial activity. A process based model developed by Bartholomeus et al. (2008) uses plant physiological processes for oxygen consumption of plant roots and physical laws of diffusion for oxygen transport through the soil to the plant roots to describe the influence of oxygen

stress on the growing process of plants. This model can be used to get better results affecting the soil status for grass growing.

6.6. Penetration resistance

Limited knowledge on the relationship between the penetration resistance and soil moisture content values for different soil types makes the penetration resistance classifications side unreliable. For only four soil types there is a penetration resistance versus hydraulic head/volumetric soil moisture graph available in literature. The relation between the penetration resistance and volumetric soil moisture for peat (B16) presented by Schothorst (1982) shows increasing penetration resistance as a function of decreasing volumetric soil moisture. Farmers and water managers experience that the penetration resistance of peat also decreases at very low values of the volumetric soil moisture. This should be investigated before it can be implemented in the classification. Also the minimum penetration resistance for machinery should be updated. Used value of 0.5 MPa was the standard in 1992, machinery changed and became bigger, but their needed penetration resistance decreases due to low pressure tires and caterpillar tracks down to 0.04 MPa (Vermeulen & Verwijs, 2007).

7. Conclusions and recommendations

The main and sub-questions of this research (see section 1.3) will be answered in section 7.1. Next, recommendations for further research will be given and the use of satellite observation data in operational water management will be discussed in section 7.2.

7.1. Conclusions

The objective of this study was:

To provide fine resolution maps that represent oxygen or water stress for root take up in and the carrying capacity of the topsoil at field scale, based on satellite observed soil moisture data and soil texture information.

To reach this objective one main research question and three sub-questions were formulated. The three sub-questions will be answered before the main research question.

I. *How can fine spatial resolution soil moisture maps be generated from available remote sensing data sources?*

Two sources of coarse spatial resolution and high temporal resolution soil moisture data were compared: (i) GLDAS-Noah (28 km x 28 km, 30 minutes), a model using satellite and ground-based data that provides soil moisture data for different depths and (ii) ASCAT (12.5 km x 12.5 km, daily), processed satellite radar data that provide the Surface Soil Moisture (SSM) for the top 5 cm or Soil Water Index (SWI) which applies a smoothing filter over the SSM data for different characteristic times T. Of these data the ASCAT-SWI product came closest to measured data for three stations from the ITC soil moisture network over 2012. The ASCAT-SWI 1 (T = 1) product was selected as source for coarse spatial and high temporal resolution (Chapter 2).

To downscale the coarse ASCAT SWI 1 data to a finer resolution, fine resolution and low temporal RADARSAT-2 HH-polarized backscatter (25 m x 25 m, 24 days with 13 fly-overs in 2012) was used. Four different downscaling methods were compared. Three methods were based on Das et al. (2011) which assumes a linear relationship between the volumetric soil moisture content derived from ASCAT SWI 1 ($\theta_{SWI\ 1}$) and the average RADARSAT-2 backscatter over the coarse ASCAT grid. This relationship varies per grid and was taken (1) constant for the entire year (derived from data for the same year), (2) constant for every 24 days the RADARSAT-2 satellite reveals new data and was taken constant and (3) variable per day based on daily θ_{SWI} data from ASCAT. For the latter two the intercept of the linear relationship was considered zero. Since these methods may result in moisture contents outside the realistic range a fourth downscaling method was developed that was based on a scaling between the minimum and maximum RADARSAT-2 backscatter values. Since the θ derived from satellite data was on average lower than measured in the field a bias correction was applied to all data. This bias correction was based on trend lines between the retrieved volumetric soil moisture content and the one measured in the field for three stations. The volumetric water content was then calculated for the other 10 stations of the ITC soil moisture network using all four downscaling methods including bias correction and compared to the field measurements. The downscaling method with a daily varying relationship gave the best result (Chapter 3 and 5).

So, a fine spatial, high temporal resolution soil moisture map (75 m x 75 m, 1 day) can be retrieved using the coarse resolution, high temporal ASCAT SWI 1 relative soil moisture product (12.5 km x 12.5 km, 1 day), fine resolution, low temporal RADARSAT-2 HH-polarized backscatter (25 m x 25 m, 24 days) and a downscaling method modified from Das et al. (2011) with a daily varying soil sensitivity parameter (β). The general trend in volumetric soil moisture content variation during the year, wet winter – dry summer, is well represented by the series of soil moisture map, but the average MAE of 0.08 m^3/m^3 over all grass covered ITCSM-stations is relatively large compared to the average porosity of Dutch soils (0.42 m^3/m^3) (Chapter 5). Uncertainty in the exact porosity of the different soils can be an explanation for this (Chapter 6).

II. *How can the water or oxygen stress for root take up and the topsoil carrying capacity of grassland be determined when the soil moisture content is known?*
When the volumetric soil moisture content is known, this content can be converted to a matric head using pF/water retention curves. Soil water retention curves are different for each soil type. However, the critical matric heads for water or oxygen stress for root take up for a given crop is identical for all soil types (Cultuurtechnische Vereniging, 1992). Less information could be found about the relation between soil moisture and carrying capacity. Based on two papers that indicated a relationship between carrying capacity in MPa and matric head or soil moisture content (Schothorst, 1982; Peerboom, 1990), critical moisture contents and matric heads were derived for all soil types in the study area. Critical values of the matric head in all situations for oxygen or water stress for root take up and the carrying capacity are combined together in a Soil-Moisture-Stress indication (SMS-i) diagram, resulting in a maximum of 15 different classes per soil type (Chapter 4).

III. *How can a clear combined map be produced that represents both the status of oxygen or water stress and the carrying capacity?*
Linking the volumetric soil moisture content of a 75 m x 75 m grid of the high spatial and temporal resolution soil moisture maps, retrieved from ASCAT SWI 1 and RADARSAT-2 data with a modified downscaling method of Das et al. (Das, Entekhabi, & Hjoku, 2011), with the SMS-i classification diagram for that grid results in a map representing the SMS-i class of each pixel. These SMS-i maps are representing both the status of oxygen or water stress and the carrying capacity in one class with a spatial resolution of 75 m x 75 m and a daily recurrent time (Chapter 5).

The answer to the research questions fulfils the objective of this research and provides an answer to the main research questions:

Can satellite derived soil moisture data be used to generate fine resolution maps of topsoil water or oxygen stress and carrying capacity of grasslands?

This research has shown that satellite derived soil moisture can be used to generate fine resolution maps of topsoil water or oxygen stress and carrying capacity of grasslands using a Soil-Moisture-Stress indication classification. Within the limitations of the used methods, especially for determining the carrying capacity, the results give a good indication of the status of the soil. The wet winter - dry summer pattern is present in the retrieved soil moisture and wet and dry spots are pointed out well

on the different maps. Also the precipitation effect is visible in the maps; after a precipitation event the status of the soil shifts to a “wetter” status on the SMS-i classification. These data may be useful for waterboards to optimize their (operational) water management and avoid too dry or too wet situations as much as possible. However, the accuracy and reliability of the data and used methods are only good enough to give an indication and more research is required to improve the SMS-i maps. Some recommendations to improve the SMS-i maps will be given in the next section.

7.2. Recommendations

Recommendations based on this research can be split up in two parts: i) recommendations for (operational) water management and ii) recommendations for further research.

(Operational) water management

- A decision has to be made about which spatial resolution is desirable for (operational) water management. This resolution should be the standard for new soil moisture products. Are products needed at field scale, or even smaller, or is plot scale fine enough to provide good information to the water managers? This recommendation is related to the vision of waterboards on what their tasks are. Do waterboards need to manage water at field scale, or leave this up to the farmers and should waterboards aim for the bigger picture (e.g., polders).
- A decision has to be made in how many classes the soil status should be presented. The SMS-i classification has now 15 classes resulting in more classes per soil type than a simpler and more clear three color traffic light classification. Can classes be combined together resulting in the three color traffic light or will this accompany loss of important information? A solution to tackle this problem can be a distinction between the classes shown for operational water management and for water managers dealing with complaints. The operational water managers can have a simple traffic light classification in which red represents “to dry”, green “ideal” and blue “to wet” and proceedings such as pumping water in, do nothing or pumping water out can be coupled to the different classifications. For the more theoretical water managers dealing with complaints, the now used SMS-i classification will be shown to give all information they need about root water uptake stress and the carrying capacity.
- Replace the topsoil in this research with the root depth of grass (approximately 0.75 m). This research only takes into account the status of the topsoil and determined that water stress for root uptake will occur for grass when the topsoil is to dry/wet. But because the root of grass can be grown up to 0.75 m deep, grass can get water from deeper layers than the topsoil.
- When no detailed soil data are available, retrieved soil moisture using the method of this research is not specific enough. Methods that are not using soil properties can be a solution to tackle this problem. The Surface Energy Balance System (SEBS) or Surface Energy Balance Algorithm for Land (SEBAL) are examples which can determine oxygen or water stress in the root zone without knowing the soil properties but are having their own, different, uncertainties.

Further research

- Maps of the different soil types in the Netherlands have to be updated. More soil types with clear distinctions between them are needed to reduce the variance within one soil type. Nowadays maps are too coarse to get specific information of a small area and because the status of the soil depends strongly on these soil types fine resolution differences are not visible.
- Determine the exact porosity at the ITCSM location. This can be done by carrying out a new field experiments or by us the bulk density of the soil samples taken by Dente et al. (2011).
- Investigate what the results will be when the reduction function of Feddes et al. (1978) will be replaced by a more smooth function displaying the relation between oxygen or water stress and the matric head. For example use Batholomeus et al. (2008) for the wet/oxygen-stress side of the reduction function.
- There is limited information available and research done on the relation between the penetration resistance and the volumetric soil moisture content or matric head for the topsoil. Most research and information about the volumetric soil moisture/matric head – penetration resistance relation is only done for sub soils because compaction problems at crop fields. These researches focus only on the sub soil because the topsoils of crop fields are cultivated yearly. There is no yearly cultivation for topsoils of grasslands and this resulting in compaction problems in this layer. Research should be done to this problem separately to the research in compaction of the sub soil.

Bibliography

Bakker, S. (2013, 02 05). Waterbeheer in kaart brengen op basis van Remote Sensing. Zwolle: Waterboard Groot Salland.

Bartalis, Z., Naeimi, V., Hasenauer, S., & Wagner, W. (2008). *ASCAT Soil Moisture Product Handbook.* Vienna University of Technology, Institute of Photogrammetry and Remote Sensing,. Vienna: Vienna University of Technology.

Bartholomeus, R., Witte, J., van Bodegom, P., van Dam, J., & Aerts, R. (2008). Critical soil conditions for oxygen stress to plant roots: Substituting the Feddes-function by a process-based modelJ. *Journal of Hydrology*, 147 - 165.

Brocca, L., Melone, F., Moramarco, T., Wagner, W., & Hasenauer, S. (2010). ASCAT soil wetness index validation through in situ and modeled soil moisture data in central Italy. *Remote Sensing of Environment, 114*, 1745-2755.

Capel, W., Delsman, J., Goijer, I., Hoogwoud, J., Jansen, H., Klein, J., . . . Otte, A. (2011). *Klimaat en Droogte.* Deventer: TAUW.

Chen, F., Mitchell, K., Schaake, J., Xue, Y., Pan, H., Koren, V., . . . Betts, A. (1996). Modeling of land surface evaporation by four schemes and comparison with FIFE observations. *Journal of Geophysical Research*, 7251-7268.

Chung, D., De Jeu, R., Dorigo, W., Hahn, S., Melzer, T., Parinussa, R., . . . Wagner, W. (2013). *Algorithm Theoretical Baseline Document.* Wien: TU Wien.

Cultuurtechnische Vereniging. (1992). *Cultuurtechnisch vademecum* (Thirth ed.). Utrecht, Utrecht, The Netherlands: Vereniging voor landinrichting.

Das, N., Entekhabi, D., & Hjoku, E. (2011). An Algorithm for Merging SMAP Radiometer and Radar Data for High-Resolution Soil-Moisture Retrieval. *IEEE Transactions on Geoscience and Remote Sensing, 49*, 1504-15-12.

Delta-T Devices Ltd. (2008). *User Manual for the Profile Probe type PR2.* Cambridge: Delta-T Devices Ltd.

Dente, L., Vekerdy, Z., Su, Z., & Ucer, M. (2011). *Twente soil moisture and soil temperature network.* Enschede: University of Twente.

Dexter, A., Czyz, E., & Gate, O. (2007). A method for prediction of soil penetration resistance. *Soil & Tillage Research*, 412-419.

Ek, M., Mitchell, K., Lin, Y., Rogers, E., Grunmann, P., Koren, V., . . . Tarpley, J. (2003). Implementation of Noah land surface model advances in the National Centers for Environmental Prediction operation mesoscale Eta model. *Journal of Geophysical Research*.

Feddes, R., Kowalik, P., & Zaradny, H. (1978). *Simulation of field water use and crop yield.* Wageningen: Center for Agricultural Publishing and Documentation.

Gyo, Y., Shi, Z., Zhou, L., Jin, X., Tian, Y., & Teng, H. (2013). Integrating remote sensing and proximal sensors for the detection of soil moisture and salinity variability in coastal areas. *Journal of Interactive Agriculture*, 723-731.

Hagemann, S., Haerter, J., & Piani, C. (2010, December). Bias correction of climate model data - the golden solution for impact models or cursed black magic? Bonn, Germany.

Herold, M., Hajnsek, I., & Schmullius, C. (2000). Multifrequency and Polarimetric Radar Remote Sensing of Grassland- geo-biohysical Parameter Retrieval with Airborne E-SAR Data. *The 20th EARSel Symposium Remote Sensing in the 22st Century: A Decade of Trans-European Remote Sensing Cooperation*, (pp. 95-102). Dresden.

Hille Ris Lambers, I., Brekelmans, F., Lensink, R., & Smit, G. (2008). *Bestaand gebruik van rijksinfrastructuur en Natura 2000-gebieden.* Culemborg: Bureau Waardenburg bv.

IPF TU Wien. (2012). *http://www.ipf.tuwien.ac.at/radar/index.php?go=ascat*. Opgeroepen op 10 05, 2013, van http://www.ipf.tuwien.ac.at: http://www.ipf.tuwien.ac.at/radar/index.php?go=ascat

KNMI. (2013). *www.knmi.nl/klimatologie/*. Opgeroepen op 04 12, 2013, van www.knmi.nl: http://www.knmi.nl/klimatologie/

Kornelsen, K., & Coulibaly, P. (2013). Advances in soil moisture retrieval from aperture radar and hydrological applications. *Journal of Hydrology*, 460-489.

Lapen, D., Topp, G., Edwards, M., Gregorich, E., & Curnoe, W. (2004). Combination cone penetration resistance/water content instrumentation to evaluate cone penetration-water content relationships in tillage research. *Soil & Tillage Research*, 51-62.

Mahrt, L., & Ek, K. (1987). The influence of atmospheric stability on potential evaporation. *Boundary Layer Meteorology*, 222-234.

Mahrt, L., & Pan, H. (1984). A two layer model of soil hydrology. *Boundary Layer Meteorology*, 1-20.

McCandless, S., & Jackson, C. (2005). Principles of Synthetic Aperture Radar. In C. Jackson, & J. Apel, *Synthetic Aperture Radar MArine USers Manual* (pp. 1-24). Washington, DC: U.S. Departement of commerce.

McKnight, T., & Hess, D. (2000). Climate zones and types: the Knöppen system. *Physical Geography: A Landscape Appreceiation*.

Mitchell, K. (2005). *The Community Noah Land-Surface Model.* National Oceanic and Atmospheric Administration.

NHI. (2008). *Deelrapportage 11: Bodem.* Utrecht: Deltares.

Pan, H., & Mahrt, L. (1987). Interaction between soil hydrology and boundary layer development. *Boundary Layer Meteorology*, 185-202.

Peerboom, J. (1990). *Waterhuishoudkundige schadefuncties op grasland.* Wageningen: STARING CENTRUM.

Perumpral, J. (1987). Cone penetration applications: a review. *Transactions of the American Society of Agricultural Engineers, 30*, 939-944.

Piani, C., Weedon, G., Best, M., Gomes, S., Viterbo, P., Hagemann, S., & Haerter, J. (2010). Statistical bias correction of global simulated daily precipitation and temperature for the application of hydrological models. *Journal of Hydrology*, pp. 199-215.

Pradhan, Y., Brooks, M., & Saunders, R. (2011). *ESCAT soil moisture climatology.* Crown.

RADARSAT International. (1995). *RADARSAT Illuminated | your guide to products and services.* Richmond,Canada: RADARSAT International.

Rodell, M., Houser, P., Jambor, U., Gottschalck, J., Mitchell, K., Meng, C.-J., . . . Toll, D. (2004). The Global Land Data Assimilation System. *American Meteorological Society*, 381-294.

Sabaghy, S., Van der Velde, R., & Salama, M. (2013). Soil moisture mapping using combined active/passive microwave observations over the east part of the Netherlands.

Sanli, F., Kurucu, Y., Esetlili, M., & Abdikan, S. (2008). Soil moisture estimation from RADARSAT-1, ASAR and PALSAR data in agricultural fields of menemen plane of western Turkey. *unknown*.

Schothorst, C. (1982). *Drainage and behaviour of peat soils.* Wageningen: Intsitute for Land and Water Management Research (ICW).

Unie van Waterschappen. (2007). *Water en Waterschappen.* Den Haag: Unie van Waterschappen.

Van Bakel, J., Schaap, J., & Van Essen, E. (2012). *Is peilverhoging in een kleipolder agrohydrologisch neutraal te realiseren?* Houten: Hoogheemraadschap De Stichtse Rijnlanden.

Van den Akker, J. (2001). *Landbouwkundige vochtsimulatiemodellen als basis voor de berekening van de initiële vochtcondities in dijken.* Wageningen: Alterra.

Verkerk, M., Kaiser, V., Van Ouwerkerk, R., & Heijkers, J. (2012, May). Remote-sensing data kunnen (nog) beter gebruikt worden. *H2O, 10*, 7-8.

Vermeulen, G., & Verwijs, B. (2007). *Inventarisatie van beschikbare technieken voor oogst en transport met lage bodemdruk.* Wageningen: Plant Research International B.V.

Wagner, W., Hahn, S., Kidd, R., Melzer, T., Bartalis, Z., Hasenauer, S., . . . Rubel, F. (2013). The ASCAT Soil Moisture Product: A Review of its Specifications, Validation Results, and Emerging Applications. *Meteorologische Zeitschrift, 22*(1), 5-33.

Wagner, W., Lemoine, G., & Rott, H. (1999). A method for estimating soil moisture from ERS scatterometer and soil data. *Remote Sening of Environment, 70*, 191-207.

Waterschap Groot Salland. (2010). *Waterbeheerplan 2010-2015.* Zwolle: Waterschap Groot Salland.

Willmott, C., & Matsuura, K. (2005). Advvantage of the mean absolute error (MAE) over the root mean square error (RMSE) in assessing average model performance. *Climate Research*, 79-82.

Wösten, H., de Vries, F., Hoogland, T., Massop, H., Veldhuizen, A., Vroon, H., . . . Bolman, A. (2013). *BOFEK2012, de nieuwe, bodemfysische schematisatie van Nederland.* Wageningen: Alterrra Wageningen UR.

Wösten, J., de Vries, F., Denneboom, J., & van Holst, A. (1988). *Generalisatie en bodemfysische vertaling van de bodemkaart van Nederland, 1:250000, ten behoeve van de PAWN-studie.* STIBOKA.

Wösten, J., Veerman, G., De Groot, W., & Stolte, J. (2001). *Waterretentie- en doorlatendheidskarakteristieken van boven- en ondergronden in Nederland: de Staringsreeks.* Wageningen: Alterra.

APPENDICES

Appendix 1 Study area

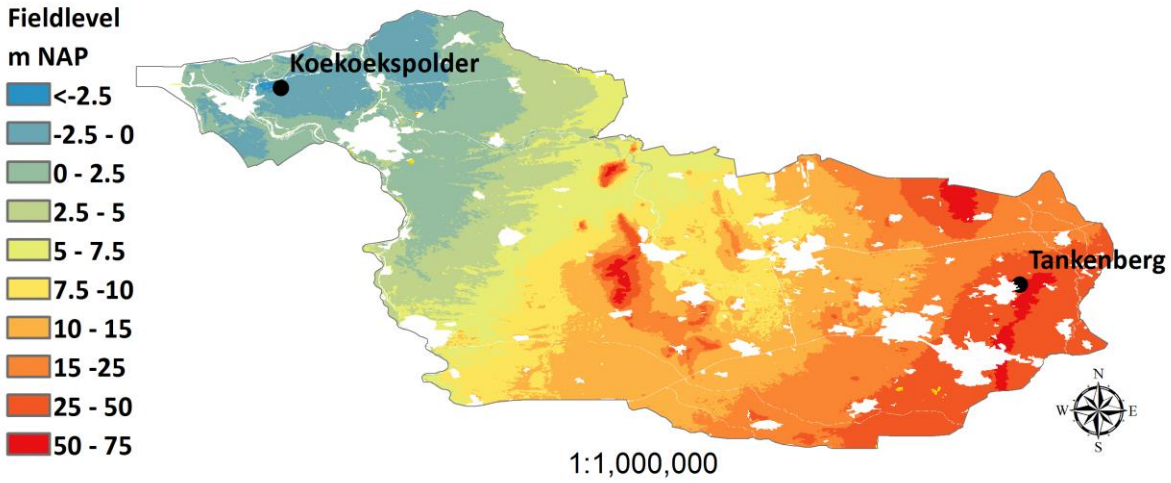

(a)

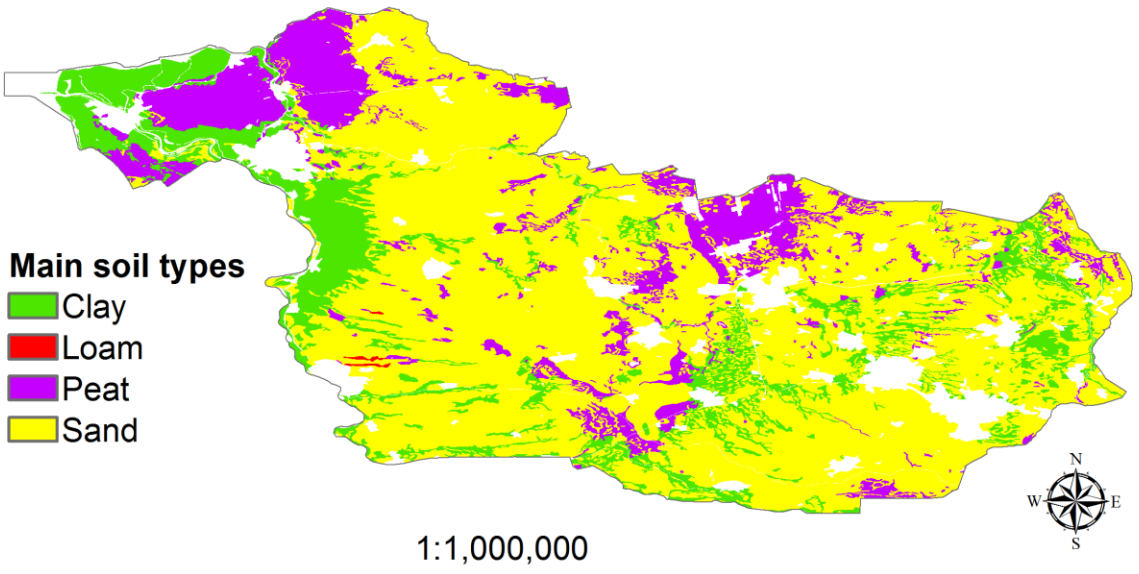

(b)

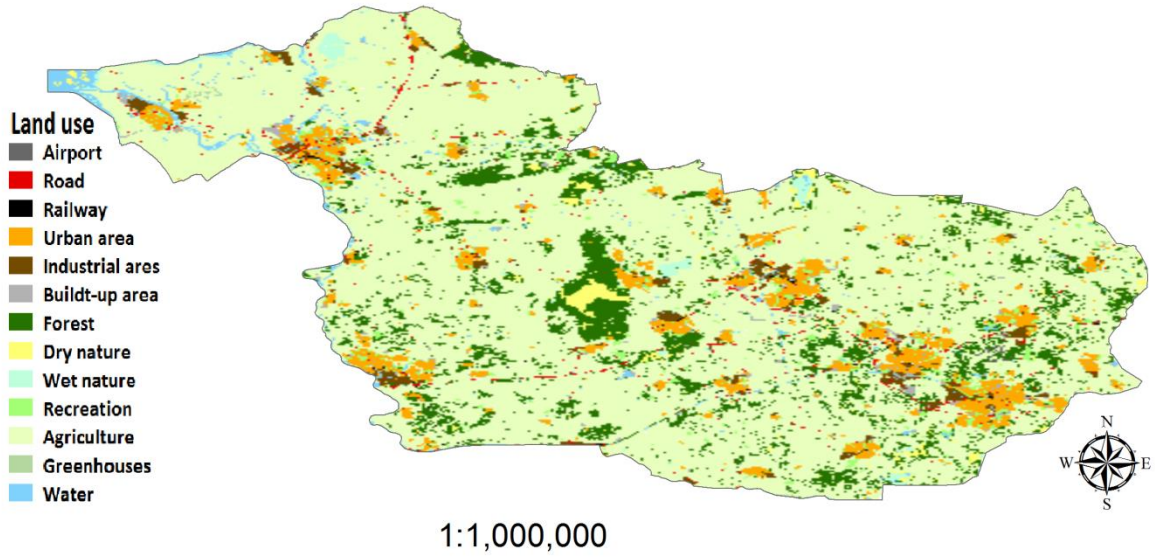

(c)

Figure 30: (a) Field level (modified from digital AHN maps), (b) main soil types (modified from digital PAWN maps)and (c) land use of the study area (Digital map Bestand Bodemgebruik of the CBS) .

Figure 31: Locations of the ITCSM-locations in the field.

Appendix 2 Classification of Dutch soil types

Table 12: PAWN-classification and related Staringreeks-classes of Dutch soil types (NHI, 2008).

Code bodem-opbouw	Omschrijving	Opmerkingen	Opeenvolgende bouwstenen Staringreeks
1	Veraarde bovengrond op diep veen		B18,O17
2	Veraarde bovengrond op veen op zand	Combinatie van veengronden en moerige gronden met zandondergrond. Associaties van moerige gronden en zandgronden vertaald naar zandgronden	B16,O17,O2
3	Kleidek op veen		B11,O17
4	Kleidek op veen op zand	Combinatie van veengronden en moerige gronden met kleidek en zandondergrond. Associaties van moerige gronden en zandgronden vertaald naar klei op zand (19)	B11,O17,O2
5	Zanddek op veen op zand	Combinatie van veengronden en moerige gronden met zanddek en zandondergrond. Associaties moerig en zand vertaald naar zand.	B2,O16.O2
6	Veen op ongerijpte klei	Combinatie van veengronden en moerige gronden met een kleiondergrond. Bij deze gronden kan het veen zowel als toplaag (Wo, Vk) en als tussenlaag (kVk, pVk) voorkomen. Associaties van moerige gronden met kleigronden zijn vertaald naar een kleigrond.	B18.O12
7	Stuifzand	Tot deze groep behoren de landduinen en de kustduinen, inclusief de stranden enz. Deze gronden hebben een laag leemgehalte en de humeuze bouwvoor ontbreekt veelal (Zd.. en Zn..A)	O1
8	Leemarm zand	Hier gaat het vooral om de jonge dekzandruggen en om de uitgestoven laagtes temidden van landduinen. Deze gronden hebben wel een toplaag (Hd21, Y21 en Zn21)	B1,O1
9	Zwaklemig fijn zand	Met name de zwaklemige zandgronden (Hn21, pZn21, pZg21, enz.)	B2,O2
10	Zwaklemig fijn zand op grof zand	Zandgronden met grind of grof zand in de ondergrond. In de bovenlaag vooral zwak lemig, soms ook lemiger.	B2,O2,O5
11	Sterk lemig fijn zand op (kei-)leem	Zandgronden met keileem en of lössleem in de ondergrond (..x, ..t). In de bovenlaag vooral sterk lemig zand, soms ook minder lemig.	B3,O2,O6
12	Enkeerdgronden (fijn zand)	Enkeergronden, gronden met een dikke eerdlaag (> 50 cm), zowel lemig als zwak lemig en leemarm. Gronden met een matig dikke eerdlaag (cHn, cY..) ingedeeld op basis van leemgehalte.	B2,O2
13	Sterk lemig zand	Lemige zandgronden	B3,O3,O2
14	Grof zand	Alle grofzandige gronden	B1,O5
15	Zavel met homogeen profiel		B8,O9
16	Lichte klei met homogeen profiel		B10,O10
17	Klei met zware tussenlaag of ondergrond		B12,O13
18	Klei op veen	Begindiepte veenondergrond 40 – 120 cm-mv.	B12,O13,O17
19	Klei op zand	Begindiepte zandondergrond 25 – 80 cm-mv.	B8,O10,,O2
20	Klei op grof zand	Begindiepte grofzandige ondergrond 25 – 120cm-mv..	B8,O10,O5
21	Leem	Alle leemgronden, inclusief keileemgronden (KX en KT)	O15

Table 13: "Buildingstones" soil types Staringreeks (Wösten et al., 2013).

Code	Omschrijving
Bovengronden	
B1	Leemarm, zeer fijn tot matig fijn zand
B2	Zwak lemig, zeer fijn tot matig fijn zand
B3	Sterk lemig, zeer fijn tot matig fijn zand
B4	Zeer sterk lemig, zeer fijn tot matig fijn zand
B5	Grof zand
B6	Keileem
B7	Zeer lichte zavel
B8	Matig lichte zavel
B9	Zware zavel
B10	Lichte klei
B11	Matig zware klei
B12	Zeer zware klei
B13	Zandige leem
B14	Siltige leem
B15	Venig zand
B16	Zandig veen en veen
B17	Venige klei
B18	Kleiig veen
Ondergronden	
O1	Leemarm, zeer fijn tot matig fijn zand
O2	Zwak lemig, zeer fijn tot matig fijn zand
O3	Sterk lemig, zeer fijn tot matig fijn zand
O4	Zeer sterk lemig, zeer fijn tot matig fijn zand
O5	Grof zand
O6	Keileem
O7	Beekleem
O8	Zeer lichte zavel
O9	Matig lichte zavel
O10	Zware zavel
O11	Lichte klei
O12	Matig zware klei
O13	Zeer zware klei
O14	Zandige leem
O15	Siltige leem
O16	Oligotroof veen
O17	Mesotroof en eutroof veen
O18	Moerig tussenlaag

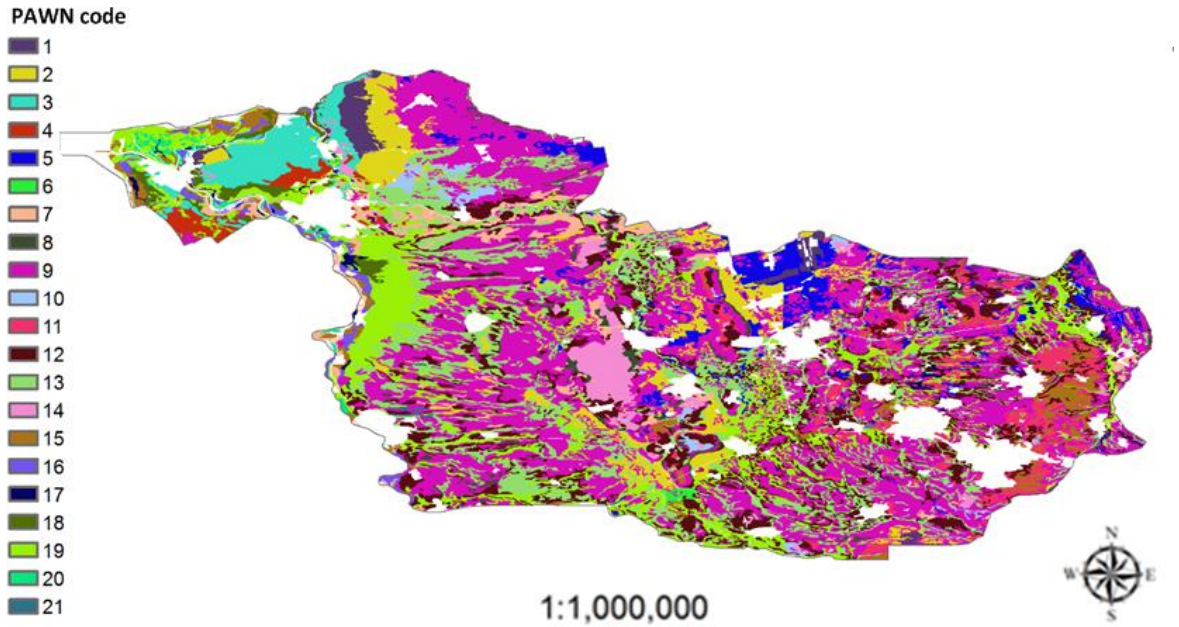

Figure 32: PAWN code map of the study area. Adapted from the digital PAWN map

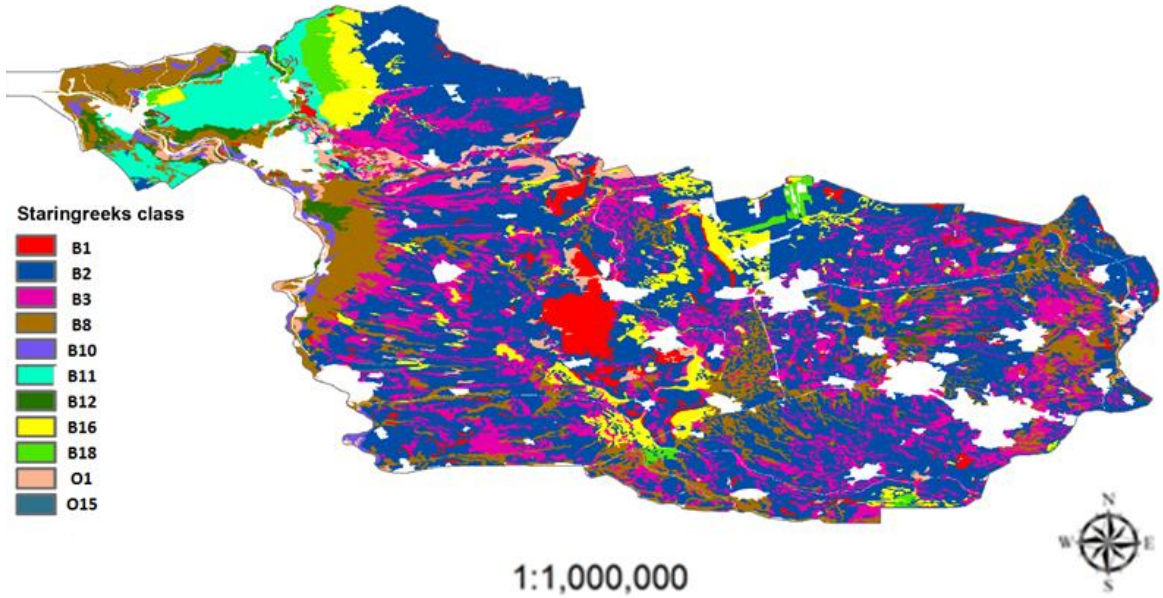

Figure 33: Staringreeks map of the study area. Modified form the digital PAWN map.

Appendix 3 Linear scaling method

The linear scaling method scales the volumetric soil moisture between dry ($\theta_{SWI\,1}$ = 0) and wet ($\theta_{SWI\,1}$ = n). This method is explained below using the scaling term S_{dry} or S_{wet} for the dry and wet situations and $\sigma^\circ_{c,min}$ and $\sigma^\circ_{c,max}$ for the minimal and maximal RADARSAT-2 backscatter over all periods, in this study -16 dB and -5 dB.

Scaling dry ($\sigma^\circ_m < \sigma^\circ_c$):

$$\theta_m = \theta_{SWI\,1} + S_{dry}\,\beta(\sigma^\circ_{min} - \sigma^\circ_c) = 0$$

$$0 = \theta_{SWI\,1} + S_{dry}\,\beta(\sigma^\circ_{min} - \sigma^\circ_c)$$

$$-\theta_{SWI\,1} = S_{dry}\,\beta(\sigma^\circ_{min} - \sigma^\circ_c)$$

$$S_{dry} = -\frac{\theta_{SWI\,1}}{\beta(\sigma^\circ_{min} - \sigma^\circ_c)}$$

$$\theta_m = \theta_{SWI\,1} + -\frac{\theta_{SWI\,1}}{\beta(\sigma^\circ_{min} - \sigma^\circ_c)}\,\beta(\sigma^\circ_m - \sigma^\circ_c)$$

$$\theta_m = \theta_{SWI\,1} - \frac{\theta_{SWI\,1}}{(\sigma^\circ_{min} - \sigma^\circ_c)}\,(\sigma^\circ_m - \sigma^\circ_c)$$

Scaling wet ($\sigma^\circ_m > \sigma^\circ_c$):

$$\theta_m = \theta_{SWI\,1} + S_{max}\,\beta(\sigma^\circ_{max} - \sigma^\circ_c) = n_{max}$$

$$n_{max} = \theta_{SWI\,1} + S_{max}\,\beta(\sigma^\circ_{max} - \sigma^\circ_c)$$

$$n_{max} - \theta_{SWI\,1} = S_{max}\,\beta(\sigma^\circ_{max} - \sigma^\circ_c)$$

$$S_{max} = \frac{n_{max} - \theta_c}{\beta(\sigma^\circ_{max} - \sigma^\circ_c)}$$

$$\theta_m = \theta_{SWI\,1} + \frac{n_{max} - \theta_{SWI\,1}}{\beta(\sigma^\circ_{max} - \sigma^\circ_c)}\,\beta(\sigma^\circ_m - \sigma^\circ_c)$$

$$\theta_m = \theta_{SWI\,1} + \frac{n_{max} - \theta_{SWI\,1}}{(\sigma^\circ_{max} - \sigma^\circ_c)}\,(\sigma^\circ_m - \sigma^\circ_c)$$

Combination dry and wet:

If $\sigma^\circ_m > \sigma^\circ_c$: $\theta_m = \theta_{SWI\,1} + \frac{n_{max} - (\theta_{SWI\,1})}{(\sigma^\circ_{max} - \sigma^\circ_c)}\,(\sigma^\circ_m - \sigma^\circ_c)$ (VIII)

Else : $\theta_m = \theta_{SWI\,1} - \frac{(\theta_{SWI\,1})}{(\sigma^\circ_{min} - \sigma^\circ_c)}\,(\sigma^\circ_m - \sigma^\circ_c)$ (IX)

Appendix 4 Critical soil moisture content values in relation to the penetration resistance

The penetration resistance will be determinate in different ways. For five of the eleven Staringreeks soil types used a relation between matric head or volumetric soil moisture content can be found in literature. These are presented in 0a. The critical values of the other soil types are obtained in 0b. 0c gives an overview of all the critical values and all the matric head values will be converted to soil moisture content values.

a. Penetration resistance relation to soil moisture in literature

Figure 34 and Figure 35 are the only two figures found in literature that present a relation between the penetration resistance and the matric head or moisture content. Peerboom (1990) presents the relation for Staringreeks B101, B103, clayey peat and "kom-clay". The used codes B101 and B103 by Peerboom are representing B1 and B3 as used in Wösten et al. (2013) is clear. Wösten et al. (2013) also mention clayey peat as a topsoil in the Staringreeks (code B18) and the assumption is made that both researchers are talking about the same soil types. "Kom-clay" is not direct mentioned in the Staringreeks, its properties are used to quantify it to the right Staringreeks code. Because "Kom-clay" is heavy clay that arises by sedimentation of small clay particles during flooding of the land by a river or the se, it is classified as Staringreeks B12 (heavy clay). Schothorst (1982) presents the relation between the penetration resistance and volumetric moisture content for peat. The peat soil with on organic matter of 40 to 50% is represented in the Staringreeks by B16: peat and sandy peat.

Table 14: Critical values of the matric head and volumetric soil moisture content available in literature from Peerboom (1990) and Schothorst (1982).

Staringreeks classification	Matric head (cm)		Volumetric soil moisture content		Derived from
	0.5 MPa	0.6 MPa	0.5 MPa	0.6 Mpa	
B1	-2	-14	-	-	Peerboom
B3	-18	-33	-	-	Peerboom
B12	-70	-90	-	-	Peerboom
B16	-	-	0.68	0.65	Schothorst
B18	-56	-78	-	-	Peerboom

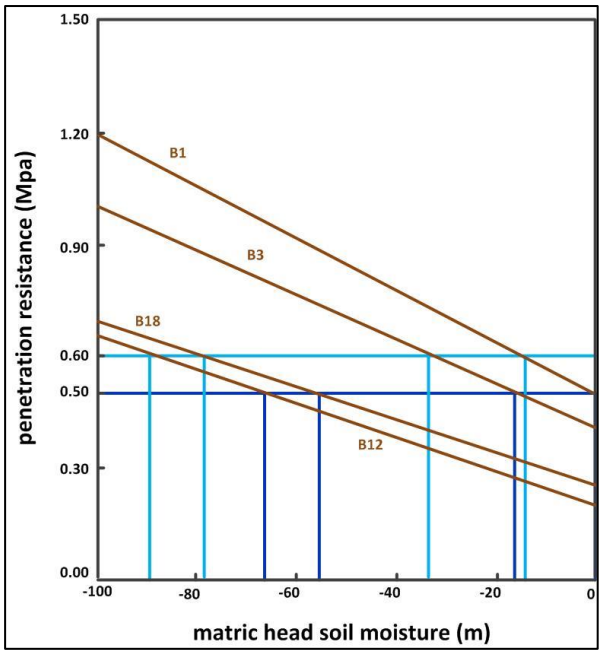

Figure 34: Relation between penetration resistance and matric head for the soil types loamless fine to moderate fine sand (B1), loamy, fine to moderate fine sand (B3), heavy peat (B12) and clayey peat (B18) (Peerboom, 1990).

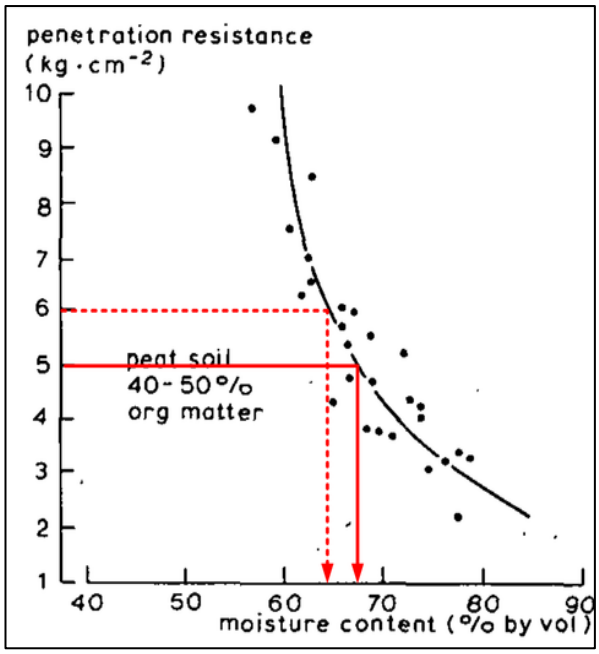

Figure 35: Relation between the penetration resistance and volume moisture content for peat (B16) (Schothorst, 1982).

b. Penetration resistance in relation to soil moisture

Linear interpolation between the critical values for the carrying capacity of the five known soil types is used to get a critical value for the soil types whose relation between penetration resistance and matric head/soil moisture content is unknown until now.

The characteristics of B1, B2 and B3 in the Staringsreeks makes is possible to get the critical matric head values for B2 by interpolation between B1 and B3. This results in a critical matric head of -10 cm for 0.5 MPa and -24 cm for 0.6 MPa. For B8, B10 and B11 the interpolation is done between B3 and B12. Equations and outcome of this interpolation can be found in Table 15.

Table 15: Linear interpolation of critical matric head for the critical penetration resistances 0.5 MPa and 0.6 MPa for the missing soil types B2, B8, B10 and B11.

Staringreeks classification	Linear interpolation equation	Critical matric head (cm)	
		0.5 Mpa	0.6 Mpa
B2	$h_{B2} = h_{B1} - \frac{\lvert h_{B1}\rvert - \lvert h_{B3}\rvert}{2}$	-10	-24
B8	$h_{B8} = h_{B3} - 5 \times \left(\frac{\lvert h_{B3}\rvert - \lvert h_{B12}\rvert}{9}\right)$	-47	-65
B10	$h_{B10} = h_{B3} - 7 \times \left(\frac{\lvert h_{B3}\rvert - \lvert h_{B12}\rvert}{9}\right)$	-58	-77
B11	$h_{B11} = h_{B3} - 8 \times \left(\frac{\lvert h_{B3}\rvert - \lvert h_{B12}\rvert}{9}\right)$	-64	-84

The soil types O1 and O15 of the subsoil, O is coming from the Dutch word “onder” that means “sub”, are treated in a different way. Assuming that the characteristics of O1 and B1 are the same, both loamless fine to moderate fine sandy soils, justify the use of the same critical values of the matric head for O1 as for B1. For O15, which have the same characteristics as B14, a linear extrapolation of the matric head between B3 and B12 is used. This extrapolation is doubtful because O15 is a loamy soil and is differs a lot in characteristics of sandy and clayey soils. Despite this, there is no better method available and the extrapolation will be used.

Table 16: Linear extrapolation of critical matric head for the critical penetration resistances 0.5 MPa and 0.6 MPa for the missing soil type O15.

Staringreeks classification	Linear interpolation equation	Critical matric head (cm)	
		0.5 Mpa	0.6 Mpa
O15	$h_{O15} = h_{B12} - 11 \times \left(\frac{\lvert h_{B3}\rvert - \lvert h_{B12}\rvert}{9}\right)$	-82	-103

c. Critical volumetric soil moisture content

The critical matric head of the soil types has to be converted to critical volumetric soil moisture contents because this will be the unit in the downscaled soil moisture maps. The conversion from matric head to volumetric soil moisture content is done using the matric head/volumetric soil moisture content relation described of Van Genuchten and used by Wösten et al. (2001) in combination with the staringreeks. An overview of these results can be found in Table 17.

Table 17: Conversion from matric head to volumetric soil moisture content of the critical values for a penetration resistance of 0.5 MPa and 0.6 MPa.

Staringreeks classification	Matric head (cm)		Soil moisture content (volumetric)		Source
	0.5 MPa	0.6 MPa	0.5 MPa	0.6 MPa	
B1	-2	-14	0.42	0.38	Derived from Peerboom (1990)
B2	-10	-24	0.39	0.36	Linear interpolation of matric head between B1 and B3
B3	-18	-33	0.43	0.41	Derived from Peerboom (1990)
B8	-47	-65	0.40	0.39	Linear interpolation of soil moisture content between B3 and B12
B10	-58	-77	0.41	0.40	
B11	-64	-84	0.55	0.54	
B12	-70	-90	0.50	0.49	Derived from Peerboom (1990)
B16			0.68	0.65	Derived from Schothorst (1982)
B18	-56	-78	0.70	0.68	Derived from Peerboom (1990)
O1	-2	-14	0.35	0.31	Matric head assumed to be equal as B1
O15	-82	-103	0.37	0.36	Linear interpolation of soil moisture content between B12 and B16 (neglecting extra clay layer in the bottom class)

Appendix 5 Soil Moisture Stress indication (SMS-i) diagrams

This appendix includes the SMS-i diagrams of the eleven soil types of the Staringreeks which are underlying the different PAWN-classifications. First the different classes are presented together with their color, secondly the SMS-i diagrams of all soils are presented.

a. Soil Moisture Stress indication classes

A I. No moisture (light red): grass growth is limited by the available amount of soil and the carrying capacity is sufficient for both machinery and cattle.

A II. Moisture stress (light orange): grass growth is limited by the available amount of soil moisture and the carrying capacity is sufficient for both machinery and cattle.

A III. Ideal growing and carrying (light green): grass growth is not limited by the available amount of soil moisture or oxygen in the soil and the carrying capacity is sufficient for both machinery and cattle.

A IV. Oxygen stress and ideal carrying capacity (light turquoise): grass growth is limited by the available amount of oxygen for took take up in the soil and the carrying capacity is sufficient for both machinery and cattle.

A V. No oxygen and Ideal carrying capacity (light blue): No oxygen is available in the soil for root take up, the carrying capacity is good for both machinery and cattle.

B I. No moisture and machinery (red): grass growth is limited by the available amount of soil moisture and the carrying capacity is only sufficient for machinery. (status excluded in this research)

B II. Moisture stress and machinery (orange): grass growth is limited by the available amount of soil moisture and the carrying capacity is only sufficient for machinery. (status excluded in this research)

B III. Ideal growing and machinery (green): grass growth is not limited by the available amount of soil moisture or oxygen in the soil and the carrying capacity is only sufficient for machinery.

B IV. Oxygen stress and machinery (turquoise): grass growth is limited by the available amount of oxygen for took take up in the soil and the carrying capacity is only sufficient for machinery.

B V. No oxygen and machinery (blue): no oxygen is available for root take-up in the soil and the carrying capacity is only insufficient for machinery.

C I. No moisture and no carrying capacity (dark red): grass growth is limited by the available amount of soil moisture and the carrying capacity is insufficient for machinery and cattle. (status excluded in this research)

C II. Water stress (dark turquoise): water availability is the restrictive factor in grass growth but there is a certain amount available for root take-up and the carrying

capacity is insufficient for both machinery and cattle.

C III. Ideal growing (dark green): grass growth is not limited by the available amount of soil moisture or oxygen in the soil but the carrying capacity is still insufficient for both machinery and cattle.

C IV. Oxygen stress (dark turquoise): oxygen availability is the restrictive factor in grass growth but there is a certain amount available for root take-up and the carrying capacity is insufficient for both machinery and cattle.

C V. No oxygen (dark blue): no oxygen is available for root take-up in the soil and the carrying capacity is insufficient for both machinery and cattle.

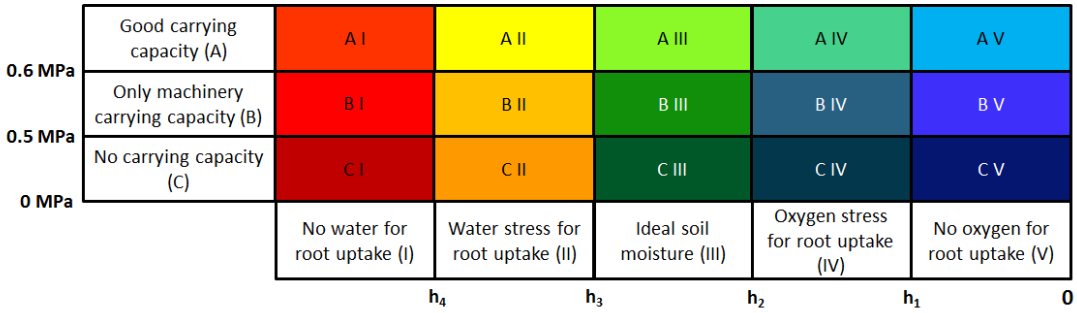

Figure 36: Soil Moisture Stress indication diagram class colours.

b. Soil Moisture Stress indication diagram per soil type

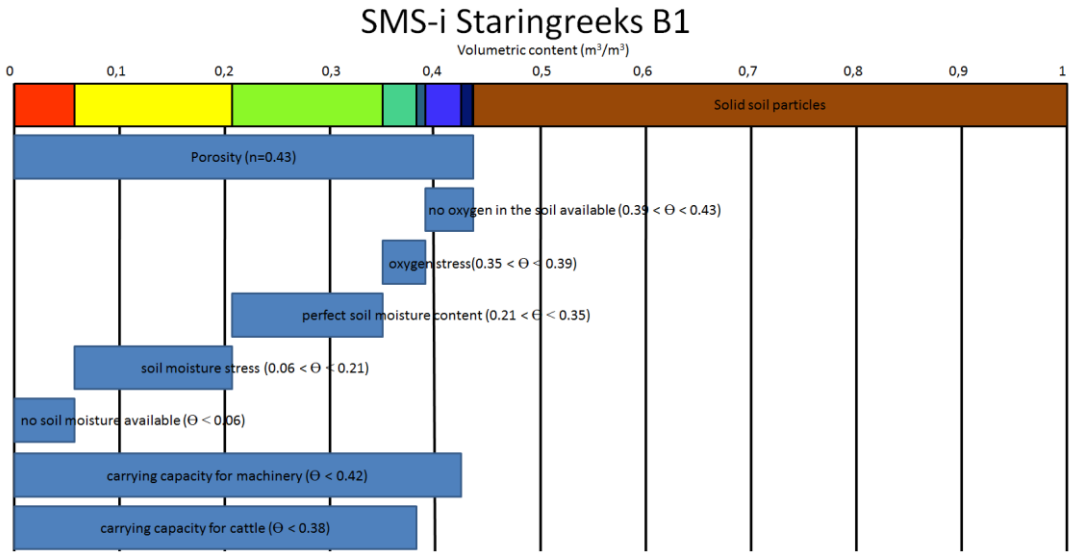

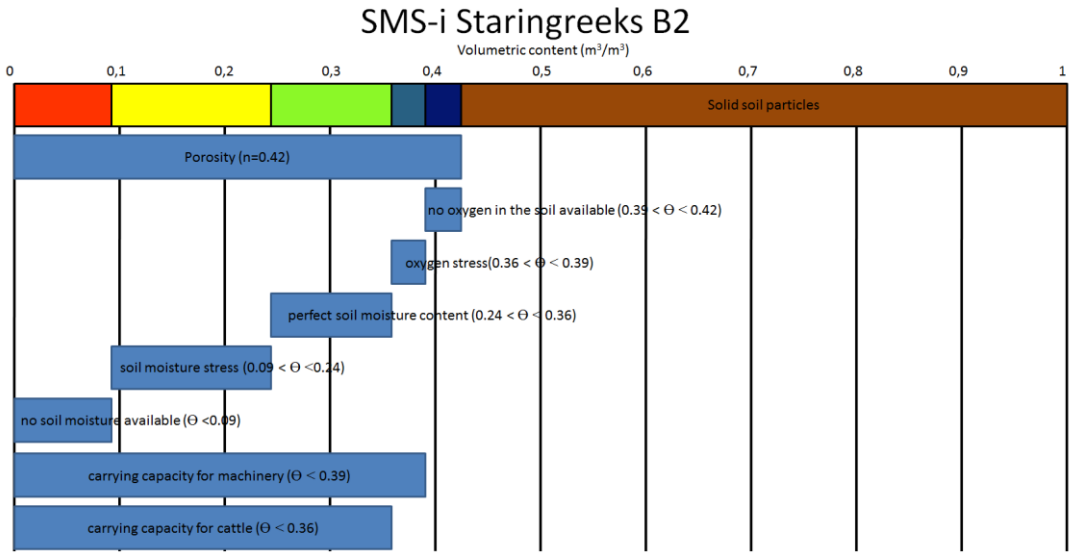
SMS-i Staringreeks B2
Volumetric content (m³/m³)
0
0,1
0,2
0,3
0,4
0,5
0,6
0,7
0,8
0,9
1
Solid soil particles
Porosity (n=0.42)
no oxygen in the soil available (0.39 < Θ < 0.42)
oxygen stress(0.36 < Θ < 0.39)
perfect soil moisture content (0.24 < Θ < 0.36)
soil moisture stress (0.09 < Θ <0.24)
no soil moisture available (Θ <0.09)
carrying capacity for machinery (Θ < 0.39)
carrying capacity for cattle (Θ < 0.36)

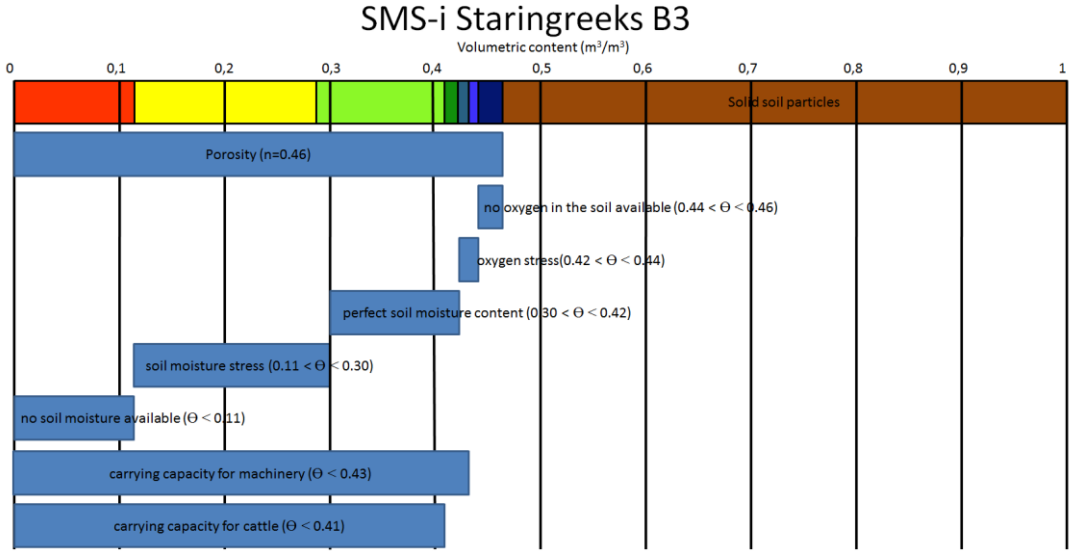
SMS-i Staringreeks B3
Volumetric content (m³/m³)
0
0,1
0,2
0,3
0,4
0,5
0,6
0,7
0,8
0,9
1
Solid soil particles
Porosity (n=0.46)
no oxygen in the soil available (0.44 < Θ < 0.46)
oxygen stress(0.42 < Θ < 0.44)
perfect soil moisture content (0.30 < Θ < 0.42)
soil moisture stress (0.11 < Θ < 0.30)
no soil moisture available (Θ < 0.11)
carrying capacity for machinery (Θ < 0.43)
carrying capacity for cattle (Θ < 0.41)

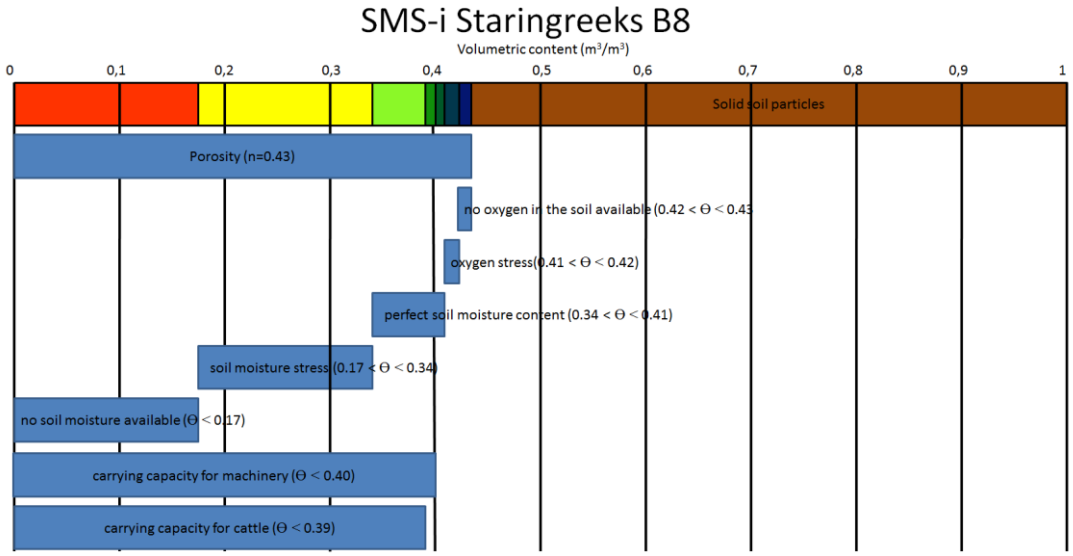
SMS-i Staringreeks B8
Volumetric content (m³/m³)
0
0,1
0,2
0,3
0,4
0,5
0,6
0,7
0,8
0,9
1
Solid soil particles
Porosity (n=0.43)
no oxygen in the soil available (0.42 < Θ < 0.43
oxygen stress(0.41 < Θ < 0.42)
perfect soil moisture content (0.34 < Θ < 0.41)
soil moisture stress (0.17 < Θ < 0.34)
no soil moisture available (Θ < 0.17)
carrying capacity for machinery (Θ < 0.40)
carrying capacity for cattle (Θ < 0.39)

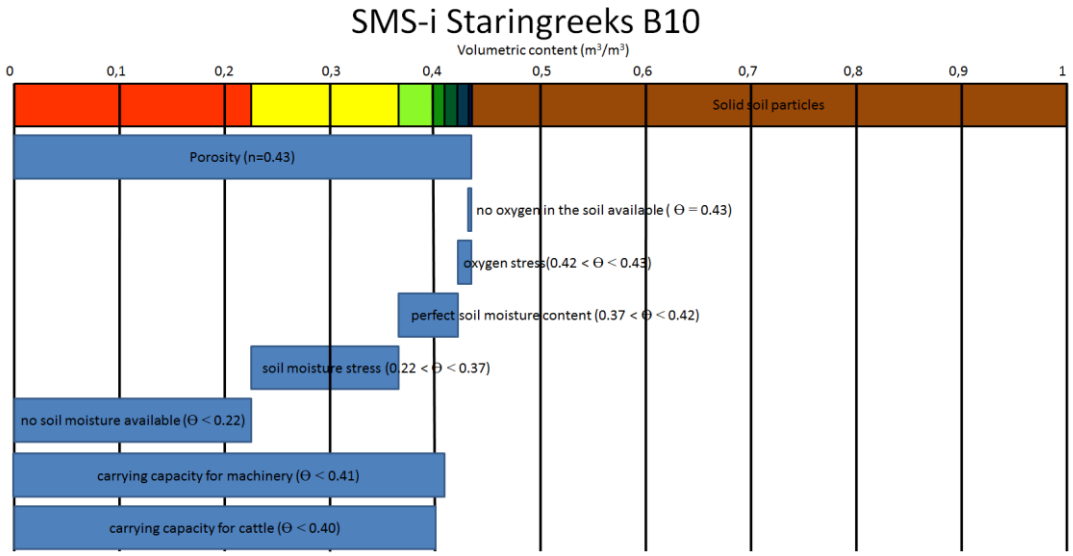
SMS-i Staringreeks B10
Volumetric content (m³/m³)
0
0,1
0,2
0,3
0,4
0,5
0,6
0,7
0,8
0,9
1
Solid soil particles
Porosity (n=0.43)
no oxygen in the soil available (Θ = 0.43)
oxygen stress(0.42 < Θ < 0.43)
perfect soil moisture content (0.37 < Θ < 0.42)
soil moisture stress (0.22 < Θ < 0.37)
no soil moisture available (Θ < 0.22)
carrying capacity for machinery (Θ < 0.41)
carrying capacity for cattle (Θ < 0.40)

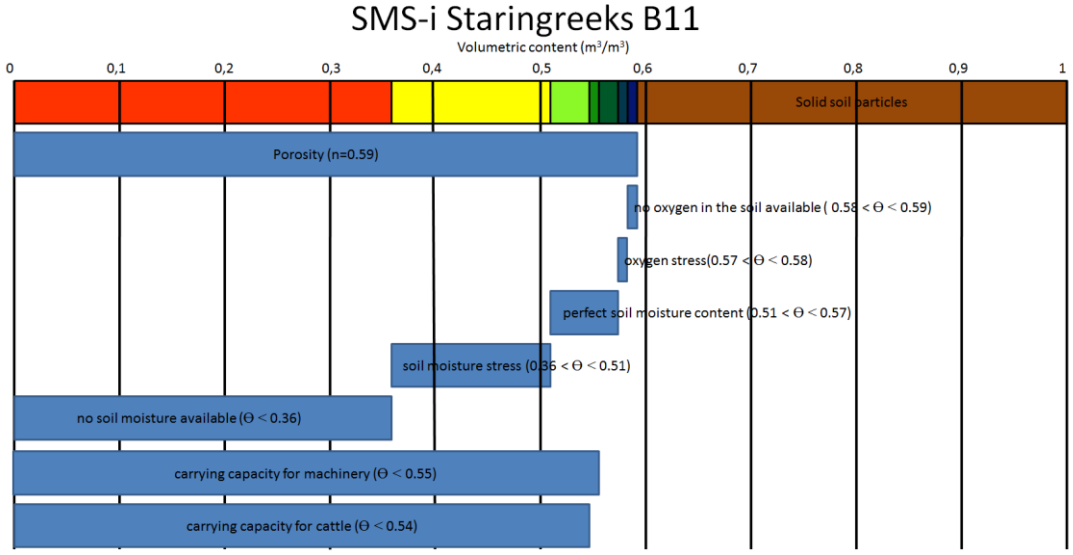
SMS-i Staringreeks B11
Volumetric content (m³/m³)
0
0,1
0,2
0,3
0,4
0,5
0,6
0,7
0,8
0,9
1
Solid soil particles
Porosity (n=0.59)
no oxygen in the soil available (0.58 < Θ < 0.59)
oxygen stress(0.57 < Θ < 0.58)
perfect soil moisture content (0.51 < Θ < 0.57)
soil moisture stress (0.36 < Θ < 0.51)
no soil moisture available (Θ < 0.36)
carrying capacity for machinery (Θ < 0.55)
carrying capacity for cattle (Θ < 0.54)

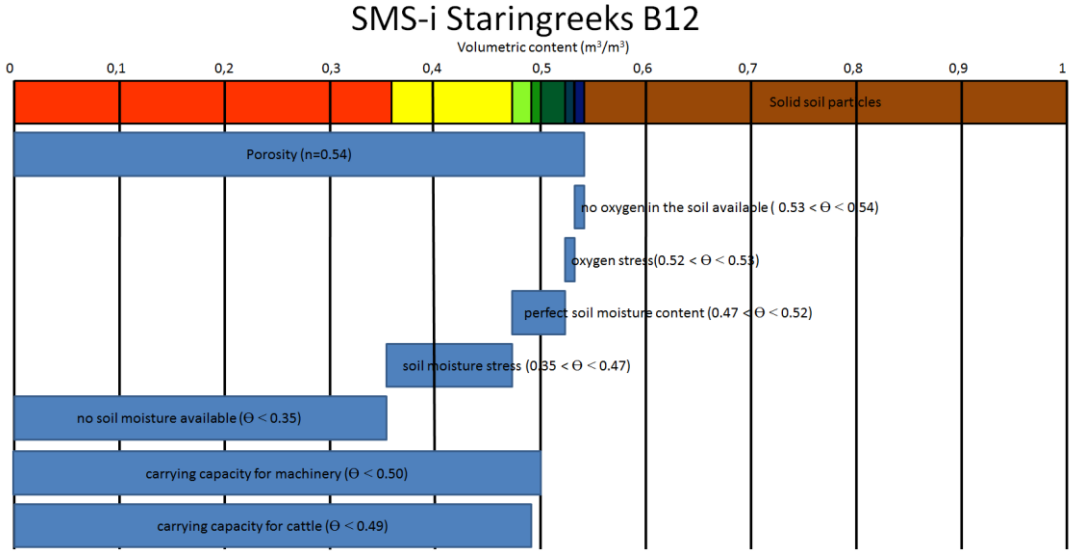
SMS-i Staringreeks B12
Volumetric content (m³/m³)
0
0,1
0,2
0,3
0,4
0,5
0,6
0,7
0,8
0,9
1
Solid soil particles
Porosity (n=0.54)
no oxygen in the soil available (0.53 < Θ < 0.54)
oxygen stress(0.52 < Θ < 0.53)
perfect soil moisture content (0.47 < Θ < 0.52)
soil moisture stress (0.35 < Θ < 0.47)
no soil moisture available (Θ < 0.35)
carrying capacity for machinery (Θ < 0.50)
carrying capacity for cattle (Θ < 0.49)

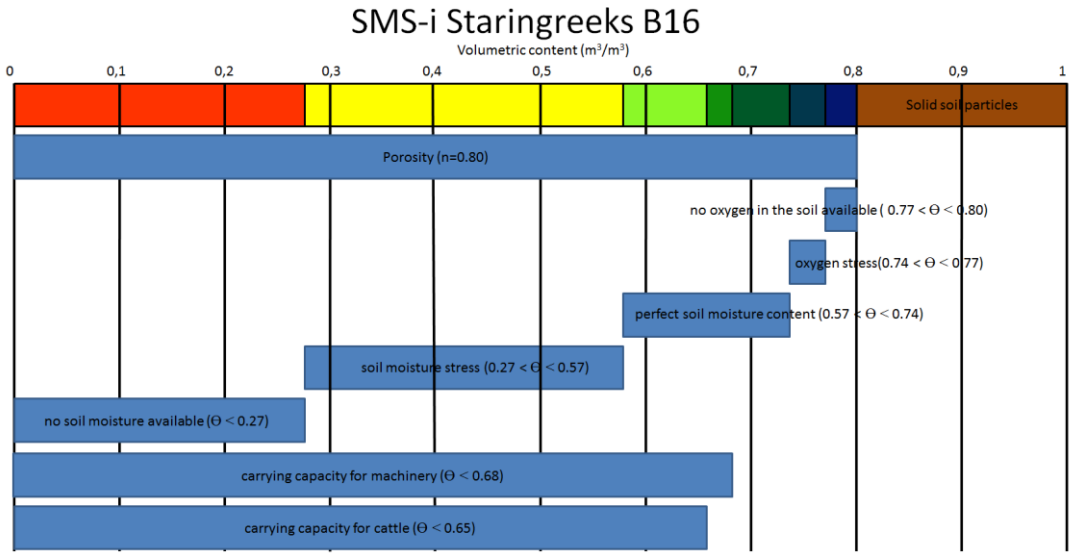
SMS-i Staringreeks B16
Volumetric content (m³/m³)
0
0,1
0,2
0,3
0,4
0,5
0,6
0,7
0,8
0,9
1
Solid soil particles
Porosity (n=0.80)
no oxygen in the soil available (0.77 < Θ < 0.80)
oxygen stress(0.74 < Θ < 0.77)
perfect soil moisture content (0.57 < Θ < 0.74)
soil moisture stress (0.27 < Θ < 0.57)
no soil moisture available (Θ < 0.27)
carrying capacity for machinery (Θ < 0.68)
carrying capacity for cattle (Θ < 0.65)

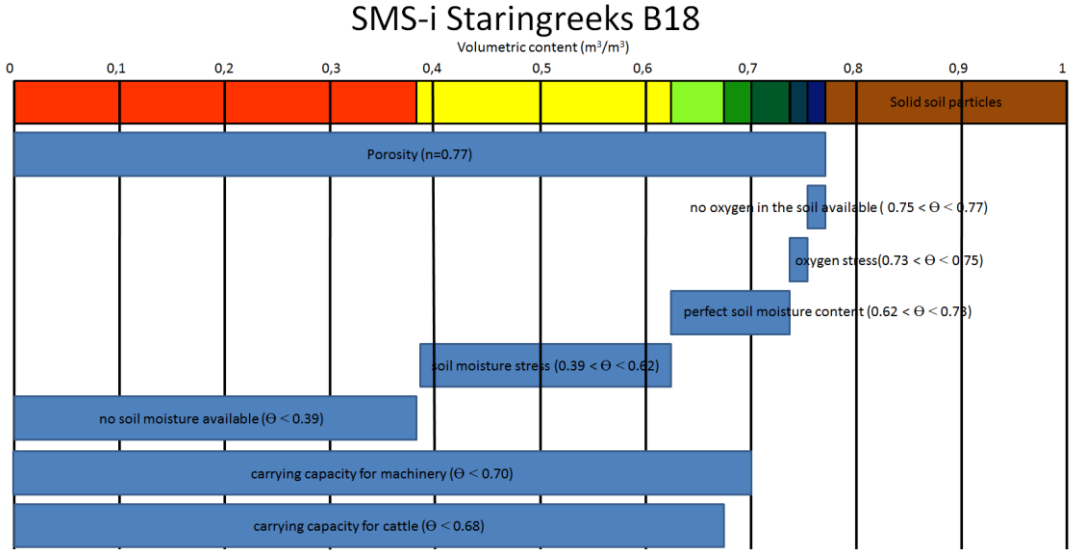
SMS-i Staringreeks B18
Volumetric content (m³/m³)
0
0,1
0,2
0,3
0,4
0,5
0,6
0,7
0,8
0,9
1
Solid soil particles
Porosity (n=0.77)
no oxygen in the soil available (0.75 < Θ < 0.77)
oxygen stress(0.73 < Θ < 0.75)
perfect soil moisture content (0.62 < Θ < 0.73)
soil moisture stress (0.39 < Θ < 0.62)
no soil moisture available (Θ < 0.39)
carrying capacity for machinery (Θ < 0.70)
carrying capacity for cattle (Θ < 0.68)

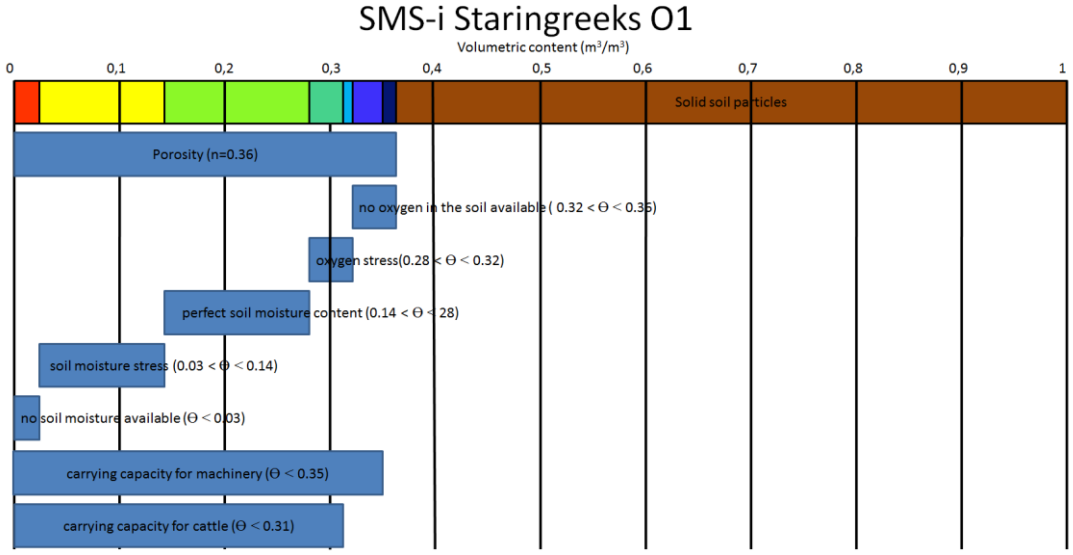
SMS-i Staringreeks O1
Volumetric content (m³/m³)
0
0,1
0,2
0,3
0,4
0,5
0,6
0,7
0,8
0,9
1
Solid soil particles
Porosity (n=0.36)
no oxygen in the soil available (0.32 < Θ < 0.36)
oxygen stress(0.28 < Θ < 0.32)
perfect soil moisture content (0.14 < Θ < 28)
soil moisture stress (0.03 < Θ < 0.14)
no soil moisture available (Θ < 0.03)
carrying capacity for machinery (Θ < 0.35)
carrying capacity for cattle (Θ < 0.31)

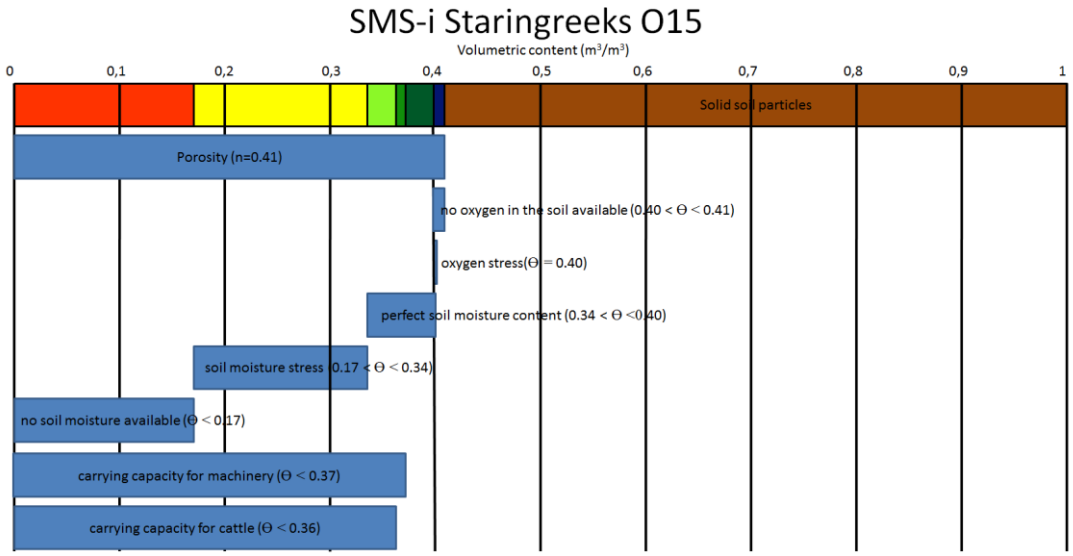
SMS-i Staringreeks O15
Volumetric content (m³/m³)
0
0,1
0,2
0,3
0,4
0,5
0,6
0,7
0,8
0,9
1
Solid soil particles
Porosity (n=0.41)
no oxygen in the soil available (0.40 < Θ < 0.41)
oxygen stress(Θ = 0.40)
perfect soil moisture content (0.34 < Θ <0.40)
soil moisture stress (0.17 < Θ < 0.34)
no soil moisture available (Θ < 0.17)
carrying capacity for machinery (Θ < 0.37)
carrying capacity for cattle (Θ < 0.36)

Appendix 6 Results

a. Soil moisture sensitivity parameter β

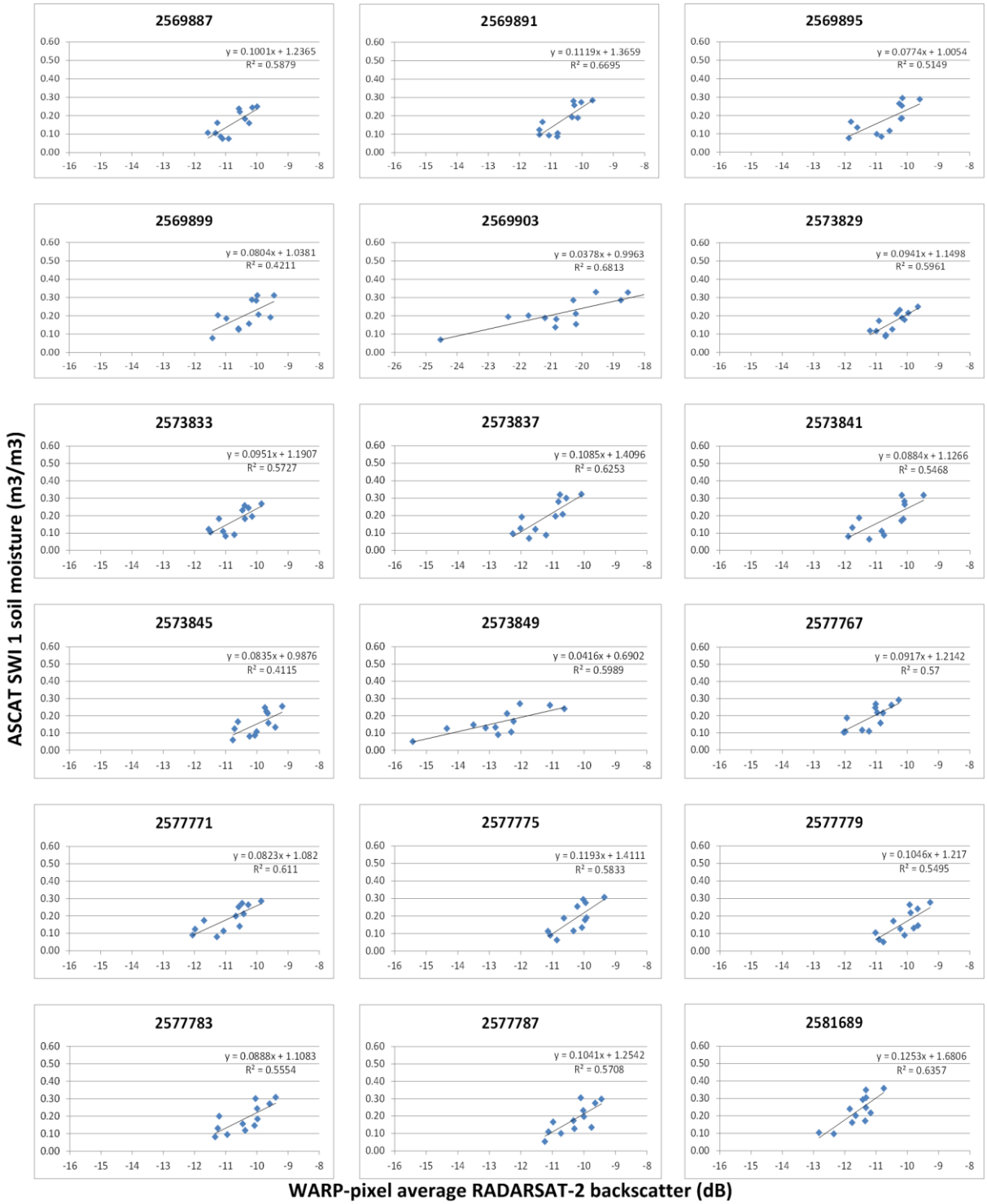

Figure 37A: $\Theta_{SWI\,1}$ versus σ_c for calculation of the yearly beta (part I).

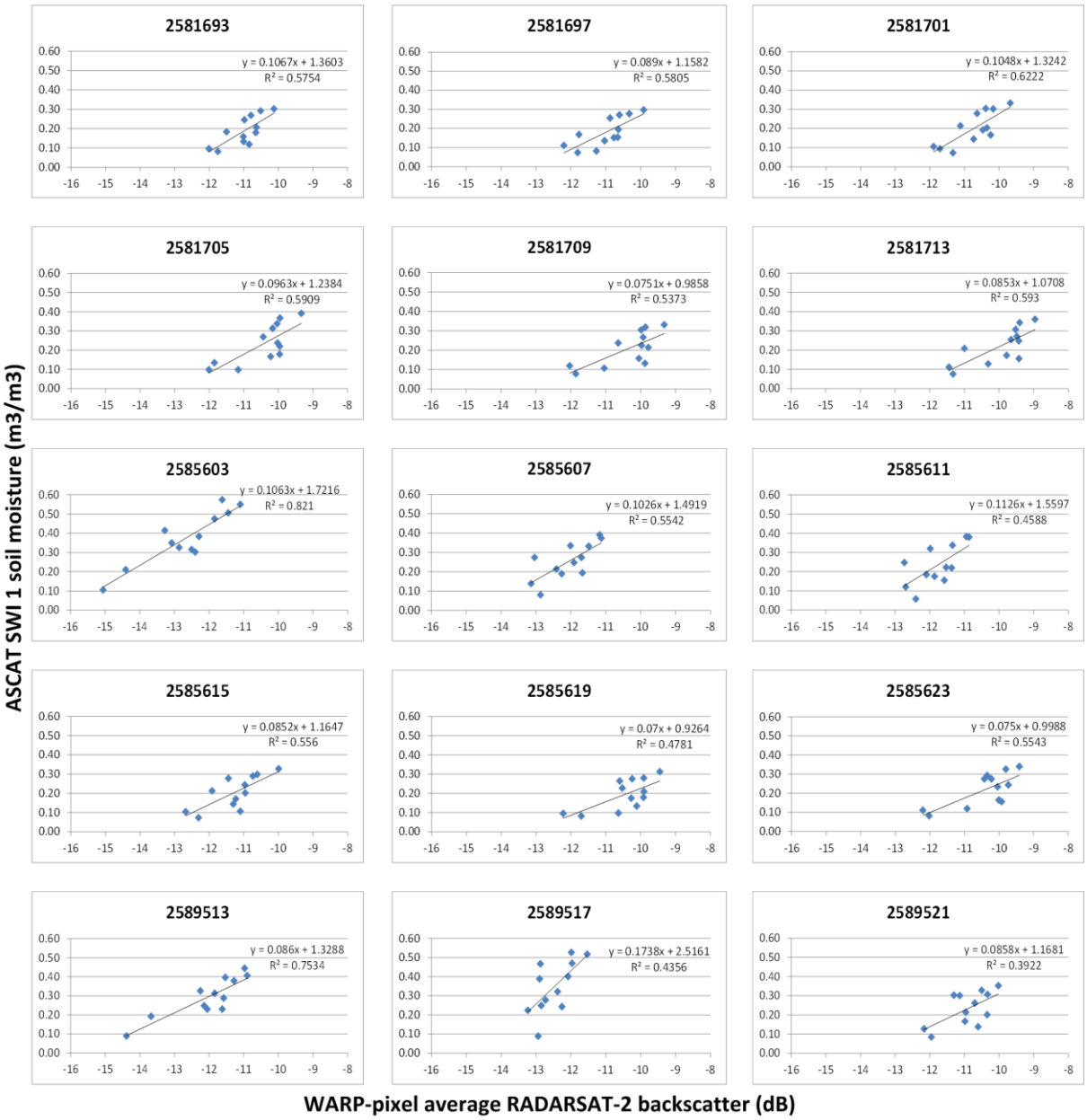

Figure 27B: $\Theta_{SWI\ 1}$ versus σ_c for calculation of the yearly beta (part II).

Table 18: Values for the 24 daily soil moisture sensitivity parameter ($\theta_{c,24}$).

	Calculation date											
WARP-ID	**12-3-2012**	**5-4-2012**	**29-4-2012**	**23-5-2012**	**16-6-2012**	**10-7-2012**	**3-8-2012**	**27-8-2012**	**20-9-2012**	**14-10-2012**	**7-11-2012**	**1-12-2012**
2569887	0.024	0.009	0.014	0.009	0.018	0.008	0.007	0.016	0.007	0.023	0.025	0.021
2569891	0.027	0.011	0.015	0.009	0.019	0.010	0.008	0.019	0.008	0.027	0.029	0.025
2569895	0.026	0.012	0.014	0.006	0.018	0.011	0.009	0.018	0.008	0.029	0.030	0.025
2569899	0.028	0.017	0.018	0.007	0.020	0.015	0.012	0.021	0.012	0.031	0.033	0.028
2569903	0.017	0.009	0.009	0.003	0.009	0.009	0.007	0.010	0.008	0.017	0.018	0.014
2573829	0.022	0.011	0.016	0.011	0.019	0.012	0.009	0.018	0.008	0.023	0.026	0.021
2573833	0.024	0.010	0.016	0.009	0.018	0.010	0.007	0.019	0.008	0.025	0.027	0.022
2573837	0.028	0.011	0.016	0.008	0.018	0.011	0.006	0.019	0.008	0.030	0.032	0.026
2573841	0.028	0.011	0.016	0.007	0.017	0.010	0.006	0.018	0.008	0.031	0.033	0.026
2573845	0.023	0.012	0.016	0.006	0.014	0.011	0.008	0.016	0.009	0.025	0.028	0.022
2573849	0.023	0.009	0.011	0.003	0.010	0.010	0.007	0.014	0.009	0.022	0.024	0.017
2573853	0.003	0.002	0.002	0.000	0.002	0.002	0.001	0.002	0.002	0.004	0.004	0.003
2577767	0.025	0.009	0.016	0.009	0.020	0.014	0.010	0.020	0.010	0.024	0.028	0.022
2577771	0.026	0.010	0.015	0.007	0.019	0.013	0.007	0.020	0.010	0.026	0.029	0.024
2577775	0.028	0.010	0.018	0.008	0.018	0.013	0.006	0.019	0.011	0.029	0.033	0.025
2577779	0.025	0.010	0.016	0.006	0.013	0.012	0.005	0.015	0.009	0.027	0.030	0.022
2577783	0.028	0.012	0.018	0.007	0.015	0.015	0.009	0.018	0.011	0.030	0.033	0.024
2577787	0.028	0.010	0.015	0.005	0.014	0.017	0.009	0.020	0.012	0.030	0.032	0.023
2581689	0.031	0.008	0.020	0.008	0.019	0.017	0.015	0.022	0.014	0.027	0.033	0.026
2581693	0.028	0.008	0.016	0.007	0.017	0.014	0.011	0.019	0.012	0.025	0.030	0.022
2581697	0.027	0.009	0.014	0.006	0.014	0.014	0.007	0.018	0.012	0.025	0.030	0.023
2581701	0.030	0.009	0.019	0.008	0.018	0.016	0.006	0.020	0.013	0.029	0.034	0.026
2581705	0.034	0.011	0.026	0.008	0.018	0.024	0.009	0.022	0.016	0.037	0.042	0.031
2581709	0.030	0.010	0.022	0.007	0.013	0.022	0.010	0.022	0.016	0.032	0.036	0.027
2581713	0.032	0.010	0.019	0.007	0.017	0.026	0.012	0.026	0.018	0.036	0.040	0.029
2585603	0.049	0.015	0.031	0.007	0.027	0.025	0.025	0.031	0.024	0.040	0.050	0.044
2585607	0.035	0.011	0.021	0.006	0.023	0.017	0.017	0.021	0.015	0.029	0.034	0.028
2585611	0.035	0.009	0.019	0.005	0.019	0.015	0.013	0.019	0.015	0.030	0.035	0.027
2585615	0.028	0.008	0.018	0.006	0.022	0.015	0.010	0.018	0.013	0.027	0.033	0.024
2585619	0.027	0.008	0.022	0.007	0.018	0.017	0.009	0.021	0.013	0.028	0.033	0.025
2585623	0.028	0.009	0.026	0.007	0.016	0.023	0.011	0.025	0.016	0.033	0.036	0.027
2589513	0.040	0.014	0.027	0.006	0.026	0.020	0.020	0.025	0.019	0.034	0.037	0.034
2589517	0.044	0.017	0.030	0.007	0.033	0.022	0.020	0.026	0.019	0.039	0.045	0.036
2589521	0.030	0.010	0.027	0.007	0.019	0.020	0.013	0.024	0.015	0.031	0.035	0.027

b. Calibration

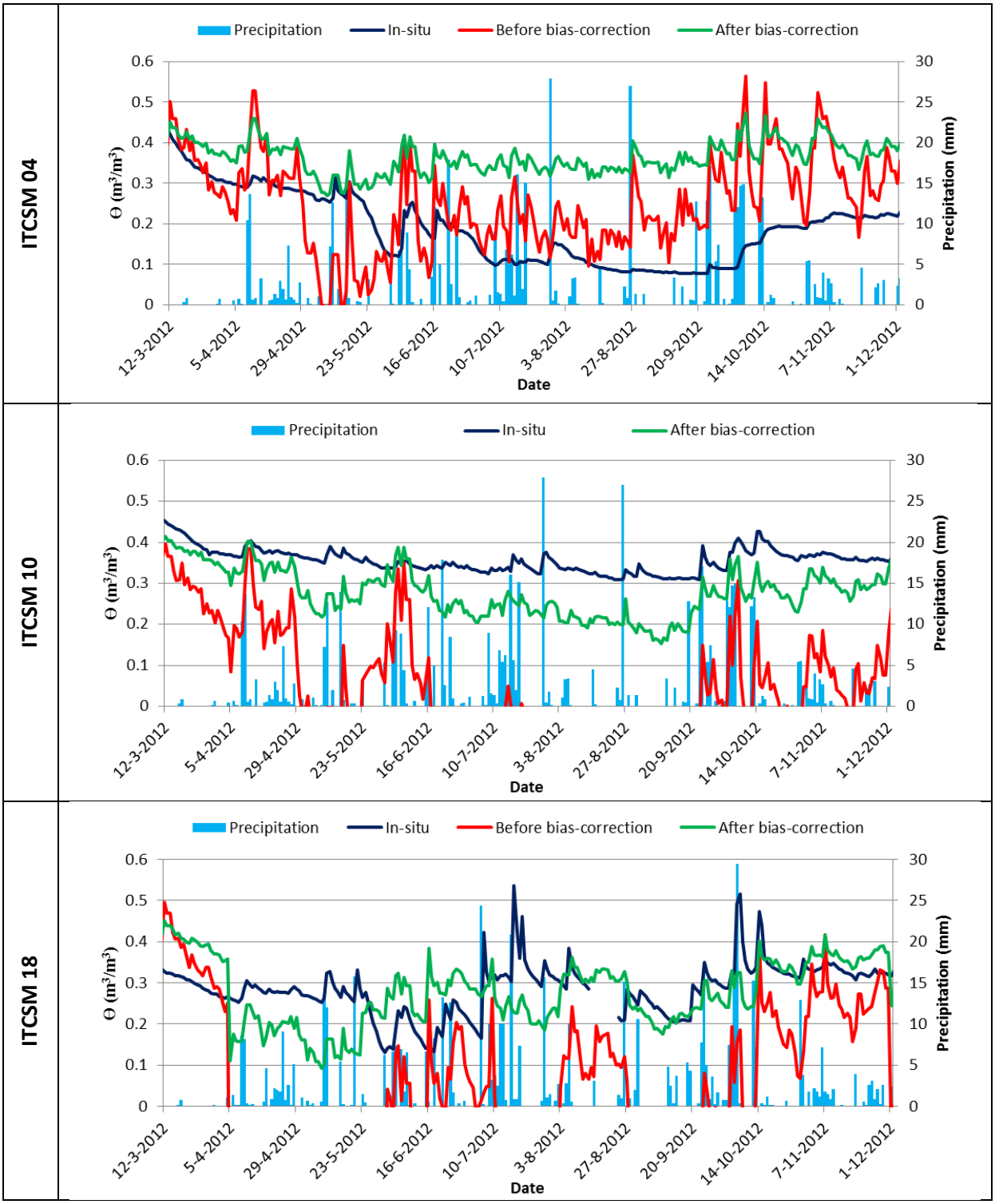

Figure 38A: Calibration results downscaling method I.

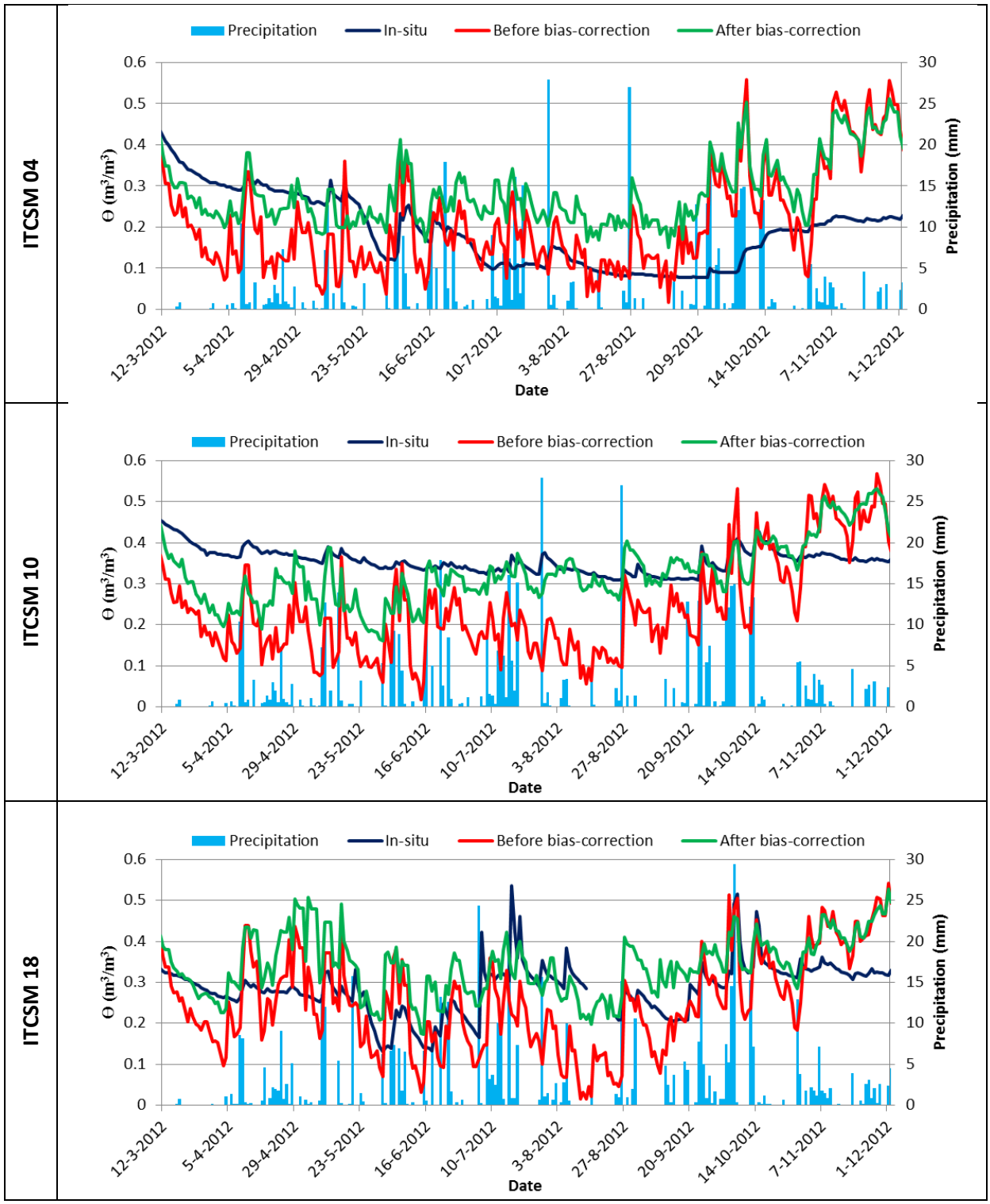

Figure 38B: Calibration results downscaling method II.

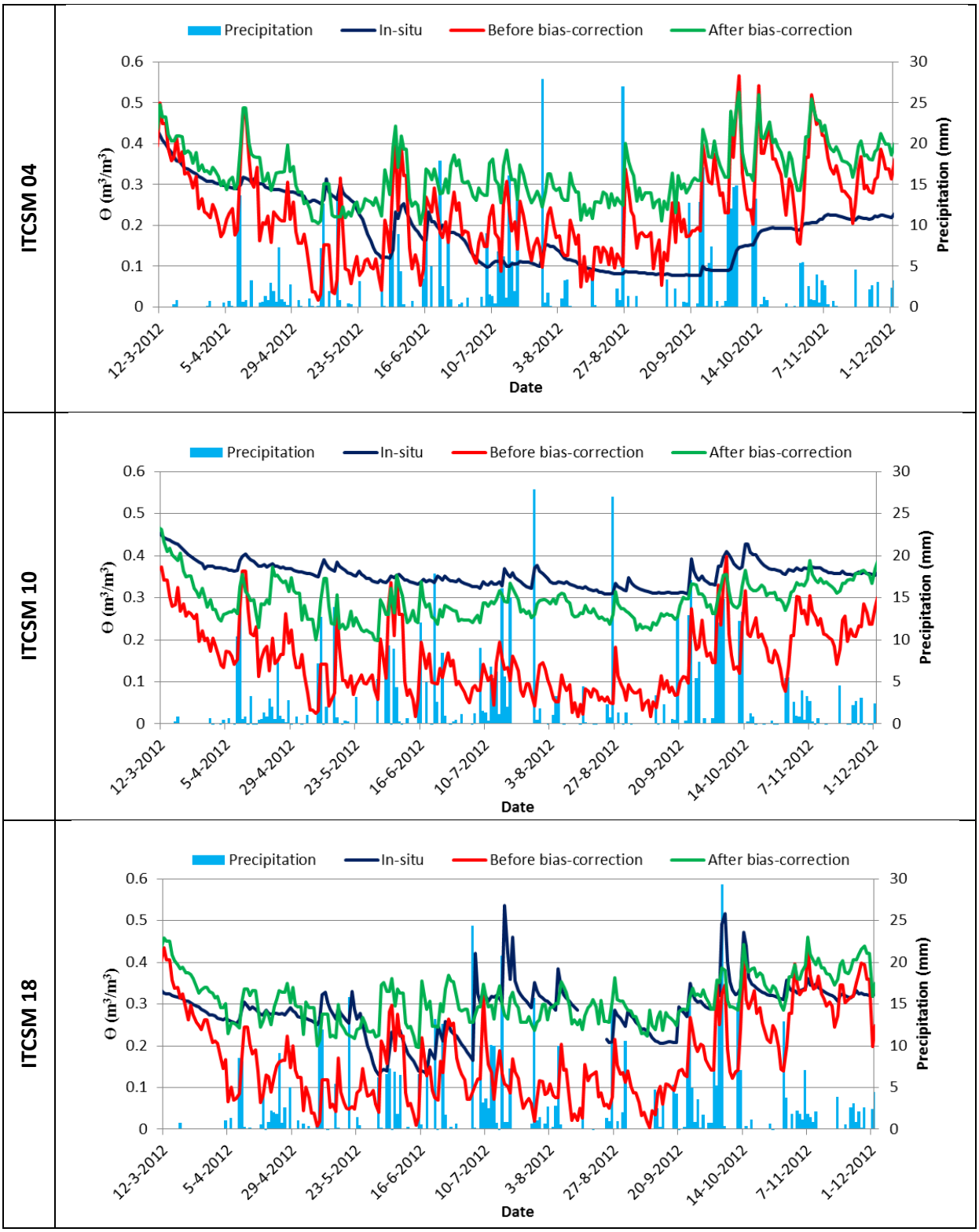

Figure 38C: Calibration results downscaling method III.

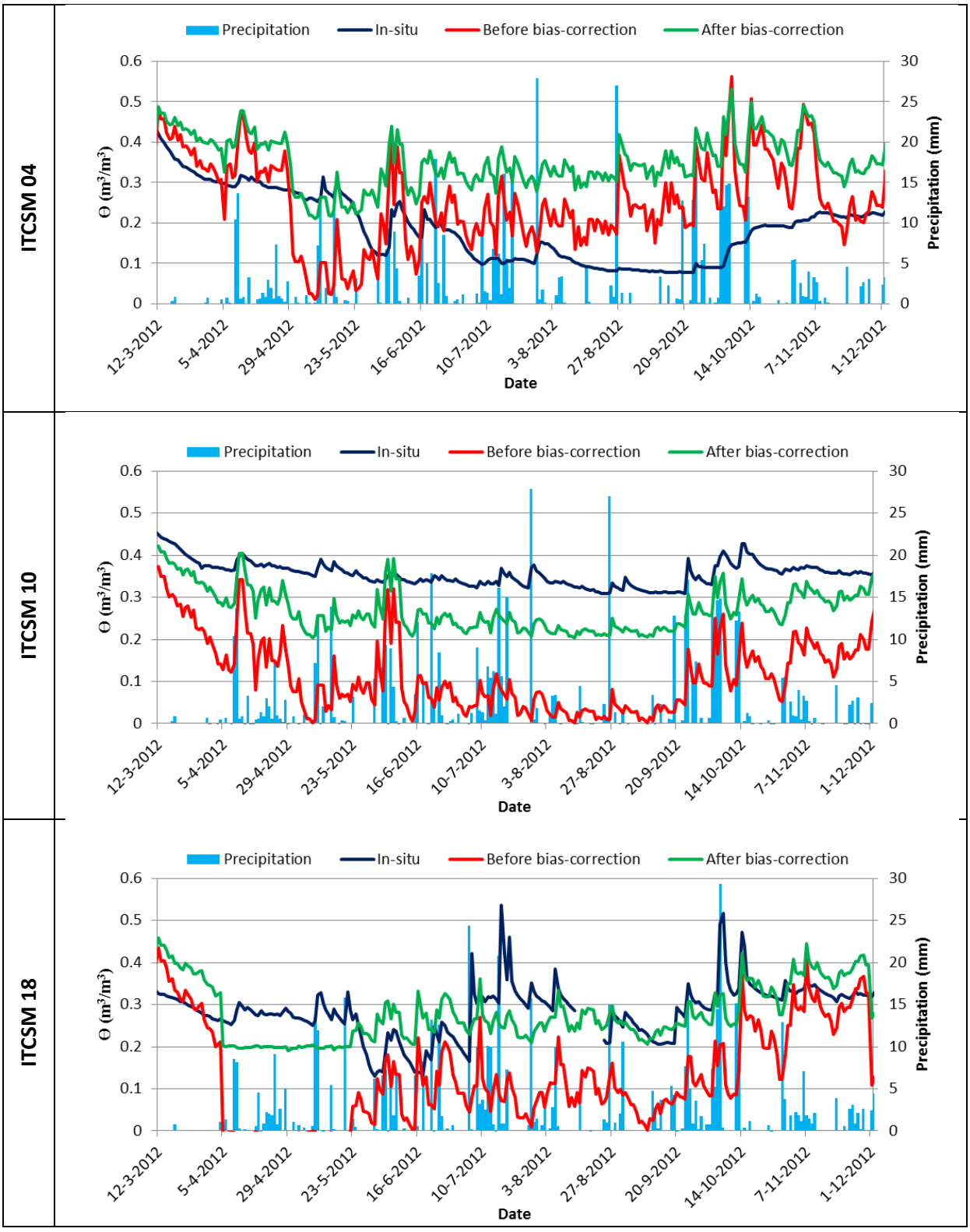

Figure 38D: Calibration results downscaling method IV.

c. Validation

Table 19: Coefficient of determination (R^2) between $\Theta_{in\text{-}situ}$ and σ_m, ASCAT SWI 1 (on RADARSAT-2 observing dates) and ASCAT SWI 1.

Station	RADARSAT-2 backscatter	ASCAT SWI 1 per 24 days	ASCAT SWI 1 per day
ITCSM 02	0.749	0.873	0.678
ITCSM 03	0.779	0.676	0.365
ITCSM 04	0.050	0.109	0.064
ITCSM 05	0.387	0.801	0.537
ITCSM 07	0.028	0.327	0.238
ITCSM 09	0.213	0.418	0.187
ITCSM 10	0.422	0.520	0.383
ITCSM 11	0.083	0.523	0.437
ITCSM 12	0.008	0.483	0.382
ITCSM 13	0.159	0.781	0.502
ITCSM 18	0.234	0.272	0.248
ITCSM 19	0.007	0.157	0.250
ITCSM 20	0.090	0.001	0.000

Appendix 7 Soil moisture station "Boetelerveld"

WGS has just started to set up their soil moisture monitoring network around the nature area Boetelerveld. Boetelerveld is wet moorland having the different land covers moorland, wood and blue-grassland (Hille Ris Lambers, Brekelmans, Lensink, & Smit, 2008). WGS monitors the soil moisture around this spot because of its ecological value. The waterboard has to manage a good soil moisture condition for the nature in Boetelerveld.

Table 20: In-situ station Boetelerveld.

Station	Coordinates (Latitude/Longitude)	Elevation (m NAP)	Land cover	Soil type (PAWM-classification)	Porosity (-)	Nearest KNMI station
WGS_ Boetelerveld	52°21'56"/6°18'53"	7	Blue-grassland	Sand	0.42	Heino

The first soil moisture measurement station is located in a blue-grassland and consists of a PR2 Profile Probe (by Delta-T Devices Ltd) measuring the soil moisture and a DL6 Soil Moisture Logger (also by Delta-T Devices Ltd) that records the data. The Profile Probe is installed in a shaft made of polycarbonate plastic and applies a 100MHZ signal to pairs of stainless steel rings on 10, 20, 30, 40, 60 and 100 cm depth. The signal transmits an electric field around 100mm in the soil and the water content of the soil surrounding the rings dominates the permittivity (permittivity of water ≈ 81, soil ≈ 4 and air ≈ 1). The permittivity results in a voltage output of the field that is translated to the soil moisture content. (Delta-T Devices Ltd, 2008).

The soil moisture probe is used in combination with a standard calibration, resulting in typical errors of 0.06m^3/m^3 including installation and sampling errors. Using a soil specific calibration can reduce this error only to 0.05m^3/m^3. Calibration is done in two steps: soil calibration and the Profile Probe response. For soil calibration distinguish is made between mineral and organic soils, both having their specific soil offset (a_0) and slope (a_1) (see Table 21) for the $\sqrt{3}$ damp soil - water content of the soil (%vol) relation resulting in equation III.

$$\sqrt{\varepsilon} = a_0 + a_1 \times \theta \qquad \text{(XIV)}$$

Table 21: Constants used for calibration and conversion to soil moisture for general soils using the Profile Probe PR2.

	a_0 (-)	a_1 (-)	Slope ($m^3/m^3/V$)	Offset (m^3/m^3)
Mineral soils	1.6	8.4	0.528	-0.146
Organic soils	1.3	7.7	0.575	-0.121

The dielectric performance off all Profile Probes is the same and can be approximated up to 0.3 m^3/m^3 by the relationship:

$$\sqrt{\varepsilon} = 0.37 + 4.43V \qquad \text{(XV)}$$

Combining both soil calibration and Profile Probe response equation makes:

$$\theta_V = \frac{(0.37+4.43V)-a_0}{a_1}\ m^3/m^3 \qquad \text{(XVI)}$$

Using the general soil constants a_0 and a_1 makes the values for the slope and offset presented in Table 21. Readings in m^3/m^3 are calculated when the readings in volts are multiplied by the slope and the offset is added.